EUROPEAN COMMISSION
5th EURATOM FRAMEWORK PROGRAMME 1998-2002
KEY ACTION : NUCLEAR FISSION

HTR-E

High-Temperature Reactor Components and Systems

CONTRACT N°
FIKI-CT-2001-00177

Delivery D25 - Workpackage 3
2.1 Concept Proposal for AMB and Diagnostic

Holger Stegemann
Steffen Gärtner

University of Applied Sciences Zittau/Görlitz

GERMANY

Dissemination level : RE
Document N°: HTR-E-04/02-D-3-2-1-2
Status : Final
Delivery No.: D25

Ref.: HZG-IPM 610334/3/2.02/F

DELIVERY D25 (Workpackage 3)

Task 2.1 Concept Proposal for AMB and Diagnostic

Authorised administrative official: Dr.-Ing. P. Reinhold
(Chancellor)

Signature

Authorised contact person: Prof. Dr.-Ing. F. Worlitz
(Project Leader)

F. Worlitz

Signature

Zittau, 02/29/2004

Zu erreichen:
Theodor-Körner-Allee 16 • 02763 Zittau
Tel.: (0 35 83) 61 0
Fax: (0 35 83) 51 06 26
Internet: http://www.hs-zigr.de

EMAS GEPRÜFTES UMWELTMANAGEMENT
Hochschule Zittau/Görlitz (FH) · Theodor-Körner-Allee 16 · 02763 Zittau
Register-Nr.: D - 144 - 00018
Diese Organisation wendet zur kontinuierlichen Verbesserung der Umweltleistung ein Umweltmanagementsystem nach der EG-Verordnung Nr. 761/2001 an, veröffentlicht regelmäßig eine Umwelterklärung, lässt das Umweltmanagementsystem und die Umwelterklärung von einem zugelassenen, unabhängigen Umweltgutachter begutachten, ist im EMAS-Register eingetragen und deshalb berechtigt, das EMAS-Zeichen zu verwenden.

Modifications

Revision	Date	Modifications
A	02/29/2004	First Issue

Summary

The document contributes to the 5th Framework Programme HTR-E Workpackage 3, Delivery D25 – Concept Proposal for AMB and Diagnostic. It describes the results of the investigations in controller algorithms and the diagnosis system.

The task is subdivided into two subtasks:
1. Concept of AMB (performed by S2M)
2. Concept of optimized controller and diagnosis algorithms with test of dynamic behaviour (performed by University Zittau/Goerlitz)

Depending on the special requirements and the results of the load analyses (task 1.2 Load Analysis, 1.2.2 Real Time Investigations, Document HTR-E-03/10-D-3-1-2-2) a concept has been designed for Active Magnetic Bearings (with controls, sensors, and power electronics) and Catcher Bearings in the first part of the document. An important aspect is the fact that sensor signals can be used for diagnosis algorithms. This allows innovations for controlling and monitoring. Three steps are necessary:
1. Concept of bearings including the control tasks.
2. Development and optimisation of controller algorithms by computer simulation depending on the analysed forces.
3. Development of diagnosis algorithms for magnetic and catcher bearings, driven and drive machine and test by computer simulation.

The dynamic behaviour (during shut-down, start up, unbalances, mechanical loads) of the Active Magnetic Bearing system was determined with the simulation tool *MLDyn* under the following conditions:
- start up
- speed levels and unbalances
- static loads
- dynamic loads (dynamic stiffness)

by using the controller algorithms:
- PID controller
- Fuzzy controller
- Fuzzy gain adaptation of PID controller

Active magnetic bearings make it possible to levitate a rotating shaft without friction or wear. Due to the functional principle of active magnetic bearings there are essential signals available without additional measurement equipment.

The second part of the document introduces a concept for the diagnosis of active magnetic bearings at rotating machines using inherently existing signals and knowledge-based methods of fuzzy logic.

Features for the diagnosis are extracted from relevant signals with signal- and model-based methods. A knowledgebase on faults at active magnetic bearings and machinery (e.g. faults in sensors, controllers and actors, unbalance, radial forces) and their characteristic features is generated by simulation and experiment. The knowledgebase is the basis for the development of a system for monitoring and fault diagnosis.

Additional to the monitoring of active magnetic bearings based on limit value checking, a concept using the combination of the extracted features and applying fuzzy logic is created for the identification and localization of appearing faults. Knowledge-based models for the diagnosis using fuzzy logic have been successfully tested and verified.

The defined fuzzy sets, operators and the selected rules realize a correct identification of occurring faults with a minimized effort of calculation. Using the concept of cascaded fuzzy logic modules the transparency of the whole systems is preserved even with a large number of symptoms and rules.

List of Symbols

Symbols – AMB control

ΔK_R	modification of PID controller gain (linguistic variable)
i	current
μ	degree of fulfillment (fuzzy logic)
n	rotor speed
N	rotational speed (linguistic variable)
ω	frequency
S	stiffness
T_I	integral action time constant of PID controller
T_N	reset time constant of PID controller
T_D	derivation action time constant of PID controller
T_V	rate time constant of PID controller
w	reference input variable (setpoint)
x	controlled variable
x_w	control error
X	deviation from setpoint of rotor displacement (linguistic variable)
$\dot{X}$	derivate of displacement (linguistic variable)
x,y,z	rotor displacement in x-, y-, z-direction
y	actuating signal
Y	controller output (linguistic variable)
$\hat{x}$	amplitude of rotor displacement
$\hat{X}$	amplitude of rotor displacement (linguistic variable)

Indexes – AMB control

0	nominal
1...6	No. of radial magnetic bearing
al	allowable
ax	axial
d	dynamic
M	measurement
max	maximum
min	minimum
n	necessary
Op	operational
R	controller
x,y,z	in x-, y-, z-direction

Symbols - Diagnostics

α	bearing specific constant
$\Delta\varphi$	phase difference
φq	vector phase angle
φ_{max}	phase angles of the maximum signal
$\underline{\Psi}$	measurement matrix of the input and output signals
$\underline{\Theta}$	parameter vector
μ	degree of fulfillment
ω	angular frequency
A	ratio between the rms values of the actuating signal and the according coil current
B	big
c	parameters
d	parameters
DW	diameter of a roller bearing
DT	rotating circle diameter of a roller bearing
$\underline{e}$	error vector
e	eccentricity
F	force
f_C	bearing cage rotation frequency
f_n	relative rotation between inner and outer ring of a roller bearing
f_I	roll over frequency of the inner bearing ring
F_u	unbalance force
Frbb	radial force between the upper and lower bearing level
Frub	radial force in the upper bearing level
Frlb	radial force in the lower bearing level
Frob	radial force below the lower or over the upper bearing level
FLM	fuzzy logic module
f_O	roll over frequency of the outer bearing ring of a roller bearing
f_R	rolling elements rotation frequency of a roller bearing
G	great
i	current
Io	pre-magnetization current
i_s	control current
i_-	negative coil current
i_+	positive coil current
k	physical constant
K_R	controller gain
m	mass
M	minus
n	rotor speed
N	normal
P	plus
$P(q)$	probability distribution
$p(q)$	probability density

$\bar{q}$	mean value
$\tilde{q}$	root mean square (rms)
q_{max}	maximum peak value
q_{min}	minimum peak value
q_{sp}	peak-to-peak value
R	ratio between the rms values of shaft displacement and the according actuating signal
rq	vector magnitude
$R(qq)$	auto correlation function
$R(qr)$	cross correlation function
s	shaft displacement
S	small
s_n	nominal air gap
t	time
u	controller output voltage
V	ratio between the rms values of the opposing coil currents
W	ratio between the rms values of the positive coil current and the according shaft displacement
$x(k-n)$	input signals
$y(k-n)$	output signals
$\underline{y}$	vector of the input signals
z	number of rolling elements

Indexes - Diagnostics

l	lower level
n	counting index
oa	other axis
rad	radial
u	upper level
x,y,z	in x-, y-, z-direction

Contents

1. Introduction/Objectives

The document contributes to the 5th Framework Programme HTR-E Workpackage 3, Delivery D25 – Concept Proposal for AMB and Diagnostic. It describes the results of the investigations in controller algorithms and the diagnosis system.

The task is subdivided into two subtasks:
1. Concept of AMB (performed by S2M)
2. Concept of optimized controller and diagnosis algorithms with test of dynamic behaviour (performed by University Zittau/Goerlitz)

Depending on the special requirements and the results of the load analyses (task 1.2 Load Analysis, 1.2.2 Real Time Investigations, Document HTR-E-03/10-D-3-1-2-2) a concept has been designed for Active Magnetic Bearings (with controller, sensors, and power electronics) and Catcher Bearings. An important aspect is the fact that sensor signals can be used for diagnosis algorithms. This allows innovations for controlling and monitoring. Three steps are necessary:
1. Concept of bearings including the control tasks.
2. Development and optimisation of controller algorithms by computer simulation depending on the analysed forces.
3. Development of diagnosis algorithms for magnetic and catcher bearings, driven and drive machine and test by computer simulation.

The dynamic behaviour (during shut-down, start up, unbalances, mechanical loads) of the Active Magnetic Bearing system is determined with the simulation tool *MLDyn* under the following conditions:
- start up
- speed levels and unbalances
- static loads
- dynamic loads (dynamic stiffness)

by using the controller algorithms:
- PID controller
- Fuzzy controller
- Fuzzy gain adaptation of PID controller

Resulting from the functional principle AMB deliver the following advantages for the implementation of a technical diagnosis system:

- The measured position signals and the actuating signals can be used for the diagnosis, therefore important diagnosis information are available without additional measurement equipment.
- With the shaft position and the coil currents the actuating forces and thus the disturbance forces can be calculated.
- The online-identification of machine parameters is possible by excitation of the shaft with defined forces.

Utilizing these advantages a diagnosis concept for AMB at rotating machines was developed.

Main aims of diagnosis are

- monitoring of the machine condition of AMB-systems,
- early detection of changes in the machine condition (faults),
- identification and localisation of faults, including the machinery e.g.
    - faults in sensors, controllers, actuators,
    - unbalances, radial forces

in order to increase the safety, reliability and lifespan of the machine and to decrease the costs for the maintenance.

The object of diagnosis is the rotating machine system as a whole, consisting of AMB, catcher bearings, drive and driven machine.

The used inputs are based on the following documents:
Framatome ANP (FRA): HTR-E – AMB and CB – Functional Requirements
HTR-E-02/06-D-3-1-1
Societe de Mechanique Magnetique (S2M): HTR-E Magnetic Bearing Concept Proposal
HTR-E 03/12 D-3-2-1-1

University Zittau/Goerlitz (Uni Zittau): HTR-E Load Analysis, HTR-E-03/10-D-3-1-2-2
HTR-E-03/01-D-3-3-1 Experimental test program FLP500

NRG: HTR-E Load Analysis – Modal and Harmonic Analysis HTR-E-04/03-D-3-1-2-1

As defined by all partners in the workpackage 3 (2nd WP meeting in Zittau) the configuration to be investigated is the GT-MHR reactor type.

2. AMB Control

2.1 Control Algorithms

The main task of the controller is to stabilize the rotor position in operation and during disturbances with the required accuracy. The reasons for the high requirements to the controller are
- system instability;
- nonlinearities in the magnetic force characteristic of the electromagnets;
- hysteresis and saturation of the magnetic core material;
- uncertain power losses in the magnetic coils and the rotor, e.g. eddy currents;
- high frequencies (small time constants in the control loop)
  $\Rightarrow$ short cyclic time for digital control.

Because of the nonlinearities and the uncertainties in the model of the magnetic force it can be advantageous to apply fuzzy logic or compensation methods for the nonlinearities to control the AMB. The tested algorithms are:
- PID controller
- Fuzzy logic controller
- Fuzzy gain adaptation of PID controller

2.1.1 PID Control

The common control algorithm used at active magnetic bearings is the PID controller. Fig. 2.1 shows the structure of the AMB control loop with implementation of the PID controller. The input variable is the shaft displacement (deviation from set point shaft position x_w). The output is the actuating variable for input voltage of the power amplifier y_R.

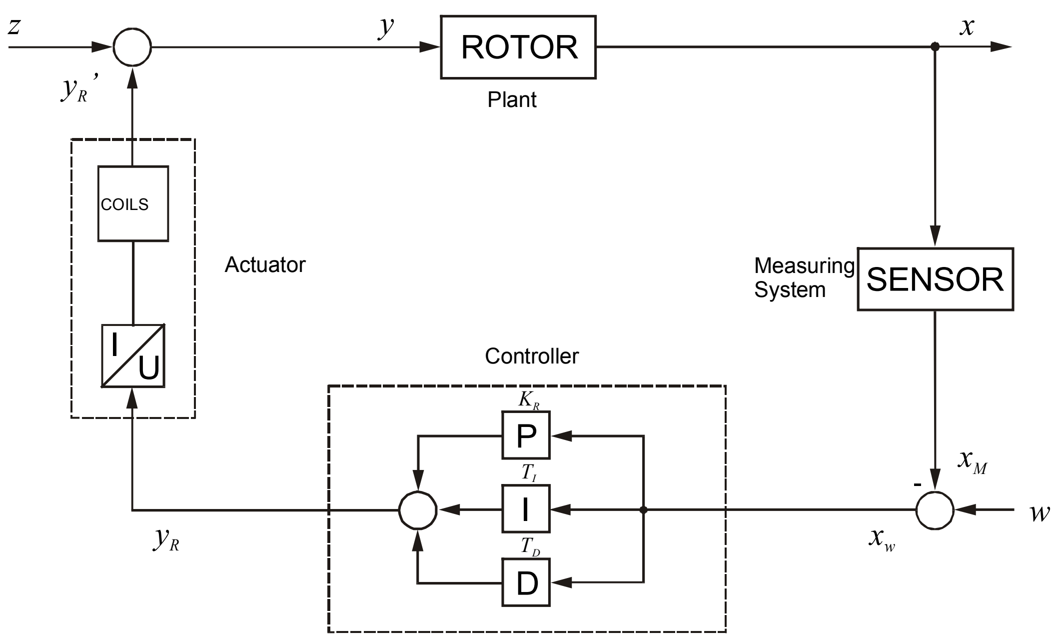

Fig. 2.1: Structure of AMB control loop with PID controller

The following differential equation is used for realization of PID algorithm:

$$y_R(t) = K_R x_w(t) + \frac{1}{T_I}\int x_w(t)dt + T_D\,\frac{dx_w(t)}{dt}$$

$$\text{with } T_I = \frac{T_N}{K_R} \text{ and } T_D = K_R \cdot T_V$$

Under assumption of minimal deviation from the working point (coil current i_0, shaft displacement s_0, speed n_0) the PID controller meets the static and dynamic requirements. For speed up of the rotor the following variants will be used:

- switching of controller parameters in different ranges (problems at switching points)
- compromise adjustment of controller parameters – no switching (non optimal control in the working point)

2.1.2 Fuzzy Control

An approach to apply non-linear control for AMB's is the usage of fuzzy logic. With fuzzy logic it's possible to integrate the expert knowledge about the machine and the process within the AMB's are used. Furthermore the uncertain power losses in the magnetic coils and the rotor (e.g. eddy currents, hysteresis) as well as the nonlinearities in the magnetic force calculation can be taken into account.

The first possibility is the application of a basic fuzzy logic controller (FLC). Fig. 2.2 shows the structure of the AMB control loop with FLC implementation. Input variables of the controller are shaft displacement x_w and derivate of displacement $\dot{x}_w$. The output is superposed by the output of the parallel connected integration part as the actuating variable y_R for input voltage of the power amplifier.

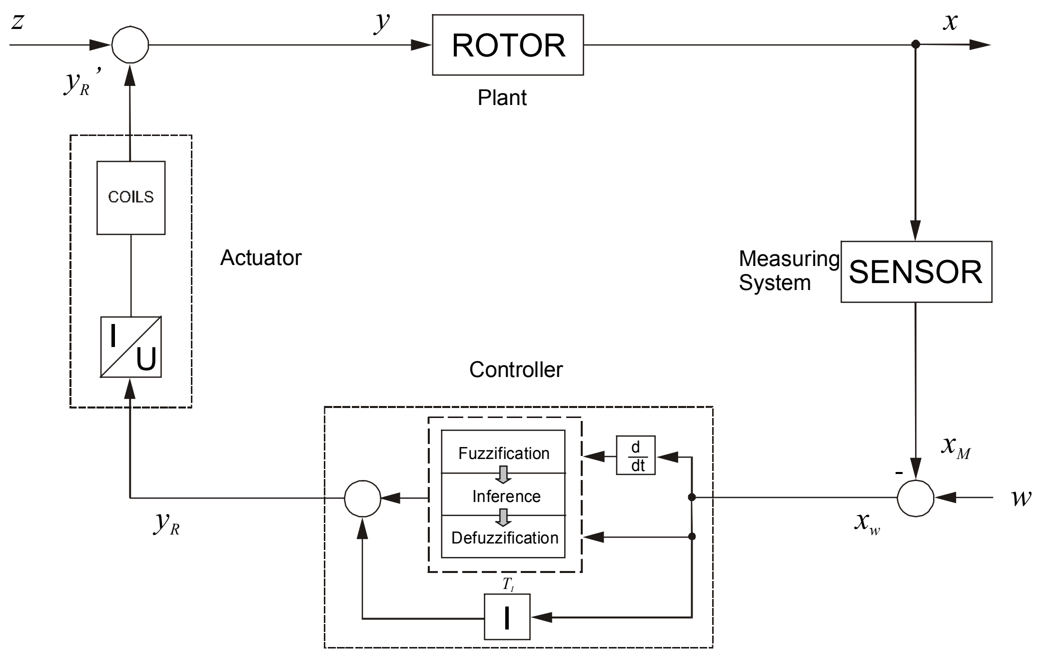

Fig. 2.2: Structure of AMB control coop with fuzzy logic controller

The fuzzy logic algorithm is subdivided into the fuzzification, the inference and the defuzzification.

Fuzzification

At the fuzzification procedure the crisp measuring values are assigned to fuzzy measures A and the degree of fulfillment (grade of membership) μ_A to these measures is calculated.
At a first step the linguistic variables, the linguistic values (sets) and their membership functions have to be defined.

linguistic varibles: X - deviation from setpoint of rotor displacement (input 1)
$\dot{X}$ - derivate of displacement (input 2)
Y - controller output (output)

fuzzy measures A of inputs and fuzzy measures B of output (sets, linguistische values):

NL - negative large
NS - negative small
ZR - zero
PS - positive small
PL - positive large

membership function: triangular shaped (λ-sets)

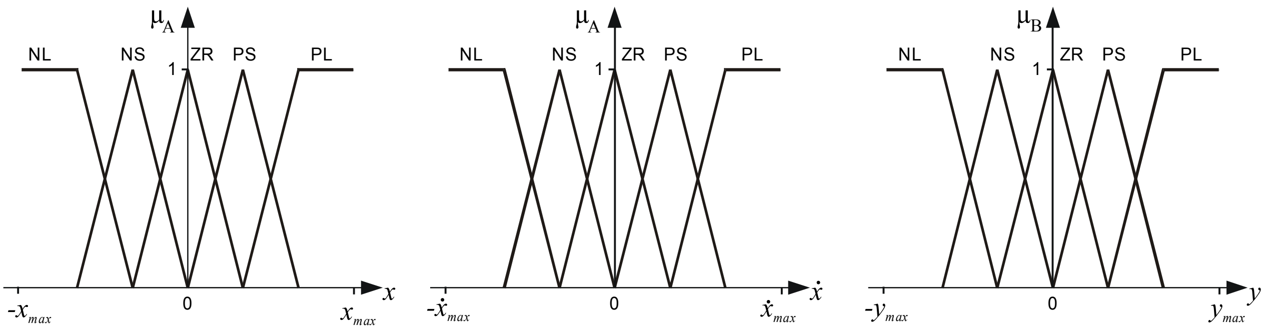

Fig. 2.3: Membership functions of linguistic variables

Afterwards the grade of membership of the linguistic inputs $\mu_A(x_w,\ \dot{x}_w)$ is calculated.

Inference

The inference describes the expert knowledge in a rule base. In the inference mechanism

From the grades of membership of the linguistic inputs $\mu_A(x_w,\ \dot{x}_w)$ the grades of membership of the fuzzy measures of the output $\mu_B(y)$ are calculated under consideration of the rule base.

The rules $R_i \ (i = 1...n)$ will be assigned in the following manner

IF <premise 1**> AND <**premise 2**> THEN <**conclusion**>**
d.h. **IF** $X = A$ **AND** $\dot{X} = A$ **THEN** $Y = B$

The rules are implemented in the rule base (Fig. 2.4).

$\dot{X}$

	Y	NL	NS	ZR	PS	PL
	NL	NL	NL	NL	NS	ZR
	NS	NL	NL	NS	ZR	PS
X	ZR	NL	NS	ZR	PS	PL
	PS	NS	ZR	PS	PL	PL
	PL	ZR	PS	PL	PL	PL

Fig. 2.4: Rule base

Defuzzification

In the last step – the defuzzifaction – the crisp output is calculated from the fuzzy result of the inference mechanism. The result is dependent on the used method of defuzzification.

2.1.3 Fuzzy gain adaptation

A different approach to apply fuzzy logic in control systems is the use as an auxiliary part of the system when the PID controller acts as the primary controller. Tuning of FLC is time consuming because it lacks practicable methods and tools for stability analysis. The adaptation approach is more advantageous, since the PID controller can be tuned and tested with practicable methods, and the Fuzzy Logic part helps in difficult operations. One possibility is the use of the gain scheduling adaptive control scheme.

The stiffness of an AMB system varies with the gain of the PID controller. The high gain at low frequencies is desired because high stiffness improves the behavior during start up operation. The problem is high gain at high frequencies as it makes the system sensitive to the vibrations because of unbalances. If the stiffness can be decreased the magnetic bearings react with forces proportional to the displacement and the shaft rotates on its axis of inertia. The magnitude of vibrations can be decreased. One method of realization is the adjusting of the gain as a function of the actual amplitude of displacement of the shaft and the rotational speed using Fuzzy Logic. In Fig. 2.5 the structure of fuzzy gain adaptation is shown.

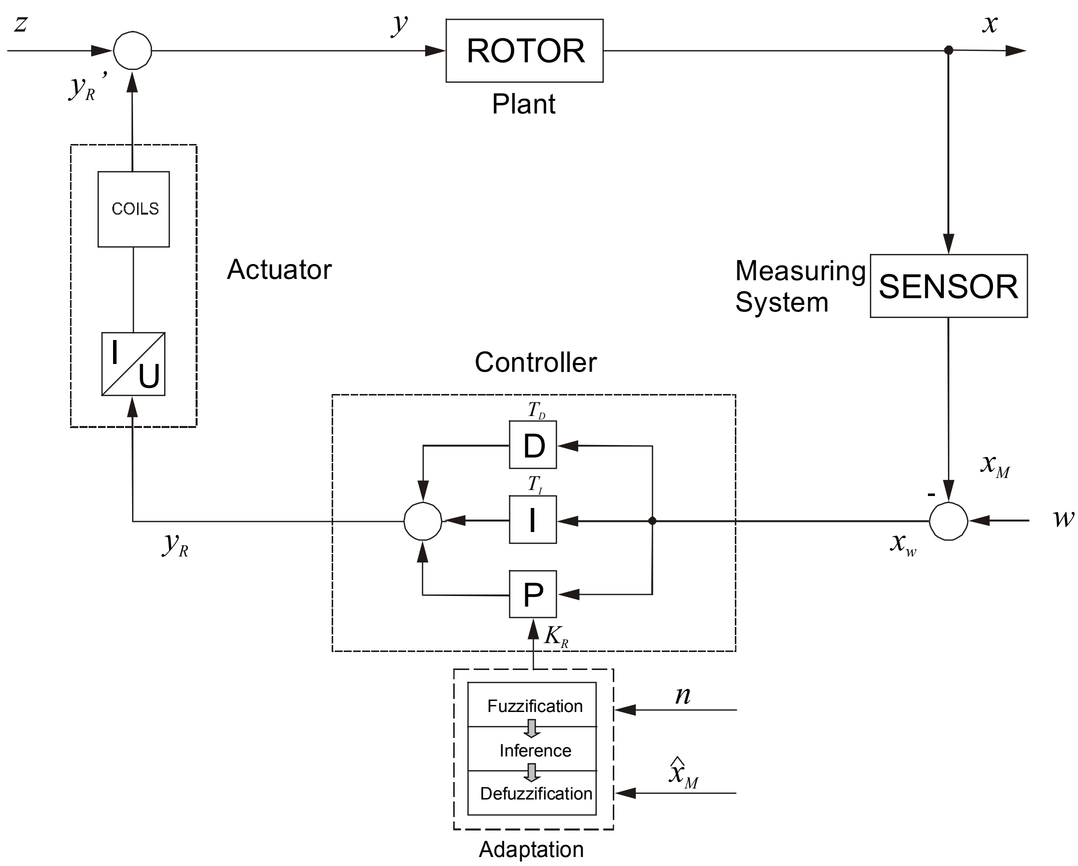

Fig. 2.5: Structure of AMB control coop with fuzzy gain adaptation of the PID controller

At a first step the linguistic variables, the linguistic values (sets) and their membership functions have to be defined.

linguistic variables:	N	- rotational speed (input 1)
	$\hat{X}$	- Amplitude of rotor displacement (input 2)
	ΔK_R	- modification of PID controller gain (output)

fuzzy measures A of inputs		*fuzzy measures B of output*	
VS	- very small	NL	- negative large
S	- small	NS	- negative small
M	- medium	ZR	- zero
L	- large	PS	- positive small
VL	- very large	PL	- positive large

membership function: triangular shaped (λ-sets)

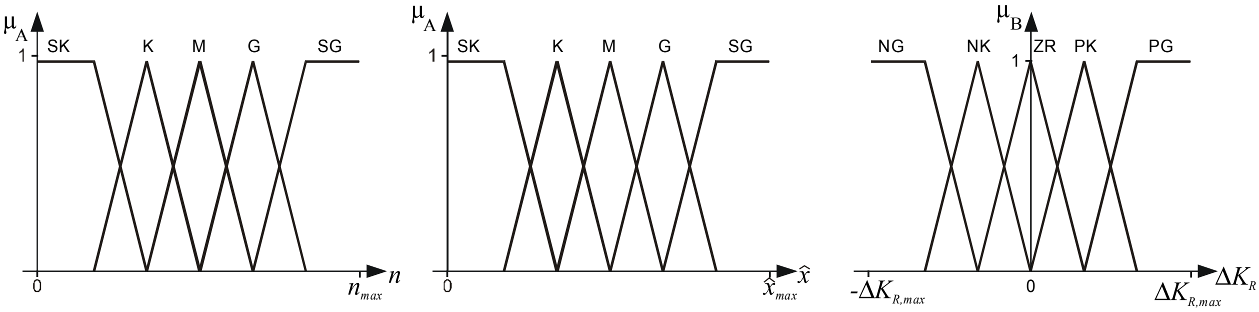

Fig. 2.6: Membership functions of linguistic variables

The adaptation rules can be derived by using the engineering knowledge about the AMB system.
The basic assumptions are:

- When the value of speed is high (therefore the system operates at high frequencies) the gain of PID controller should be decreased.
- When the value of amplitude of displacement is high and the value of speed is also high the system is heavily vibrating and the gain has to be reduced.

An example of a rule-base is shown in Fig. 2.7. The gain is the sum of a start value K_{R0} and a change of ΔK_R. For both the input variables three sets are used. The characteristic field of the adaptation is represented in Fig. 2.8.

Displacement \ Speed	S	M	L
S	ZR	ZR	ZR
M	PS	NS	NS
L	PL	NS	NL

Fig. 2.7: Rule-base for fuzzy gain adaptation (Output is ΔK_R)

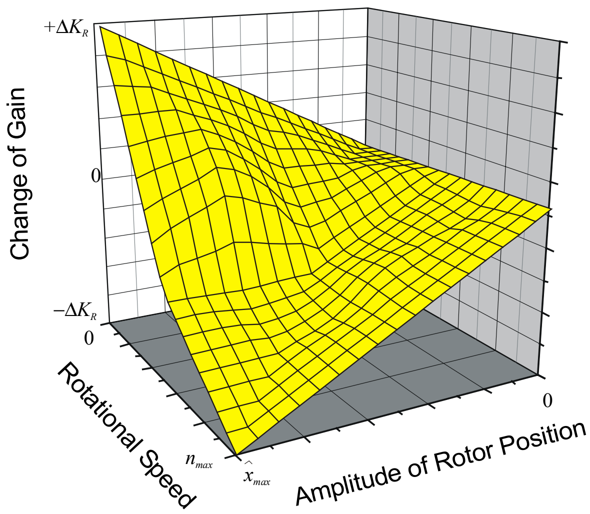

Fig. 2.8: Characteristic field of the fuzzy gain adaptation (example)

2.2 Test and Optimization

2.2.1 Parametrization of simulation tool and criteria for optimization

The tests of controller algorithms were performed with the simulation tool *MLDyn*. *MLDyn* was especially developed for theoretical investigations in the field of active magnetic bearing systems. This tool has been parameterized according the specifications of the turbomachine geometry and the AMB concept –see document HTR-E-03/10-D-3-1-2-2 Load Analysis.

At the optimization process the parameters of the used controllers are adapted with help of simulation calculations. Optimization was performed with respect to the disturbance behaviour as the unbalance loads have an essential effect to the operation of an active magnetic bearing.

Quality criteria will be used for controller tuning based on the tests (Table 1). Aim of the optimization is the minimization of these criteria primarily the main criteria.

The following tests will be used

- start up (rotor lift-up)
- speed levels and unbalance loads (sinusoidal disturbance)
- static loads
- dynamic loads (dynamic stiffness)

	Quality Criteria	
Simulation	**Main Criterion**	**Secondary Criterion**
start up	overshoot	rise time and settling time
speed levels and unbalance loads	amplitude of rotor displacement	-
static loads	overshoot	bearing forces
dynamic loads	dynamic stiffness	bearing forces

Table 1: Quality criteria for controller optimization

2.2.2 Tests

2.2.2.1 Start up

Radial AMB‘s

At the start-up operation the shaft must be lifted from an arbitrary position in the catcher bearings to the setpoint position (mainly center position). A minimal overshoot and a short settling time are required.

PID controller

Simulation-based optimization with *MLDyn* contains the varying of controller gain K_R. In Fig. 2.9 the overshoot of the rotor position at all radial AMB‘s is shown during the start-up. The overshoot depends on the adjusted controller gain K_R – increased gain results in minimal overshoot. In the investigated range of controller gain the radial AMB‘s are able to start up the rotor.

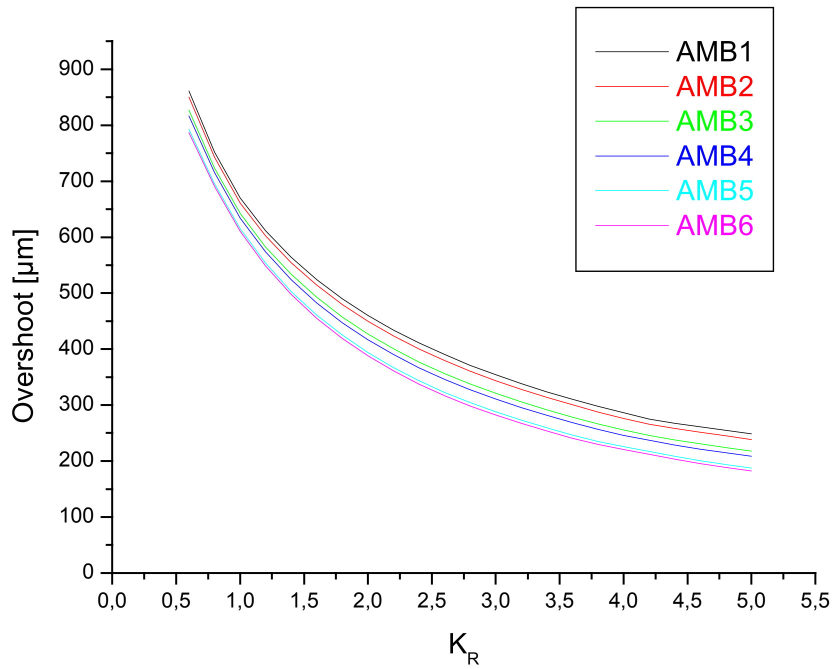

Fig. 2.9: Overshoot vs. controller gain for radial AMB 1...6

Fuzzy controller

For optimization of a fuzzy logic controller different methods can be applied:
- algorithms (fuzzification, inference, defuzzifcation methods)
- membership functions (shape, No. of sets, distribution, spread, grade of overlapping)
- rule base (No. of rules, fullness, plausibility)

Most practicable in simulation-based optimization are the varying of number of input and output sets resp. distribution of these sets.

The tests with *MLDyn* result in membership functions of all linguistic variables (input and output) with 5 triangular sets (see Fig. 2.3).

In Fig. 2.10 the overshoot of the rotor position at all radial AMB‘s is shown during the start up. The overshoot depends on the adjusted distribution of set „ $\dot{X}$ “.
Distribution = -1 means compression of the set at the border of the definition range.
Distribution = 1 means compression of the set at the center of the definition range.

For minimal overshoot the set for „ $\dot{X}$ “ should be compressed at the center (Fig. 2.11).

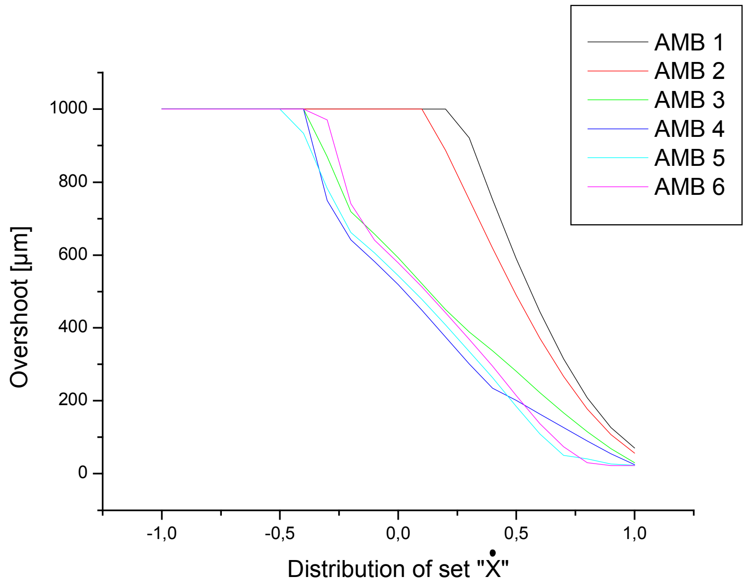

Fig. 2.10: Overshoot vs. normalized distribution of set „ $\dot{X}$ “ for radial AMB 1...6

In comparison with the PID controller the overshoot can be significantly minimized.

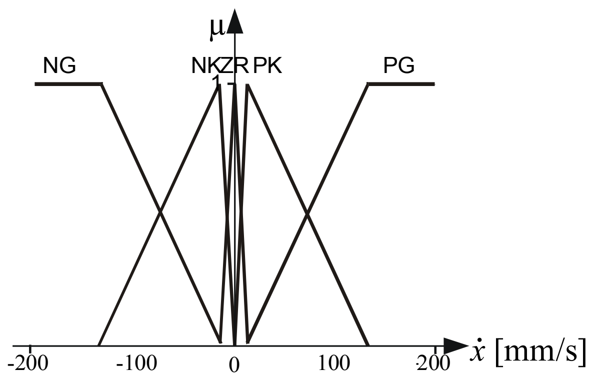

Fig. 2.11: Optimized membership function of set „ $\dot{X}$ “ (distribution = 1)

Fuzzy gain adaptation

For fuzzy adaption the same methods for optimization can be applied as used at the fuzzy controller.
Simulation-based optimization with *MLDyn* contains the varying of number of input and output sets resp. distribution of sets. The membership functions are triangular shaped. The tests result in membership functions of all linguistic variables with 3 triangular sets for the input variable $\hat{X}$ (since $N = 0$ at start up) and 5 sets for the output varible „ΔK_R. The starting value K_{R0} amounts 1.5. The range of ΔK_R is limited from -0.5 to 5.0.

Fig. 2.12 shows the overshoot of the rotor position at all radial AMB's during the start-up. Exemplarily for the investigations the overshoot is shown depending on the adjusted distribution of set „ΔK_R" For minimal overshoot the set for „ΔK_R" should be compressed at the border of the definition range (Fig. 2.13).

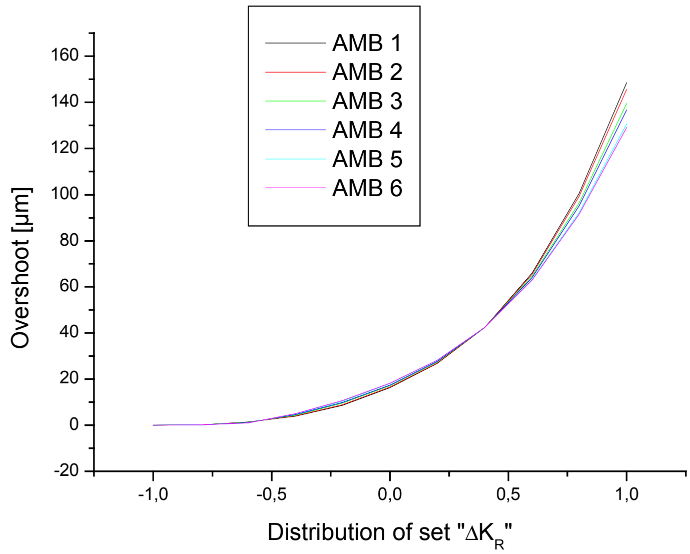

Fig. 2.12: Overshoot vs. normalized distribution of set „ΔK_R" for radial AMB 1...6

In comparison with the PID controller the overshoot can be significantly minimized.

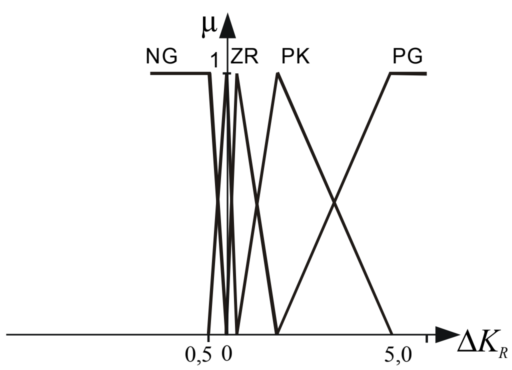

Fig. 2.13: Optimized membership function of set „ΔK_R" (distribution = -1)

Axial AMB

At the start-up operation the shaft must be lifted from the lower position in the catcher bearings to the setpoint position (mainly center position). The weight load of 105×10^4 N must be compensated.

PID controller

Simulation-based optimization with *MLDyn* contains the varying of controller gain K_R. In the investigated range of controller gain no overshoot occur. Fig. 2.14 shows the settling time vs. the controller gain. Settling time has a maximum at K_R =1.5. With higher gain the settling time decreases.

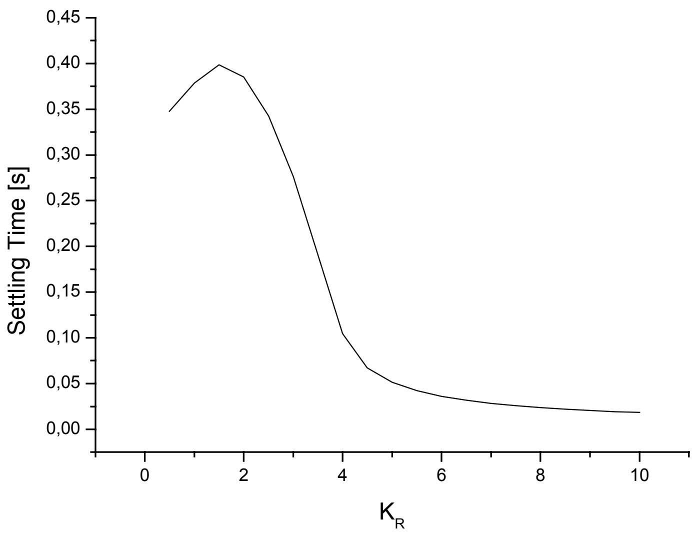

Fig. 2.14: Settling time vs. controller gain for axial AMB

Fuzzy controller

Simulation-based optimization with *MLDyn* contains the varying of number of input and output sets resp. distribution of sets. The membership functions are triangular shaped. The tests result in membership functions of all linguistic variables (input and output) with 5 triangular sets (see Fig. 2.3).

Fig. 2.15 shows the settling time vs. the distribution of set „ $\dot{X}$ “. The settling time is decreasing if the set for „ $\dot{X}$ “ is compressed at the center (Fig. 2.16). In comparison with the PID controller the same values of the settling time near 0.02 s can be reached.

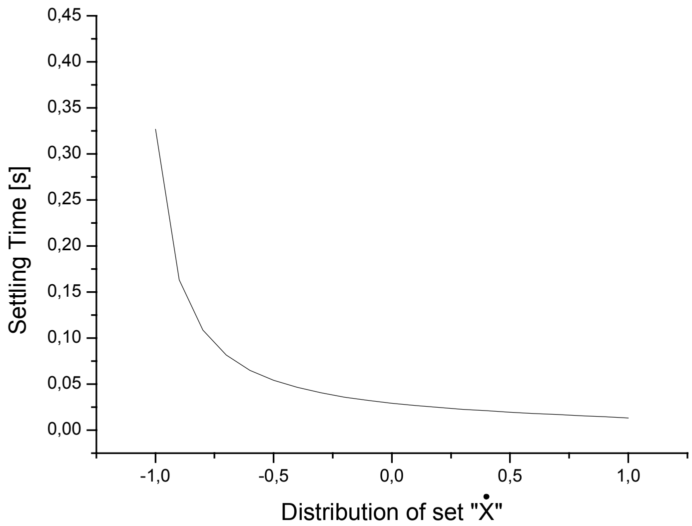

Fig. 2.15: Settling Time vs. normalized distribution of set „$\dot{X}$“ for axial AMB

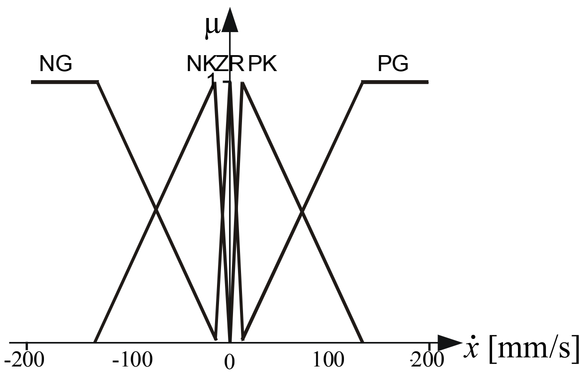

Fig. 2.16: Optimized membership function of set „$\dot{X}$“(distribution = 1)

Fuzzy gain adaptation

Simulation-based optimization with *MLDyn* contains the varying of number of input (only amplitude of rotor displacement) and output sets resp. distribution of sets. The membership functions are triangular shaped. The tests result in membership functions of all linguistic variables with 3 triangular sets for both the input variables (N and $\hat{X}$) and 5 sets for the output varible („ΔK_R). The starting value K_{R0} amounts 1.5. The range of ΔK_R is limited from -0.5 to 5.0.

Fig. 2.17 shows the settling time vs. the distribution of set „ΔK_R“. Settling time has a maximum at a distribution of –0.25. For minimal overshoot the set for „ΔK_R“ should be compressed at the border of definition range (Fig. 2.18). In comparison with the PID controller the same values of the settling time near 0.02 s can be reached.

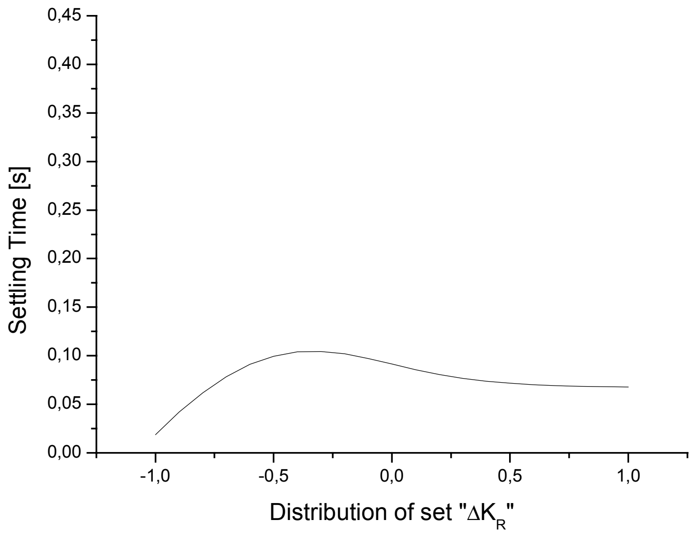

Fig. 2.17: Settling Time vs. normalized distribution of set „ΔK_R“ for axial AMB

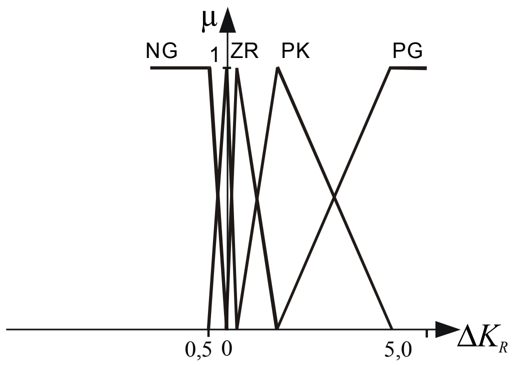

Fig. 2.18: Optimized membership function of set „ΔK_R“ (distribution = -1)

2.2.2.2 Speed levels and unbalances

High loads at the shaft can occur due to resonances vibrations at critical speeds. The reason for these vibrations are unbalances. The unbalances are caused by the eccentricity of the center of gravity and deviation moments. The eccentricity e = 10 µm is given by the FRA requirements.
The arising force is proportionally to the square of the rotational speed.

PID controller

Simulation-based optimization with *MLDyn* contains the varying of controller gain K_R. Fig. 2.19 shows the maximum amplitude of rotor position and the bearing force vs. the controller gain and the rotational speed exemplarily for the radial AMB 1.

NOTE: The amplitude of rotor position and the bearing force for AMB 1...6 can be seen on Annex 1.

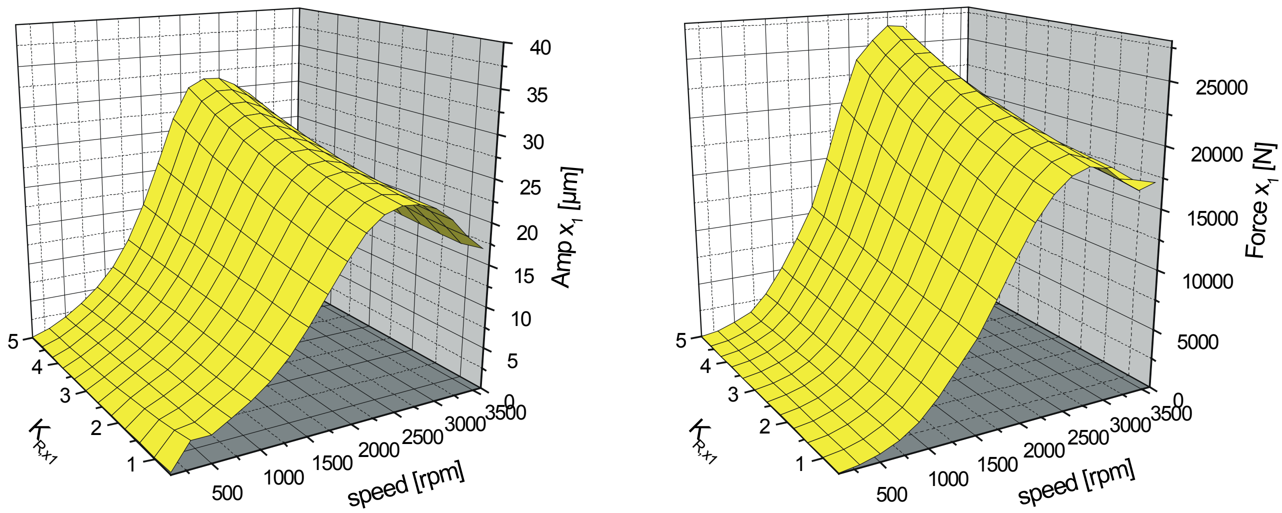

Fig. 2.19: Amplitude of rotor position and bearing force vs. speed and controller gain for radial AMB 1

The amplitude of rotor position varies with the controller gain and the rotational speed. Increased amplitudes occur at the nominal speed of 3,000 rpm but the radial AMB‘s are able to react the loads caused by unbalances up to full speed (3,600 rpm).

Fuzzy controller

Simulation-based optimization with *MLDyn* contains the varying of number of input and output sets resp. distribution of sets. The membership functions are triangular shaped. The tests result in membership functions of all linguistic variables (input and output) with 5 triangular sets (see Fig. 2.3).

Fig. 2.20 shows the maximum amplitude of rotor position and the bearing force vs. the distribution of set „$\dot{X}$“ and the rotational speed exemplarily for the radial AMB 1.

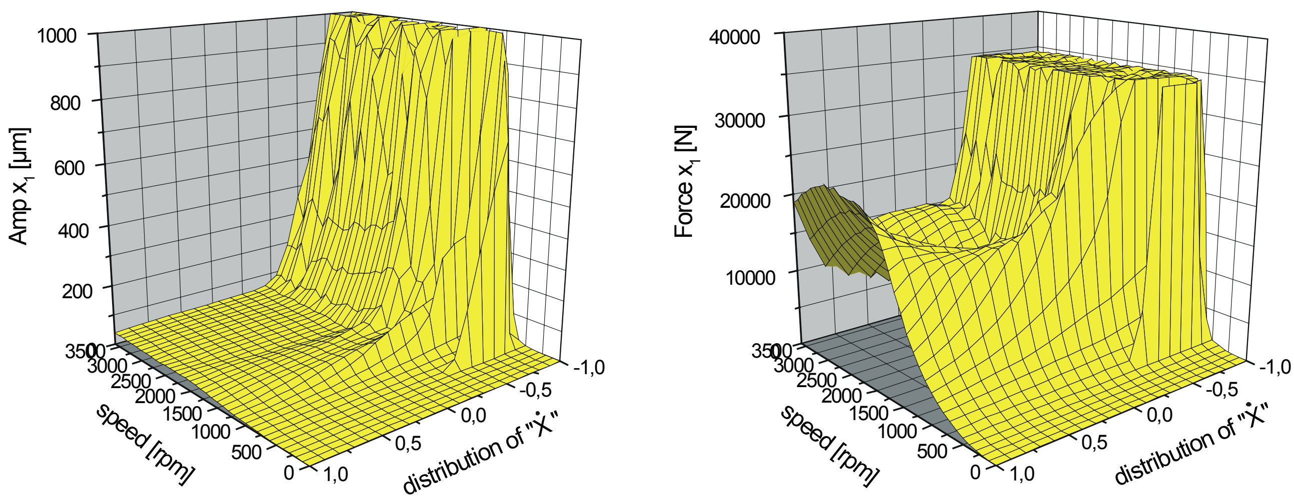

Fig. 2.20: Amplitude of rotor position and bearing force vs. speed and normalized distribution of set „$\dot{X}$“ for radial AMB 1

NOTE: The amplitude of rotor position and the bearing force for AMB 1...6 can be seen on Annex 1.

The amplitude of rotor position varies with the distribution of set „ $\dot{X}$ “ and slightly with the rotational speed. For minimal amplitudes and bearing forces at all speeds the set of „ $\dot{X}$ “ should be compressed at the center (Fig. 2.21). In this case the amplitude as well as the bearing forces can be decreased in comparison with the PID controller.

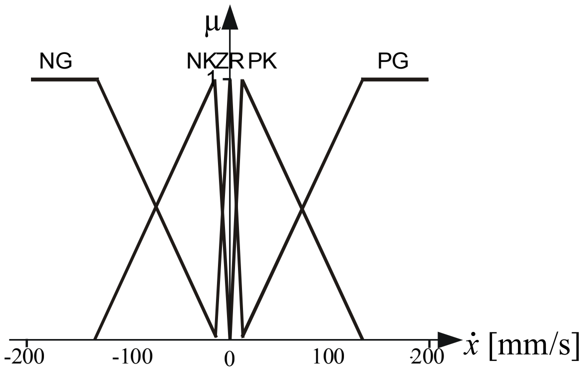

Fig. 2.21: Optimized membership function of set „ $\dot{X}$ “(distribution = 1)

Fuzzy gain adaptation

Simulation-based optimization with *MLDyn* contains the varying of number of input and output sets resp. distribution of sets. The membership functions are triangular shaped. The tests result in membership functions of all linguistic variables with 3 triangular sets for both the input variables (N and $\hat{X}$) and 5 sets for the output varible („ΔK_R). The starting value K_{R0} amounts 1.5. The range of ΔK_R is limited from -0.5 to 5.0.

Fig. 2.22 shows the maximum amplitude of rotor position and the bearing force vs. the distribution of set „ΔK_R“ and the rotational speed exemplarily for the radial AMB 1. There is only a small indepence on the variation of distribution of set „ΔK_R“. The amplitude of rotor displacement is nearly linear dependent on the rotor speed. With gain adaptation of K_R the amplitude of rotor displacement can be decreased in comparison with the PID controller.

NOTE: The amplitude of rotor position and the bearing force for AMB 1...6 can be seen on Annex 1.

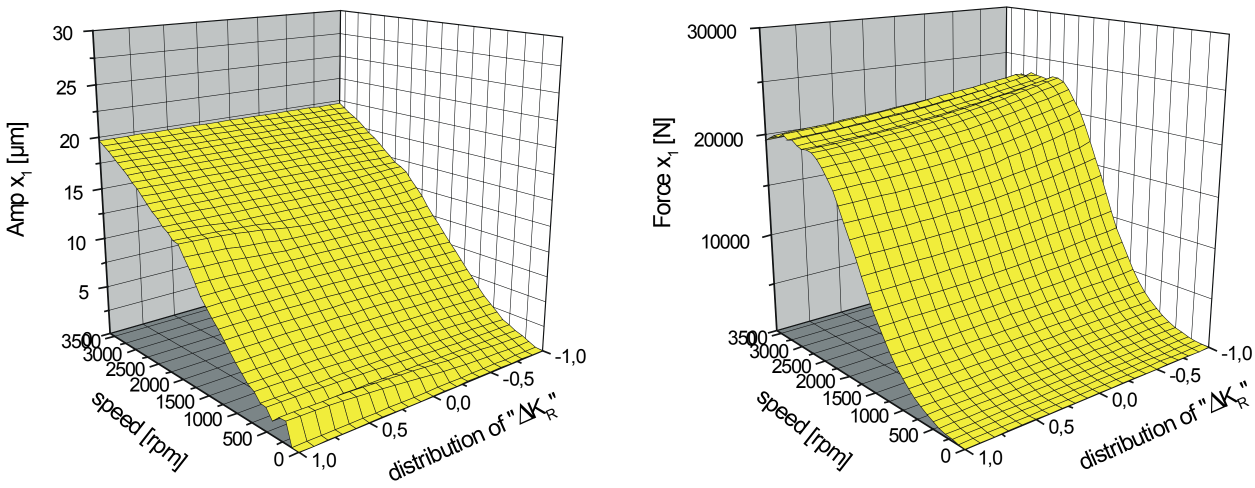

Fig. 2.22: Amplitude of rotor position and bearing force vs. speed and normalized distribution of set „ΔK_R“ for radial AMB 1

2.2.2.3 Static loads

Radial AMB‘s

According the FRA requirements a static load of 8500 N is acting between radial AMB 2 and 3. The operational speed is 3000 rpm.

PID controller

By variation of controller gain the amplitude of rotor position and the bearing forces were investigated. Fig. 2.23 shows the results for radial AMB 2.

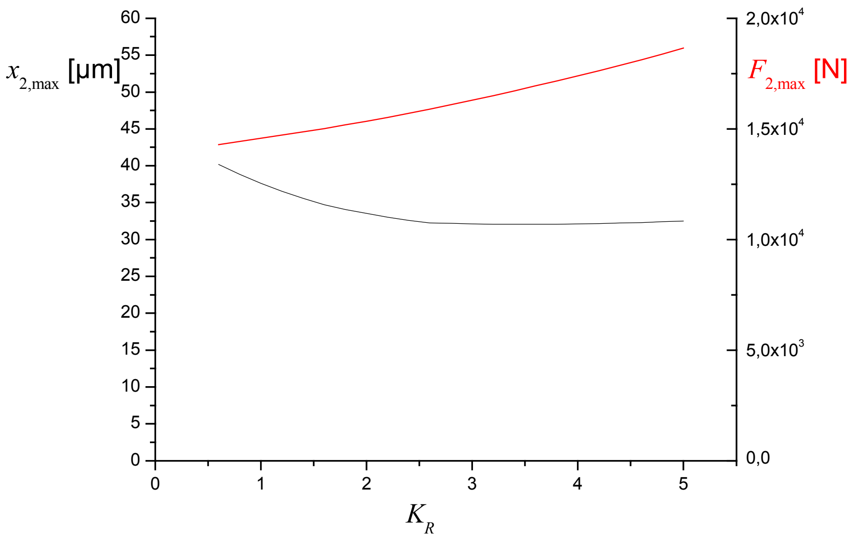

Fig. 2.23: Amplitude of rotor position and bearing force vs. controller gain for radial AMB 2

Obviously, the amplitude decreases with higher controller gain but therefore higher bearing forces are necessary (higher stiffness).
In the full range of gain the radial AMB's are able to react the static loads.

NOTE: The amplitude of rotor position and the bearing force for AMB 1...6 can be seen on Annex 1.

Fuzzy controller

Simulation-based optimization with *MLDyn* contains the varying of number of input and output sets resp. distribution of sets. The membership functions are triangular shaped. The tests result in membership functions of all linguistic variables (input and output) with 5 triangular sets.

Fig. 2.24 shows the amplitude of rotor position and the bearing force vs. the distribution of set „ $\dot{X}$ " for the radial AMB 2. To minimize the amplitude and the bearing force the set of „ $\dot{X}$ " should be compressed at the center. A good compromise is a distribution of 0.4 (see Fig. 2.25). In comparison with the PID controller the amplitude and the bearing forces can be decreased by variation of fuzzy sets.

NOTE: The amplitude of rotor position and the bearing force for AMB 1...6 can be seen on Annex 1.

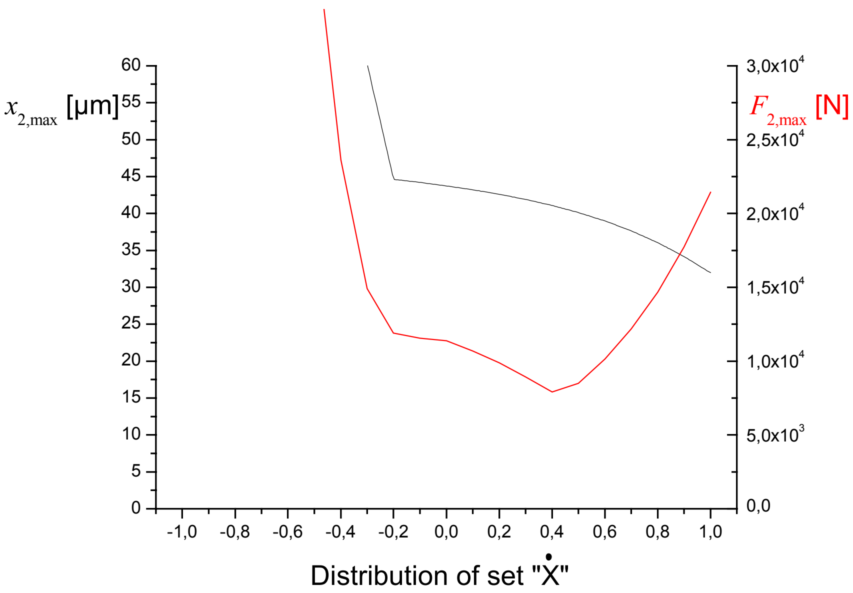

Fig. 2.24: Amplitude of rotor position and bearing force vs. normalized distribution of set „ $\dot{X}$ " for radial AMB 2

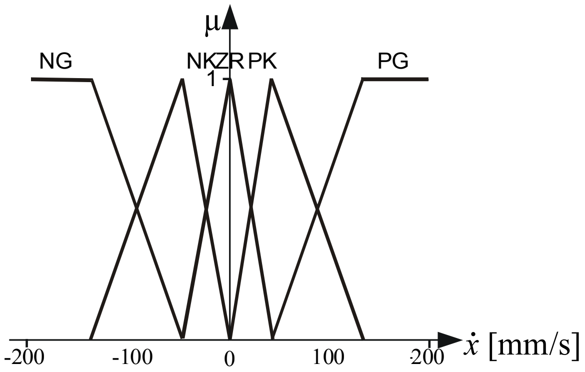

Fig. 2.25: Optimized membership function of set „ $\dot{X}$ “(distribution = 0.4)

Fuzzy gain adaptation

Simulation-based optimization with *MLDyn* contains the varying of number of input and output sets resp. distribution of sets. The membership functions are triangular shaped. The tests result in membership functions of all linguistic variables with 3 triangular sets for both the input variables (N and $\hat{X}$) and 5 sets for the output varible („ΔK_R). The starting value K_{R0} amounts 1.5. The range of ΔK_R is limited from -0.5 to 5.0.

Fig. 2.26 shows the amplitude of rotor position and the bearing force vs. the distribution of set „ΔK_R“ for the radial AMB 2. The amplitude decreases if the set of „ΔK_R“ is compressed at the border of definition range but higher forces are necessary.
A good compromise is a distribution of 0.3 (see Fig. 2.27). In comparison with the PID controller the amplitude can be decreased by variation of fuzzy sets for gain adaptation.

NOTE: The amplitude of rotor position and the bearing force for AMB 1...6 can be seen on Annex 1.

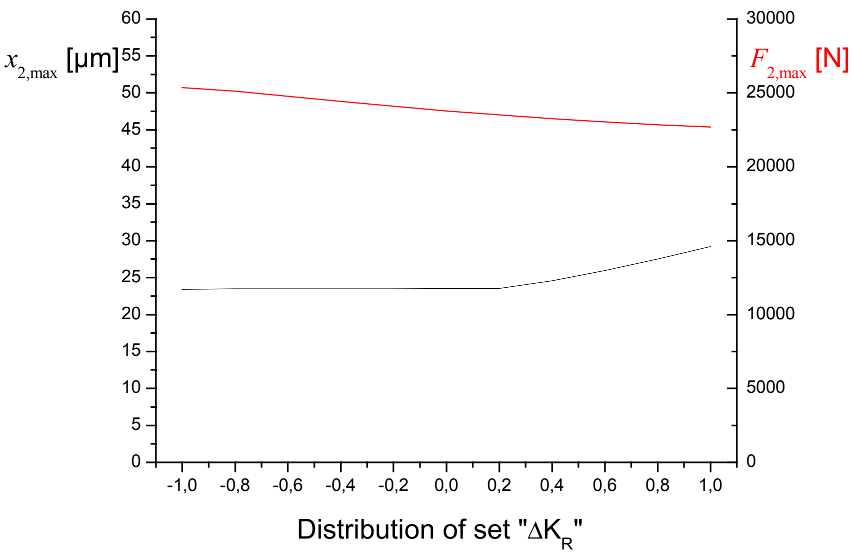

Fig. 2.26: Amplitude of rotor position and bearing force vs. normalized distribution of set „ΔK_R“ for radial AMB 2

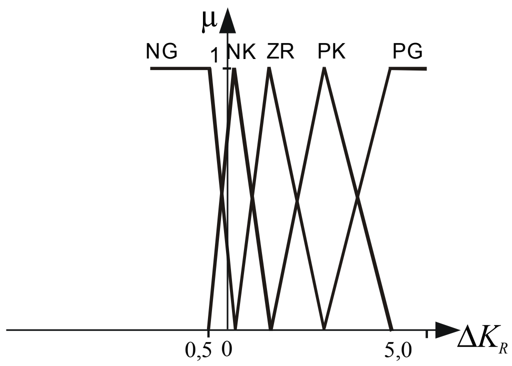

Fig. 2.27: Optimized membership function of set „ΔK_R“ (distribution = 0.3)

Axial AMB

Static loads are caused by the load from the turbomachine rotor mass and aerodynamical axial forces (from turbine and compressors). The axial load amounts +639238 N (signed sum of axial forces due to weight load, turbine, high pressure and low pressure compressor) and was calulated by NRG.

PID controller

Fig. 2.28 shows the amplitude of rotor position and the bearing force vs. the variable controller gain for the axial AMB.
The amplitude decreases with higher controller gain but therefore higher bearing forces are necessary (higher stiffness). In the full range of gain the axial AMB is able to react the static loads.

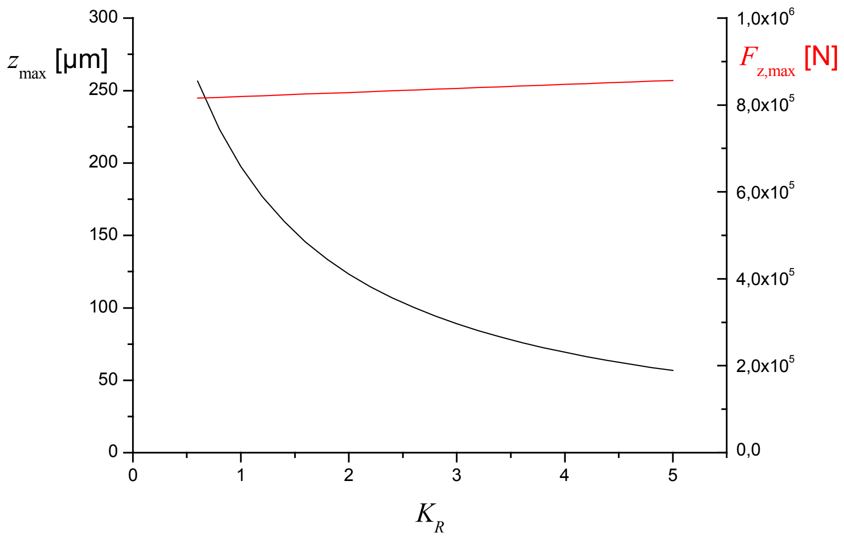

Fig. 2.28: Amplitude of rotor position and bearing force vs. controller gain for axial AMB

Fuzzy controller

Simulation-based optimization with *MLDyn* contains the varying of number of input and output sets resp. distribution of sets. The membership functions are triangular shaped. The tests result in membership functions of all linguistic variables (input and output) with 5 triangular sets (see Fig. 2.3).

Fig. 2.29 shows the amplitude of rotor position and the bearing force vs. the distribution of set „ $\dot{X}$ “ for the axial AMB . To minimize the amplitude and the bearing force the set of „ $\dot{X}$ “ should be compressed at the center. A good compromise is a distribution of 0.7 (see Fig. 2.30). In comparison with the PID controller the amplitude of rotor displacement can be decreased.

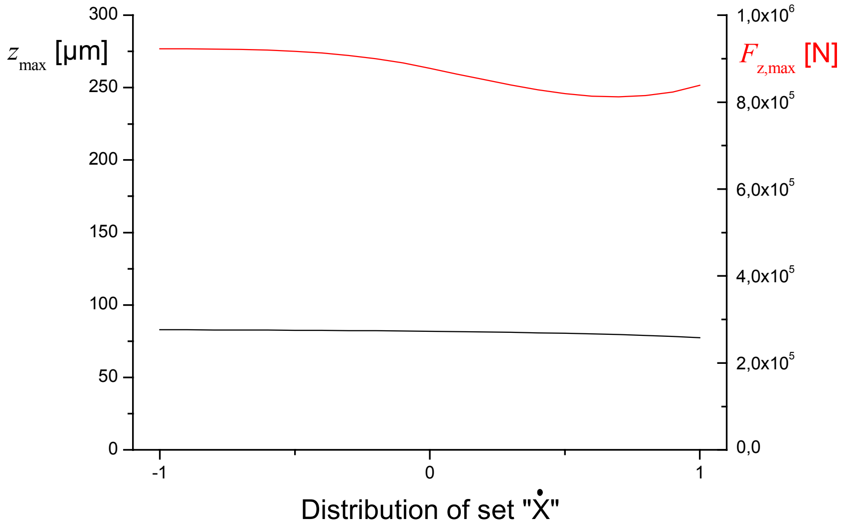

Fig. 2.29: Amplitude of rotor position and bearing force vs. normalized distribution of set „ $\dot{X}$ “ for axial AMB

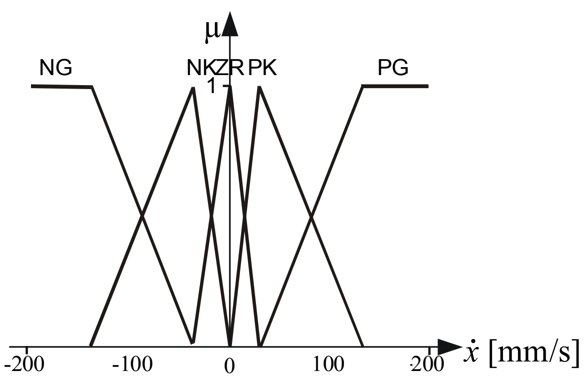

Fig. 2.30: Optimized membership function of set „ $\dot{X}$ “(distribution = 0.7)

Fuzzy gain adaptation

Simulation-based optimization with *MLDyn* contains the varying of number of input and output sets resp. distribution of sets. The membership functions are triangular shaped. The tests result in membership functions of all linguistic variables with 3 triangular sets for both the input variables (N and $\hat{X}$) and 5 sets for the output varible („ΔK_R). The starting value K_{R0} amounts 1.5. The range of ΔK_R is limited from -0.5 to 5.0.

Fig. 2.31 shows the amplitude of rotor position and the bearing force vs. the distribution of set „ΔK_R“ for the axial AMB. The bearing force is nearly undependent on the distribution. To minimize the amplitude the set of „ΔK_R“ should be compressed at the border of definition range (Fig. 2.32). In comparison with the PID controller the amplitude of rotor displacement can be decreased by variation of the fuzzy set.

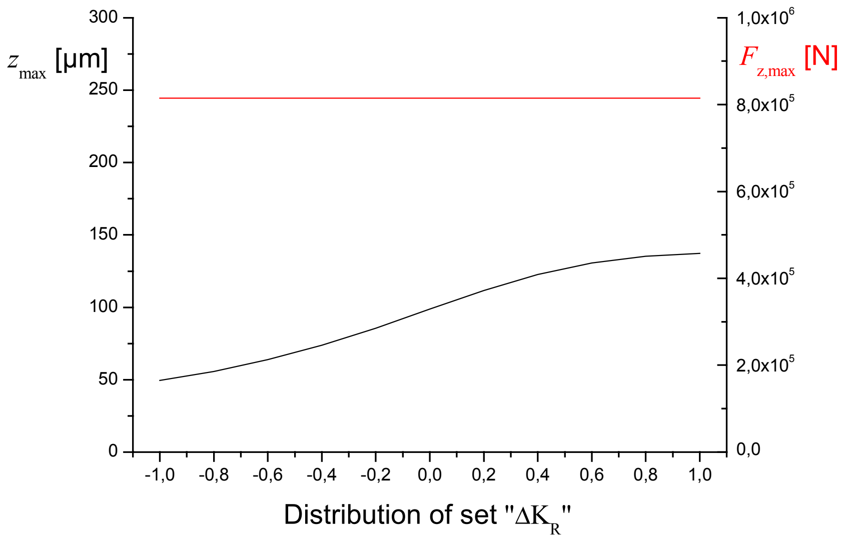

Fig. 2.31: Amplitude of rotor position and bearing force vs. normalized distribution of set „ΔK_R“ for axial AMB

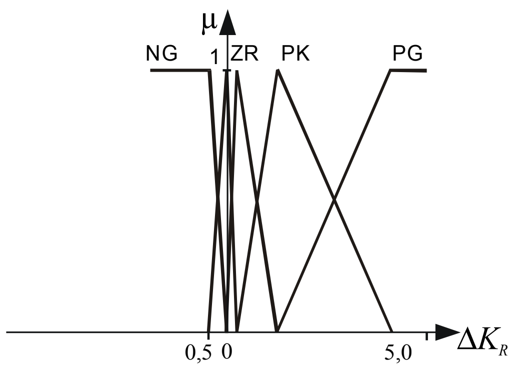

Fig. 2.32: Optimized membership function of set „ΔK_R“ (distribution = -1)

Confidential

2.2.2.4 Dynamic loads – Design on dynamic stiffness (DDS)

Radial AMB's

For the design of the AMB's it is necessary to consider the behavior at dynamic loads acting on the shaft. Based on the static loads an amplitude of the disturbance force of 8500 N is used for the investigation. Additionally the frequency of the load is changed between 0 and 500 Hz to check the range up to tenfold the rotor speed.

PID controller

The controller gain was adjusted between 0.6 and 5.0. Fig. 2.33 shows the bearing force vs. the freqency of the load and the controller gain for radial AMB 2.

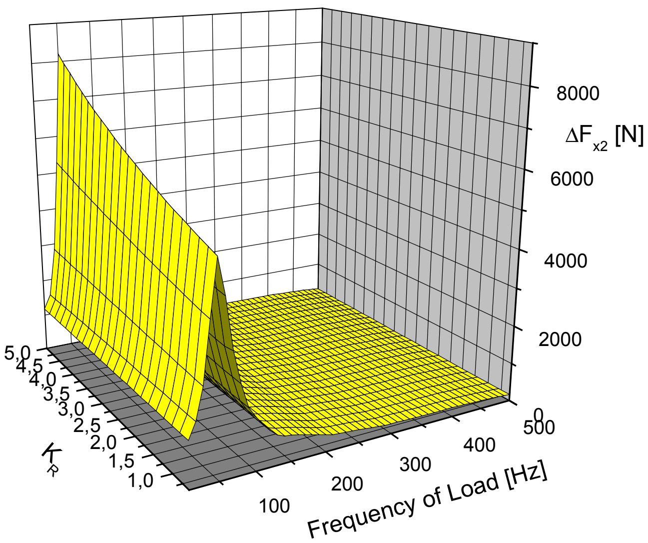

Fig. 2.33: Bearing force vs. freqency of load and controller gain for radial AMB 2

As seen on Fig. 2.33 high forces occur at 50 Hz that corresponds to the nominal speed of 3000 rpm.

The basis for the optimal design is firstly the knowledge about the rotor dynamic behaviour during operation and secondly the specific loads acting on the rotor.
In the design phase the simulation-based method for the AMB **Design regard to the parameter Dynamic Stiffness (DDS)** is applicable to the theoretical proof of the reliability performance of active magnetic bearing systems (see document HTR-E-03/10-D-3-1-2-2). This is based on the Simulation Tool *MLDyn*. Necessary dynamic stiffness S_n is introduced as a criterion for reliability and allowable rotor displacement as a criterion for quality.

To avoid contact with the catcher bearings not more than 80% of radial gap between catcher bearing and rotor are allowed. The allowable rotor displacement X_{al} as quality criterion is assumed with 400 µm.

The design force F_D of both types of radial AMB's is 6*10^4 N (for 6t bearing) resp. 12*10^4 N (for 12t bearing). With a reserve of 10% the maximum force $F_{\max}$ amounts 6.6*10^4 N resp. 13.2*10^4 N.
Then the necessary stiffness S_n amounts **165 N/µm** resp. **330 N/µm**.

Fig. 2.34 shows the stiffness S_d (ω) exemplarily for AMB 2 (12t bearing) which was calculated with the simulation tool *MLDyn*.

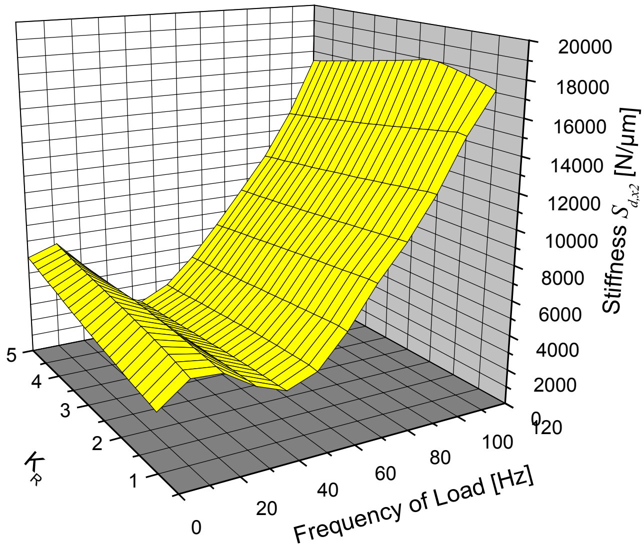

Fig. 2.34: Dynamic stiffness vs. freqency of load and controller gain for radial AMB 2

Resonance frequencies are expected in the range 0-110 Hz (FRA requirements and NRG calcultions), i.e. $\omega_{\max}$ is 110 Hz. The operating frequency ω_{op} is in the range below $\omega_{\max}$.

The minimal operating stiffness $S_{op,min}$ in the range between 0-110Hz amounts 1861 N/µm and is higher then S_n = 330 N/µm.

Therefore the criteria $S_{Op} > S_n$ is fulfilled in the operating range and for all controller gains K_R.

NOTE: The bearing force and the dynamic stiffness for AMB 1...6 can be seen on Annex 3.

Table 2 shows the necessary and the minimum operating stiffness for all radial AMB's. The criteria $S_{Op} > S_n$ is fulfilled for all bearings.

radial AMB	necessary stiffness S_n	minimum operating stiffness $S_{Op,\,min}$
1	165 N/µm	1025 N/µm
2	330 N/µm	1861 N/µm
3	330 N/µm	1627 N/µm
4	165 N/µm	973 N/µm
5	165 N/µm	513 N/µm
6	165 N/µm	456 N/µm

Table 2: Necessary and the minimum operating stiffness for radial AMB's

Fuzzy controller

Simulation-based optimization with *MLDyn* contains the varying of number of input and output sets resp. distribution of sets. The membership functions are triangular shaped. The tests result in membership functions of all linguistic variables (input and output) with 5 triangular sets (see Fig. 2.3).

Fig. 2.35 shows the bearing force vs. the freqency of the load and the distribution of set „$\dot{X}$" for radial AMB 2.

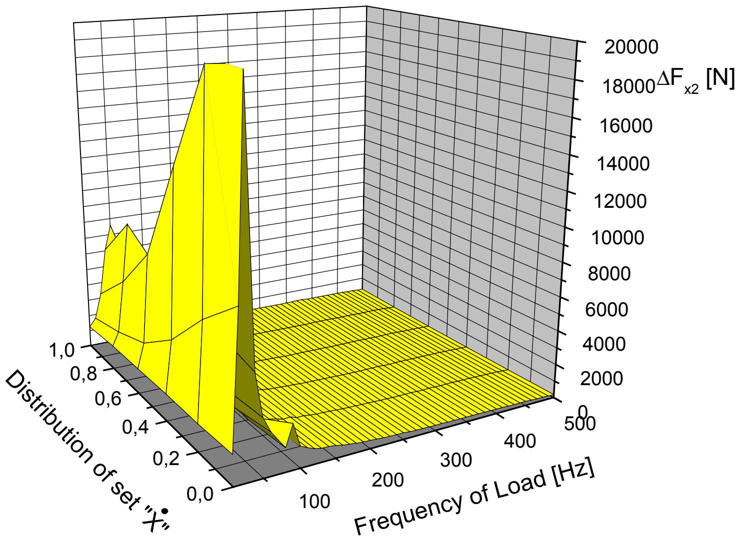

Fig. 2.35: Bearing force vs. freqency of load and normalized distribution of set „$\dot{X}$" for radial AMB 2

As seen on Fig. 2.35 high forces occur at 50 Hz that corresponds to the nominal speed of 3000 rpm.

The necessary stiffness S_n amounts **165 N/µm** resp. **330 N/µm**.

Fig. 2.36 shows the stiffness S_d (ω) exemplarily for AMB 2 (12t bearing) which was calculated with the simulation tool *MLDyn*.

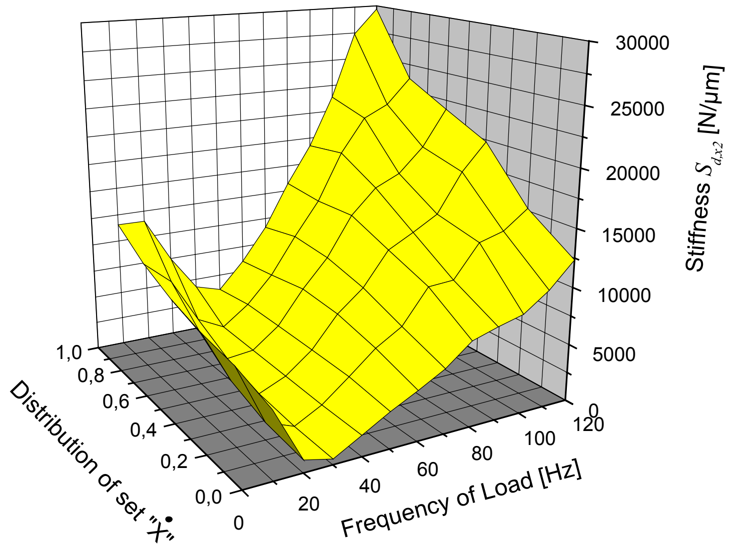

Fig. 2.36: Dynamic stiffness vs. freqency of load and normalized distribution of set „$\dot{X}$" for radial AMB 2

Resonance frequencies are expected in the range 0-110 Hz (FRA requirements and NRG calcultions), i.e. ω_{max} is 110 Hz. The operating frequency ω_{op} is in the range below ω_{max}.

The minimal operating stiffness $S_{op,min}$ in the range between 0-110 Hz amounts 481 N/µm and is higher then S_n = 330 N/µm. To increase the operating stiffness the set of „$\dot{X}$" should be compressed at the center of the definition range. Then $S_{op,min}$ is 3540 N/µm.

Therefore the criteria $\boldsymbol{S_{Op} > S_n}$ is fulfilled in the operating range and for the distribution of set „$\dot{X}$" between 0...1.

NOTE: The bearing force and the dynamic stiffness for AMB 1...6 can be seen on Annex 1.

Table 3 shows the necessary and the minimum operating stiffness for all radial AMB's. The criteria $\boldsymbol{S_{Op} > S_n}$ is fulfilled for all bearings. In comparison with the PID controller the minimum operating stiffness can be increased.

radial AMB	**necessary stiffness S_n**	**minimum operating stiffness $S_{Op,\,min}$** (set „$\dot{X}$" compressed at the center)
1	165 N/µm	1926 N/µm
2	330 N/µm	3540 N/µm
3	330 N/µm	4371 N/µm
4	165 N/µm	2182 N/µm
5	165 N/µm	1029 N/µm
6	165 N/µm	904 N/µm

Table 3: Necessary and the minimum operating stiffness for radial AMB's

Fuzzy gain adaptation

Simulation-based optimization with *MLDyn* contains the varying of number of input and output sets resp. distribution of sets. The membership functions are triangular shaped. The tests result in membership functions of all linguistic variables with 3 triangular sets for both the input variables (N and $\hat{X}$) and 5 sets for the output varible („ΔK_R). The starting value K_{R0} amounts 1.5. The range of ΔK_R is limited from -0.5 to 5.0.

Fig. 2.37 shows the bearing force vs. the freqency of the load and the distribution of set „ΔK_R" for radial AMB 2.

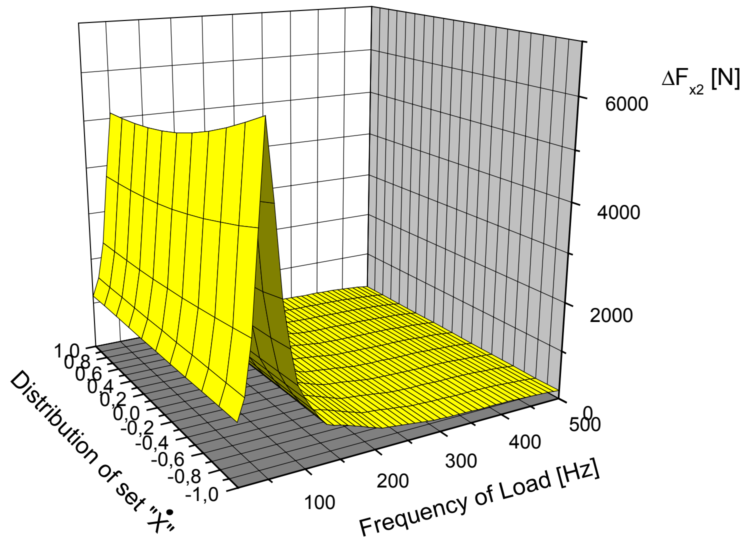

Fig. 2.37: Bearing force vs. freqency of load and normalized distribution of set „ΔK_R" for radial AMB 2

As seen on Fig. 10 high forces occur at 50 Hz that corresponds to the nominal speed of 3000 rpm.

The necessary stiffness S_n amounts **165 N/µm** resp. **330 N/µm**.

Fig. 2.38 shows the stiffness S_d (ω) exemplarily for AMB 2 (12t bearing) which was calculated with the simulation tool *MLDyn*.

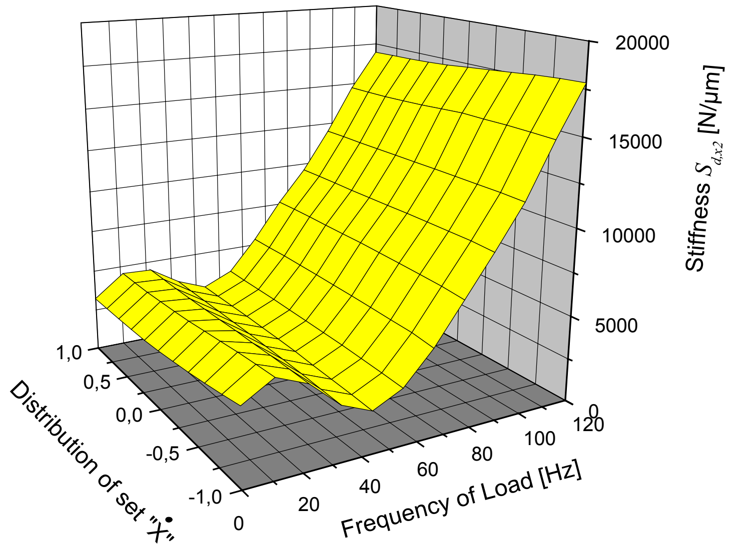

Fig. 2.38: Dynamic stiffness vs. freqency of load and normalized distribution of set „ΔK_R" for radial AMB 2

Resonance frequencies are expected in the range 0-110 Hz (FRA requirements and NRG calcultions), i.e. ω_{max} is 110 Hz. The operating frequency ω_{op} is in the range below ω_{max}.

The minimal operating stiffness $S_{op,min}$ in the range between 0-110 Hz amounts 2378 N/µm and is higher then S_n = 330 N/µm. To increase the operating stiffness the set of „ΔK_R" should be compressed at the border of the definition range. Then $S_{op,min}$ is 2718 N/µm.

Therefore the criteria $\boldsymbol{S_{Op} > S_n}$ is fulfilled in the operating range and for the distribution of set „ΔK_R" between -1...1.

NOTE: The bearing force and the dynamic stiffness for AMB 1...6 can be seen on Annex 1.

Table 4 shows the necessary and the minimum operating stiffness for all radial AMB's. The criteria $S_{Op} > S_n$ is fulfilled for all bearings. In comparison with the PID controller the minimum operating stiffness can be increased.

radial AMB	**necessary stiffness S_n**	**minimum operating stiffness $S_{Op,\ min}$** (set „ΔK_R" compressed at the border)
1	165 N/µm	1355 N/µm
2	330 N/µm	2718 N/µm
3	330 N/µm	1699 N/µm
4	165 N/µm	963 N/µm
5	165 N/µm	507 N/µm
6	165 N/µm	451 N/µm

Table 4: Necessary and the minimum operating stiffness for radial AMB's

Axial AMB

The axial load depends on the aerodynamical forces in the range 0-60 Hz regarding the rotational speed 0-3600 rpm (NRG calculation).

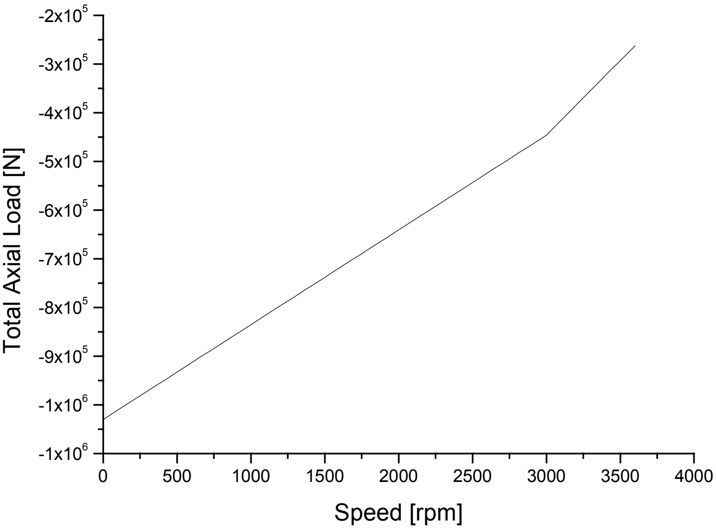

Fig. 2.39: Total axial load vs. rotational speed (NRG calculation)

PID controller

The controller gain is changed between 0.5 and 5.0. Fig. 2.40 shows the bearing force vs. the freqency of the load and the controller gain for the axial AMB.

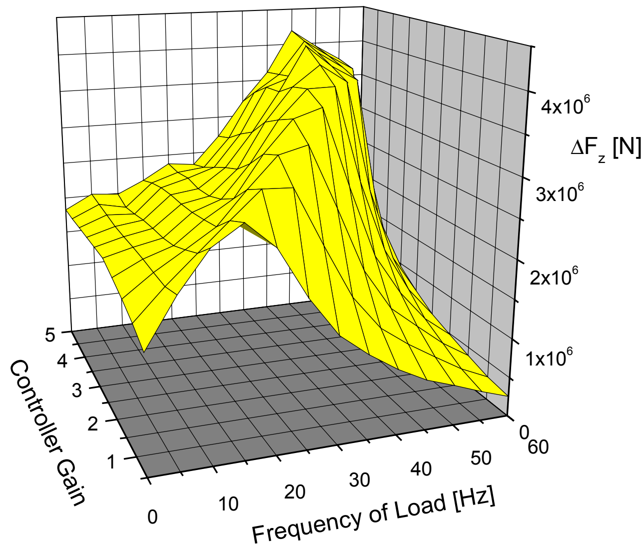

Fig. 2.40: Bearing force vs. freqency of load and controller gain for axial AMB

As seen on Fig. 2.40 high forces occur between 20 to 50 Hz depending on the controller gain. For minimal bearing forces a small gain should be used.

For the DDS-Method the allowable rotor displacement X_{al} must be fixed. Using 80% of axial gap between catcher bearing and rotor disk X_{al} amounts 400 µm.

The design force F_D of axial AMB is 2x1.090 $*10^6$N. With a reserve of 10% the maximum force $F_{\max}$ amounts $2.398*10^6$ N.

Then the necessary stiffness S_n amounts **5995 N/µm**.

Fig. 2.41 shows the stiffness S_d (ω) for the axial AMB which was calculated with the simulation tool *MLDyn*.

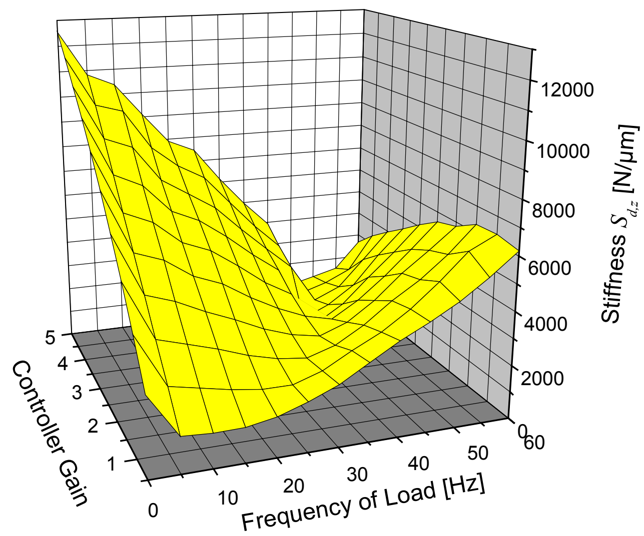

Fig. 2.41: Dynamic stiffness vs. freqency of load and controller gain for axial AMB

Resonance frequencies are expected in the range 0-60 Hz (FRA requirements and NRG calcultions), i.e. $\omega_{\max}$ is 60 Hz. The operating frequency ω_{op} is in the range below $\omega_{\max}$.

The minimal operating stiffness $S_{op,min}$ in the range between 0-60Hz amounts 1011N/µm and is **lower** then S_n = 5995 N/µm.

Therefore the criteria $\boldsymbol{S_{Op} > S_n}$ is **not fulfilled** in the operating range. For controller gains K_R in the investigated range the neccessary stiffness is not obtained.

By using the PID controller the axial AMB needs to be further optimized regarding the time constants of the coils (inductivity) to meet the criteria of the DDS method. A way to decrease the time constants can be the development and usage of more powerful power amplifiers (higher closed loop voltage).

Fuzzy controller

Simulation-based optimization with *MLDyn* contains the varying of number of input and output sets resp. distribution of sets. The membership functions are triangular shaped. The tests result in membership functions of all linguistic variables (input and output) with 5 triangular sets (see Fig. 2.3).

Fig. 2.42 shows the bearing force vs. the freqency of the load and the distribution of set „ $\dot{X}$ “ for the axial AMB.

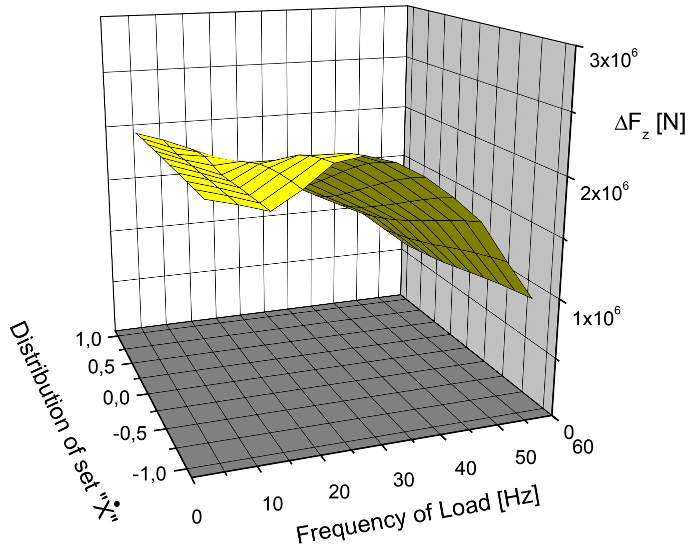

Fig. 2.42: Bearing force vs. freqency of load and normalized distribution of set „ $\dot{X}$ “ for axial AMB

As seen on Fig. 14 higher forces occur between 0 to 30 Hz depending on the distribution of set „ $\dot{X}$ “. For minimal bearing forces the set should be compressed at the center.

For the DDS-Method the allowable rotor displacement X_{al} must be fixed. Using 80% of axial gap between catcher bearing and rotor disk X_{al} amounts 400 µm.

The design force F_D of axial AMB is 2x1.090 *10^6N. With a reserve of 10% the maximum force $F_{\max}$ amounts 2.398*10^6 N.

Then the necessary stiffness S_n amounts **5995 N/µm**.

Fig. 2.43 shows the stiffness S_d (ω) for the axial AMB which was calculated with the simulation tool *MLDyn*.

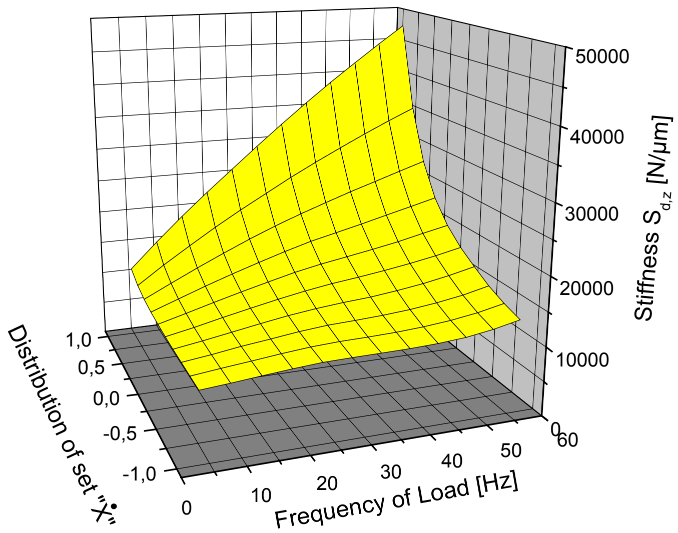

Fig. 2.43: Dynamic stiffness vs. freqency of load and normalized distribution of set „$\dot{X}$“ for axial AMB

Resonance frequencies are expected in the range 0-60 Hz (FRA requirements and NRG calcultions), i.e. ω_{max} is 60 Hz. The operating frequency ω_{op} is in the range below ω_{max}.

The minimal operating stiffness $S_{op,min}$ in the range between 0-60Hz amounts 7895 N/µm and is **higher** then S_n = 5995 N/µm.

Therefore the criteria $\boldsymbol{S_{Op} > S_n}$ is **fulfilled** in the operating range and for the whole distribution of the set „$\dot{X}$“ by using the fuzzy controller. Maximum stiffness can be reached if the set is compressed at the center of definition range.

Fuzzy gain adaptation

Simulation-based optimization with *MLDyn* contains the varying of number of input and output sets resp. distribution of sets. The membership functions are triangular shaped. The tests result in membership functions of all linguistic variables with 3 triangular sets for both the input variables (N and $\hat{X}$) and 5 sets for the output varible („ΔK_R). The starting value K_{R0} amounts 1.5. The range of ΔK_R is limited from -0.5 to 5.0.

Fig. 2.44 shows the bearing force vs. the freqency of the load and the distribution of set „ΔK_R“ for the axial AMB.

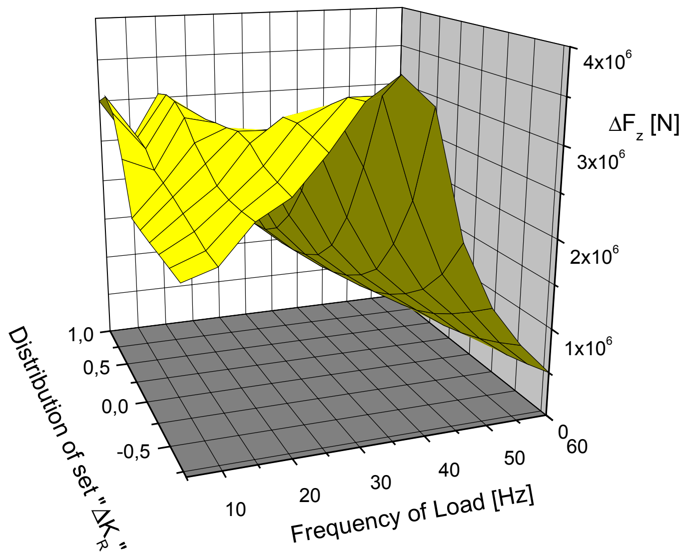

Fig. 2.44: Bearing force vs. freqency of load and normalized distribution of set „ΔK_R“ for axial AMB

As seen on Fig. 2.44 higher forces occur between 0 to 30 Hz depending on the distribution of set „ΔK_R“. For minimal bearing forces the set should be compressed at the center.

For the DDS-Method the allowable rotor displacement X_{al} must be fixed. Using 80% of axial gap between catcher bearing and rotor disk X_{al} amounts 400 µm.

The design force F_D of axial AMB is 2x1.090 *10^{6}N. With a reserve of 10% the maximum force $F_{\max}$ amounts 2.398*10^6 N.

Then the necessary stiffness S_n amounts **5995 N/µm**.

Fig. 2.45 shows the stiffness S_d (ω) for the axial AMB which was calculated with the simulation tool *MLDyn*.

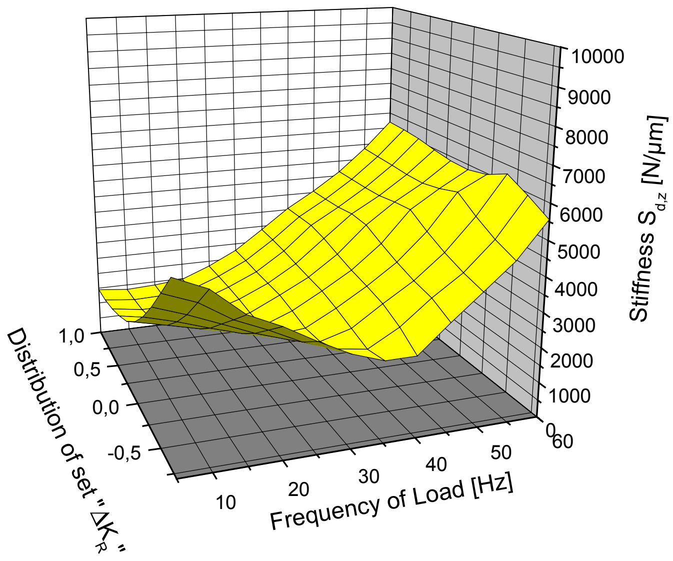

Fig. 2.45: Dynamic stiffness vs. freqency of load and normalized distribution of set „ΔK_R“ for axial AMB

Resonance frequencies are expected in the range 0-60 Hz (FRA requirements and NRG calcultions), i.e. ω_{max} is 60 Hz. The operating frequency ω_{op} is in the range below ω_{max}.

The minimal operating stiffness $S_{op,min}$ in the range between 0-60Hz amounts 1351 N/µm and is **lower** then S_n = 5995 N/µm. It is higher than by using the PID controller with fixed parameters but not sufficient.

Therefore the criteria $\boldsymbol{S_{Op} > S_n}$ is **not fulfilled** in the operating range and for the whole distribution of the set „ΔK_R“ by using the fuzzy gain adaptation of the PID controller.

Here similar conclusions can be made like using the PID controller with fixed parameters.

2.3 Conclusion

With help of the simulation tool *MLDyn* tests of the controller algorithms
- PID controller
- Fuzzy logic controller
- Fuzzy gain adaptation of PID controller

were performed at:
- start up (rotor lift-up)
- speed levels and unbalance loads (sinusoidal disturbance)
- static loads
- dynamic loads (dynamic stiffness)

At the optimization process the parameters of the used controllers were adapted with help of simulation calculations. For evaluation of the different control algorithms the quality criteria (see Table 1) were used. Aim of the optimization is the minimization of these criteria primarily the main criteria.

Table 5 and 6 show an overview about the results of the different tests and the optimized controllers. In comparison with the PID controller the behavior of the AMB control loop can be improved by using the nonlinear fuzzy controller or the fuzzy gain adaptation of the PID controller.

Radial AMB's			
Tests/ Controller	**PID controller**	**Fuzzy controller**	**Fuzzy gain adaptation of PID controller**
Start up	- increased gain → minimal overshoot, - radial AMB's able to start rotor	- 5 triangular sets for input and output, - optimized distribution of set „ $\dot{X}$ at the center of definition range → minimal overshoot, - radial AMB's able to start rotor	- 3 triangular sets for input and 5 triangular sets for output, - optimized distribution of set „ΔK_R at the border of definition range→ most minimal overshoot - starting value K_{R0}=1.5 - radial AMB's able to start rotor
Speed and unbalances	- increased amplitudes and bearing forces at nominal speed (3000 rpm), - radial AMB's able to react the loads up to full speed (3600 rpm), - minimal displacement achievable with small gain	- increased amplitudes and bearing forces at nominal speed (3000 rpm), - radial AMB's able to react the loads up to full speed (3600 rpm), - minimal displacement achievable with distribution of set „ $\dot{X}$ at the center of definition range	- linear dependency of amplitude from speed - radial AMB's able to react the loads up to full speed (3600 rpm), - no influence of distribution of set „ΔK_R" - most minimal displacement achievable
Static loads	- amplitude decreases with higher controller gain, but higher bearing forces necessary (higher stiffness), - radial AMB's able to react the static loads	- smaller amplitudes if set of „ $\dot{X}$ " is compressed at the center, - radial AMB's able to react the static loads	- smallest amplitudes but highest bearing forces, - radial AMB's able to react the static loads
Dynamic loads	- high bearing forces at 50 Hz - DDS method: criteria fulfilled (operating stiffness>necessary stiffness)	- high bearing forces at 50 Hz - DDS method: criteria fulfilled (operating stiffness>necessary stiffness) - highest operating stiffness (if set of „ $\dot{X}$ " is compressed at the center)	- high bearing forces at 50 Hz - DDS method: criteria fulfilled (operating stiffness>necessary stiffness)

Table 5: Results of the tests with used AMB control algorithms

Axial AMB			
Tests/ Controller	**PID controller**	**Fuzzy controller**	**Fuzzy gain adaptation of PID controller**
Start up	- no overshoot, - settling time maximum at controller gain=1.5, - gain > 1.5 → decreased settling time, - axial AMB able to start up rotor	- 5 triangular sets for input and output, - optimized distribution of set „ $\dot{X}$ at the center of definition range → minimal settling time, - axial AMB able to start up rotor	- 3 triangular sets for input and 5 triangular sets for output, - optimized distribution of set „ΔK_R“ at the border of definition range→ most minimal settling time - starting value K_{R0}=1.5 - range of ΔK_R limited -0.5-5,0 - axial AMB able to start up rotor
Static loads	- amplitude decreases with higher controller gain, but higher bearing forces necessary (higher stiffness), - axial AMB able to react the static loads	- smaller amplitudes, - optimized distribution of set „ $\dot{X}$ at the center of definition range, - axial AMB able to react the static loads	- smallest amplitudes, - optimized distribution of set „ΔK_R“ at the border of definition range, - axial AMB able to react the static loads
Dynamic loads	- high bearing forces at 50 Hz - DDS method: criteria **not fulfilled** (operating stiffness<necessary stiffness)	- smallest forces - highest stiffness - DDS method: criteria **fulfilled** (operating stiffness>necessary stiffness)	- high bearing forces at 40 Hz - higher stiffness - DDS method: criteria **not** fulfilled (operating stiffness>necessary stiffness)

Table 6: Results of the tests with used AMB control algorithms

3. AMB diagnostics
3.1 Diagnosis process

The principal of the diagnosis process is shown in Fig. 3.1 [1].

The data acquisition delivers measurement values from the technical process. In the feature extraction section features are calculated from the variety of the single measurement values. It is assumed that changes in the process (faults) are represented by changes in the magnitudes of the features.

In the feature extraction there are signal-based and model-based concepts applicable. Signal-based concepts use methods of signal analysis. Model-based concepts use analytical or knowledge-based redundancy of the system to generate features which are hardly accessible by mere measurement.

The extracted actual values of the feature are monitored on exceeding of limits and trends, the exceeding of a limit characterizes the occurrence of a fault.

In the process of fault diagnosis information about the cause, size, location and consequences of the fault are generated. If possible the necessary counter action (therapy) is to decide.

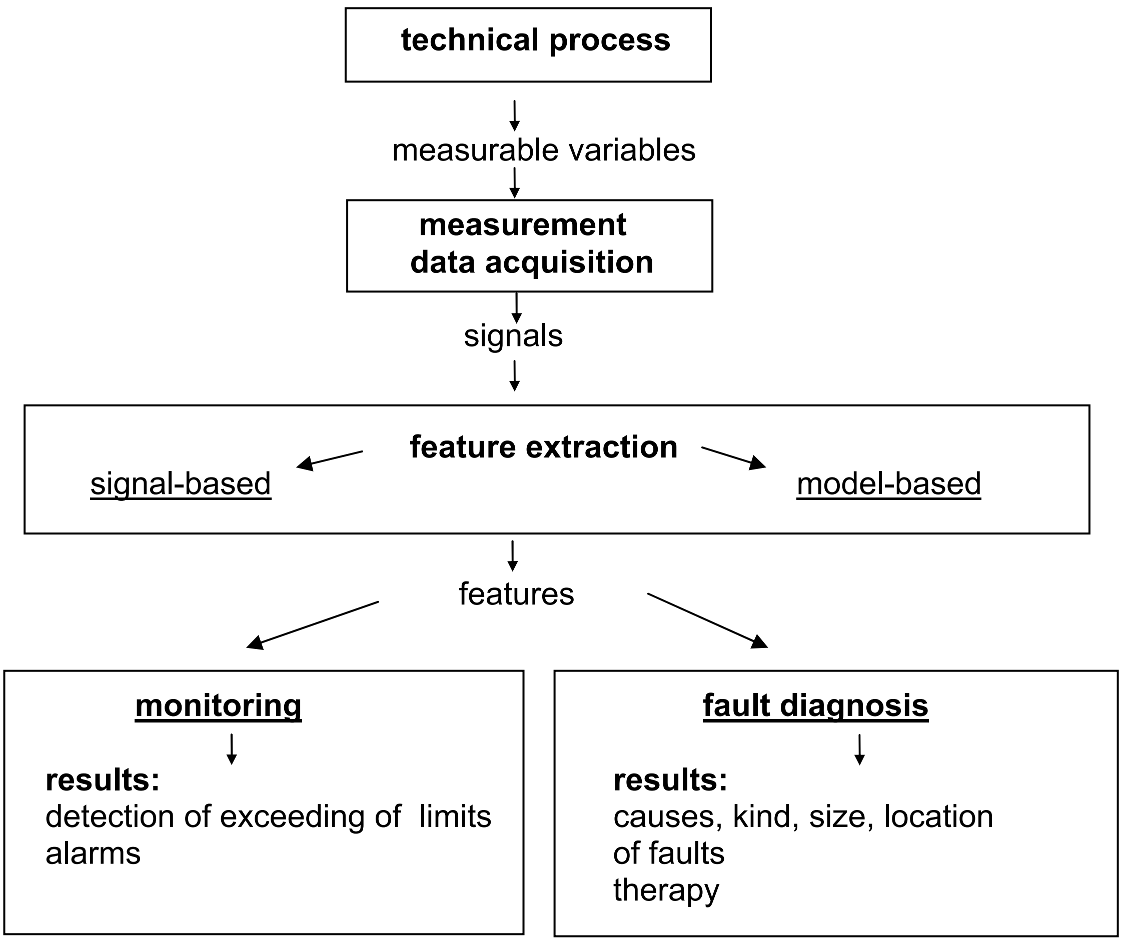

Fig 3.1: Principle of the diagnosis process

Based on this diagnosis process the realisation of the diagnosis concept was carried out in the steps:

1. Analysis of the available signals
2. Analysis and selection of feature extraction methods
3. Analysis of typical faults at components of rotating machine system with AMB
4. Acquisition of a knowledgebase by simulation and experiment
5. Development, testing and verification of knowledge-based models for the fault diagnosis
6. Technical realisation on an Windows-PC

3.2 Available signals and feature extraction

At the AMB machine the following **signals** are available:

- the shaft position signals s (shaft displacement)
- the actuating signals *u* (controller output)
- the actuating currents (coil currents) i_+ *and* i_- through the magnetic coils (for each direction two electromagnets are fixed opposite each other as positive and negative coils)

in

- *x*- und *y*-direction of the different level radial bearings
- *z*-direction (axial bearing)

The control current i_s per axis were calculated by

$$i_s = (i_+ - i_-)/2. \tag{3.1}$$

The pre-magnetization currents of the coil systems were calculated with the equation

$$Io = (i_+ + i_-)/2. \tag{3.2}$$

The produced magnetic force on the shaft depends on the shaft displacement and the coil currents and were calculated by

$$F = k_1 \cdot \left(\frac{i^2_+}{(k_2 + 2(s_{nom} - s))^2} - \frac{i^2_-}{(k_2 + 2(s_{nom} + s))^2} \right). \tag{3.3}$$

with:

F	force per direction	i_+, i_-	coil currents
s_n	nominal air gap	s	shaft displacement
k	physical constants		

Combining the x-and y-signals of the different level radial bearings the phase angle φ and magnitude r of the signal vectors of each level were calculated

$$rq = \sqrt{q\_x^2 + q\_y^2} \tag{3.4}$$

$$\varphi q = \arctan(\frac{q\_y}{q\_y}) \tag{3.5}$$

Features have been extracted from this signals by means of signal- and model-based methods.

Utilizing **signal-based methods** the following features are available:

- (arithmetic) mean value $\overline{q} = \frac{1}{N}\sum_{i=1}^{N} q_i$ (3.6)
- root mean square (rms) $\tilde{q} = \sqrt{\frac{1}{N}\sum_{i=1}^{N}(q_i - \overline{q})^2}$ (3.7)
- maximum peak value $q_{max} = MAX\,(q(t))$ (3.8)
- minimum peak value $q_{min} = MIN\,(q(t))$ (3.9)
- peak-to-peak value $q_{sp} = q_{max} - q_{min}$ (3.10)

- probability distribution $P(q)$ and probability density $p(q)$
- auto correlation function $R(qq)$ and cross correlation function $R(qr)$
- amplitude spectrum and characteristic frequencies *a_fft(q)*, *f_fft(q)*

This primary features were used to generate additional combined features:

- Ratio R between the rms values of shaft displacement and the according actuating signal

  $$R = \frac{\tilde{s}}{\tilde{u}} \tag{3.11}$$

- Ratio A between the rms values of the actuating signal and the according coil current

  $$A = \frac{\tilde{u}}{\tilde{i}} \tag{3.12}$$

- Ratio V between the rms values of the opposing coil currents

  $$V = \frac{\tilde{i}_+}{\tilde{i}_-} \tag{3.13}$$

- Ratio W between the rms values of the positive coil current and the according shaft displacement

  $$W = \frac{\tilde{i}_+}{\tilde{s}} \tag{3.14}$$

- Phase difference $\Delta\varphi$ between the phase angles φ_{max} of the maximum signal vectors of the different level radial bearings

In order to detect changes in the parameters of the controllers and the actuators (power amplifier and coils) **model-based methods** of parameter estimation were applied [2]. The data acquisition was carried out in discrete time intervals. For the parameter estimation the time discrete transfer function of the subsystem

$$G(z) = \frac{Y(z)}{X(z)} = \frac{a_0 + a_1 z^{-1} + \ldots + a_n z^{-n}}{1 + b_1 z^{-1} + \ldots + b_n z^{-n}} \tag{3.15}$$

was transformed into the difference equation [3]

$$y(k) + c_1 y(k-1) + \ldots + c_n y(k-n) = d_0 x(k) + d_1 x(k-1) + \ldots + d_n x(k-n) \tag{3.16}$$

y(*k-n*) ... output signals *x*(*k-n*) ... input signals
c_n, d_n ... parameters

With the measured input signals x(m) and output signals y(m) as well as the errors e(m) between the model output and the output of the real system using the vector of the input signals $\underline{y}^T$

$$\underline{y}^{T} = y(k) + y(k+1) + \ldots + y(k+M-1)\,, \tag{3.17}$$

the measurement matrix of the input and output signals $\underline{\Psi}$

$$\underline{\Psi} = \begin{bmatrix} -y(k-1) & \ldots -y(k-n) & x(k) & \ldots x(k-n) \\ -y(k) & \ldots -y(k-n+1) & x(k+1) & \ldots x(k-n+1) \\ \ldots & & \ldots & \\ -y(k+M-2) & \ldots -y(k-n+M-2) & x(k+M-1) & \ldots x(k-n+M-1) \end{bmatrix}, \tag{3.18}$$

the parameter vector $\underline{\Theta}^{T}$

$$\underline{\Theta}^{T} = \left[c_1 \ldots c_n \quad d_0 \ldots d_n\right], \tag{3.19}$$

and the error vector $\underline{e}^T$

$$\underline{e}^{T} = \left[e(k) \quad e(k+1) \quad \ldots \quad e(k+M-1)\right] \tag{3.20}$$

the over-determined linear equation system was created

$$\underline{y} = \underline{\Psi} \cdot \underline{\Theta} + \underline{e}\,. \tag{3.21}$$

Minimizing the quadratic error $\underline{e}^{T} \cdot \underline{e}$ by utilizing the Least-Square-Method the parameter vector $\underline{\Theta}$ of the current parameters of the system can be calculated from equation (3.21) with

$$\underline{\Theta} = \left[\underline{\Psi}^{T} \cdot \underline{\Psi}\right]^{-1} \cdot \underline{\Psi}^{T} \cdot \underline{y}\,. \tag{3.22}$$

3.3 Acquisition of a knowledgebase by simulation and experiment

The usability of the selected signals and features and the typical behaviour of the features by normal operation and by operation with faults have been investigated by simulation and experiment. The results were accumulated in a knowledgebase which serves as basis for the monitoring and the fault diagnosis.

The following faults and effects were analyzed:

- the spectra of the signals
- rotor speed dependence of the features
- changes of controller parameters
- offset errors and gain errors of sensors and actuators
- displacement of the sensors and bearings
- changing of the nominal air gap
- radial forces and unbalances
- disturbances caused by the electric drive
- rotating of the shaft in the retainer bearings

Simulations were performed with the simulation system *MLDyn*. This system consists of a module with the mathematical model of the rotor and modules with models of the sensors, controllers and actuators. All module parameters can be adapted to different AMB systems. For experiments the test facility FLP 500 [4] was used. The FLP 500 is a 240 kW asynchronous machine with a vertical rotor. The rotor has a weight of 1.3 t and is fully magnetically levitated. The maximum speed of the rotor is 7200 rpm.

Exemplarily the following results of simulations and experiments are presented.

Spectra of the signals

The spectra were sampled with a frequency of 160 kHz. The characteristic frequencies of the spectra give information about the function of the power amplifiers, the sensors and disturbance signals.

Fig. 3.2 shows the amplitude spectrum of a coil current signal. Characteristic frequencies are the switching frequency of the power amplifier (17 kHz) and its harmonics. Changes of the switching frequency (e. g. frequency drift, deformation of the puls signal) can by detected with the spectrum analysis.

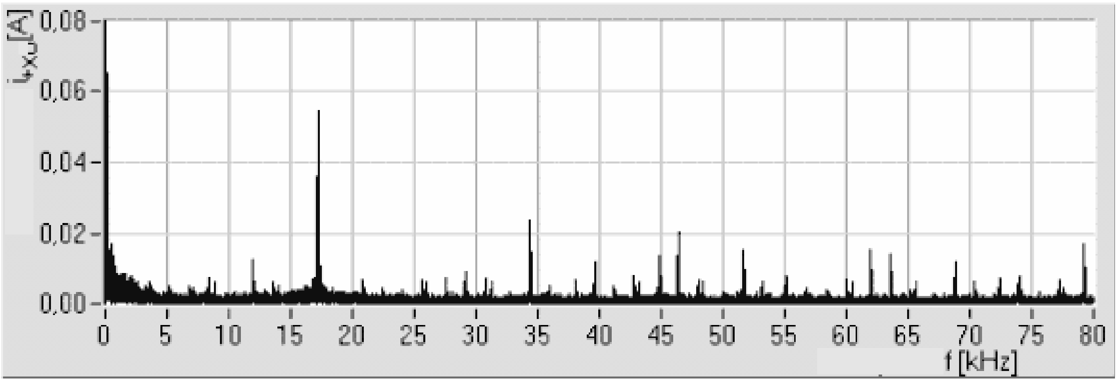

Fig. 3.2: Amplitude spectrum of the coil current i_{+xu}

Reference values and speed dependence of the features

In order to detect deviations from the normal state the magnitudes of the signals and features in this state (reference values) and the dependence of this feature from the rotor speed have been analysed at the FLP 500.

The rms values show an increase of the magnitudes to an maximum of 12 µm (shaft displacement in Fig. 3.3) respectively 900 mV (controller output in Fig. 3.4) at a critical rotor speed of 2200 rpm. Regarding the disturbance signals of about +-5 µm respectively +- 100 mV and the existing remaining unbalances of the rotor this speed dependencies are not significant.

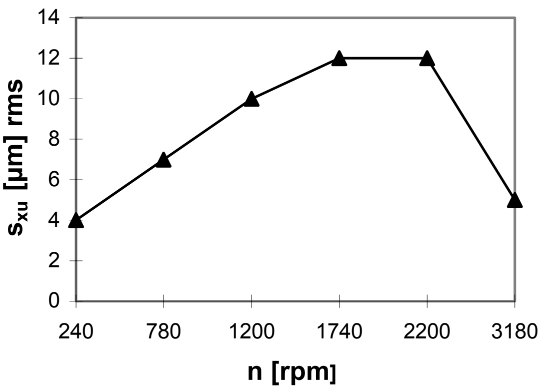

Fig. 3.3: Shaft displacement s_{xu}, (rms) by varying auf n

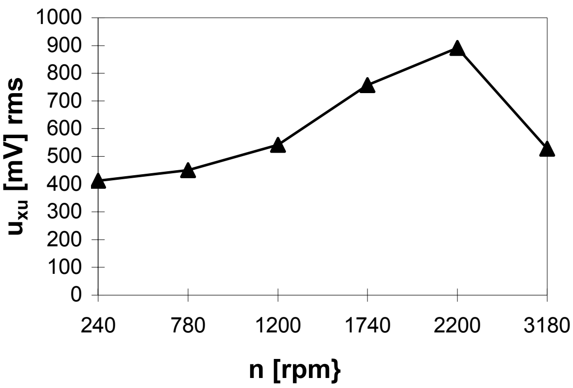

Fig. 3.4: Controller output u_{xu} (rms) by varying of n

Influence of parameters of the controller and power amplifier

With the simulation tool *MLDyn* the influence of the changing of controller parameters on the features has been analyzed. Fig. 3.5 and Fig. 3.6 show the influence of the controller gain K_R and the pre-magnetization current *Io* of the power amplifier on the rms values of the shaft displacement. The reference setting of K_R is 1,3 and of *Io* is 12 A. Simulation has been done with an increasing of *Io* to 15 A and 20 A and varying of K_R to 0,8 and 1,8. The main effect is an increase of the critical speed by increasing of K_R. Increasing *Io* results in an increased magnitude of the rms values. This increase has to be respected at the process of limit value checking and in development of the diagnoses models.

This simulation results have been verified with experiments.

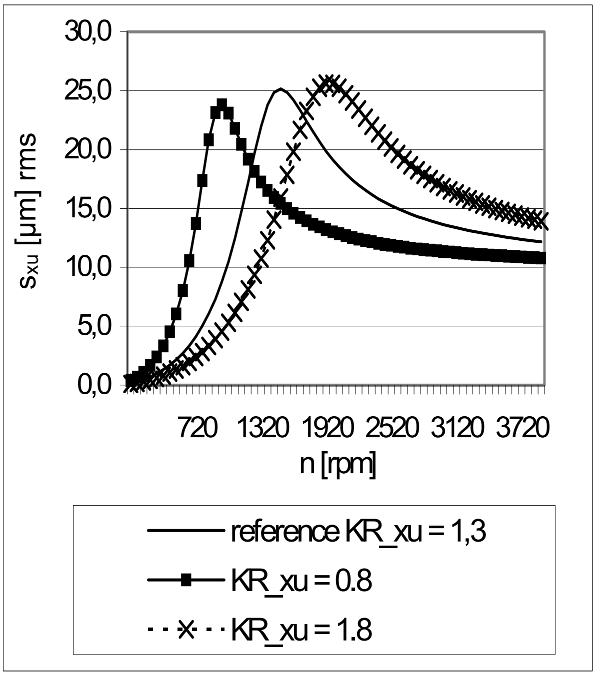

Fig. 3.5: Shaft displacement s_{xu} (rms) by varying of K_R

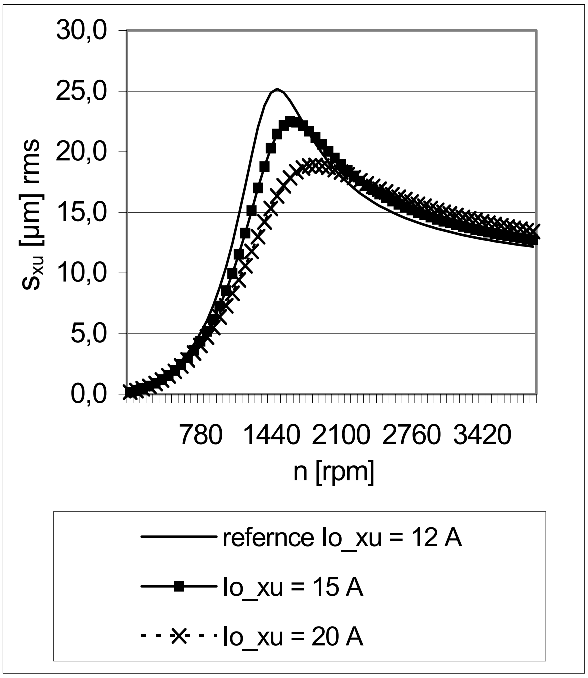

Fig. 3.6: Shaft displacement s_{xu} (rms) by varying of I_0

It can be seen that the setting of the controller parameters has a significant influence of the behaviour of the whole system. To identify the actual parameters the use of model-based parameter estimation methods has been analyzed.

Detection of parameter changes in the AMB control loop by use of parameter estimation methods

Investigations on the application of parameter estimation methods were carried out at the components controller and power amplifier.

The behaviour versus time of the estimated parameters of the PID-controller shows Figure 3.7. The simulated fault (changing of the system parameter) occurs at t = 100 ms. The fault is clearly recognizable in the change of the estimated parameters d_0, d_1 and d_2 (equation 3.19).

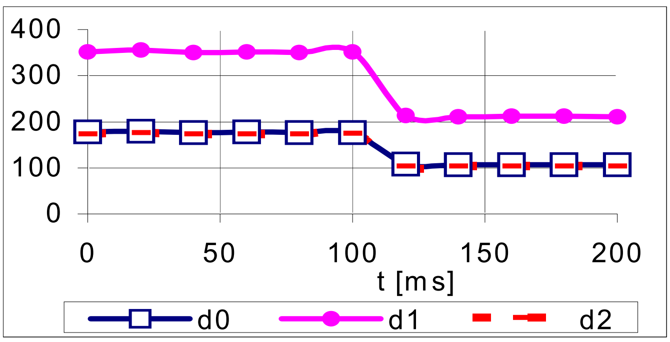

Fig. 3.7: Estimated parameters of the PID-controller

Effects of sensor errors (offset error)

Fig. 3.8 and 3.9 show the shaft displacement s_{xu} and the coil current i_{-xu} versus time when a sensor offset occurs at t = 0,18 s. Characteristic features of this fault are the continuously altered mean values of the coil currents, the mean value of the shaft displacement and the peak values of displacement and current right after the occurrence of the fault.

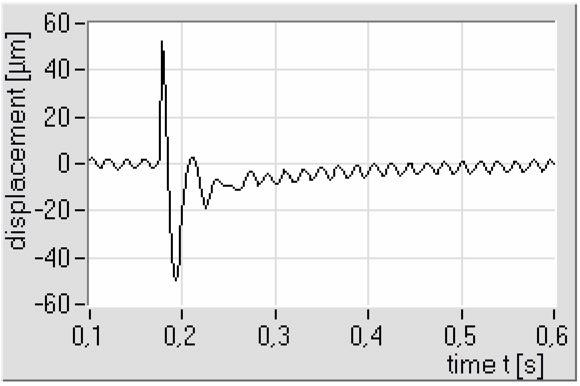

Fig. 3.8: Shaft displacement s_{xu} at sensor offset

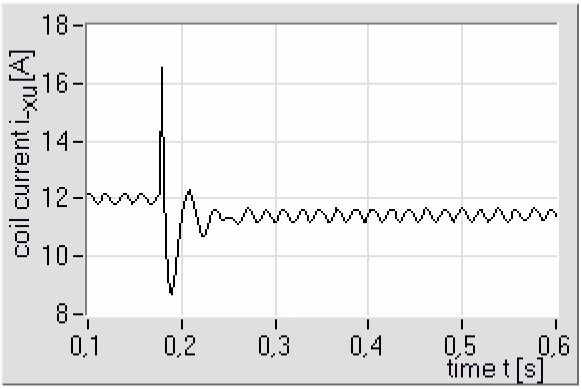

Fig 3.9.: Coil current i_{-xu} at sensor offset

Influence of radial disturbance forces

The influence of static radial forces on the extracted features is shown in Figure 3.10. The radial force is acting in *y*-direction beginning from *t* = 1.6 s.

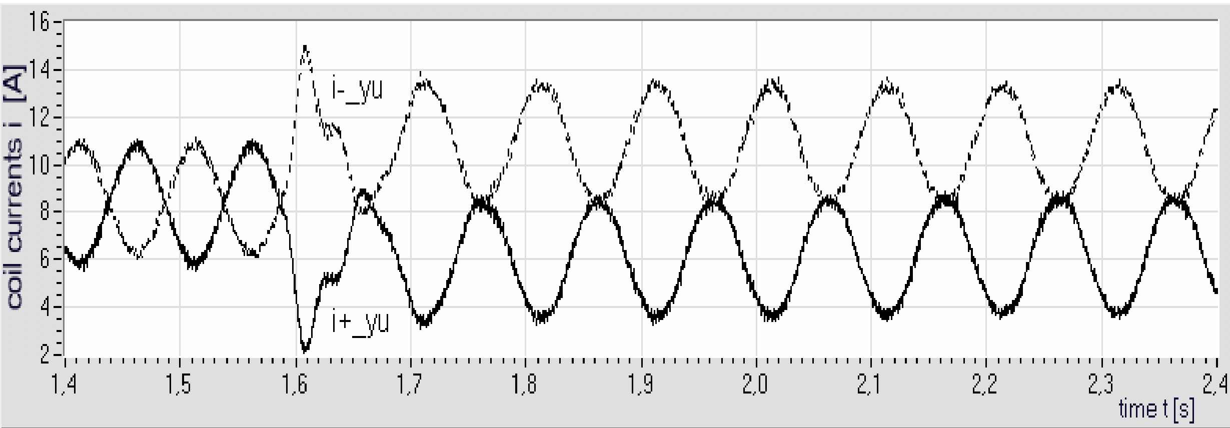

Fig. 3.10: Coil currents i_{+yu} and i_{-yu} with the radial force acting at t = 1.6 s

Characteristic features are the mean values of the coil currents $\bar{i}_{+yu}$ und $\bar{i}_{-yu}$ and the calculated vectors of the actuating forces. With help of these force vectors the radial force is locatable.

Influence of rotor unbalances

The Fig. 3.11b and 3.12b show the influence of rotor unbalances on the shaft displacement and the coil current.

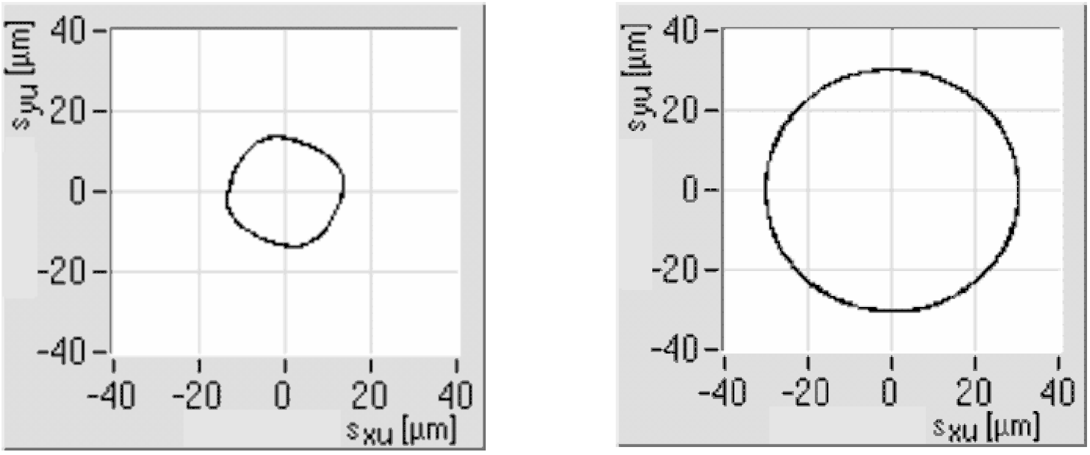

a) reference b) with unbalance acting

Fig 3.11: shaft displacement orbit s_{yu} vs. s_{xu}

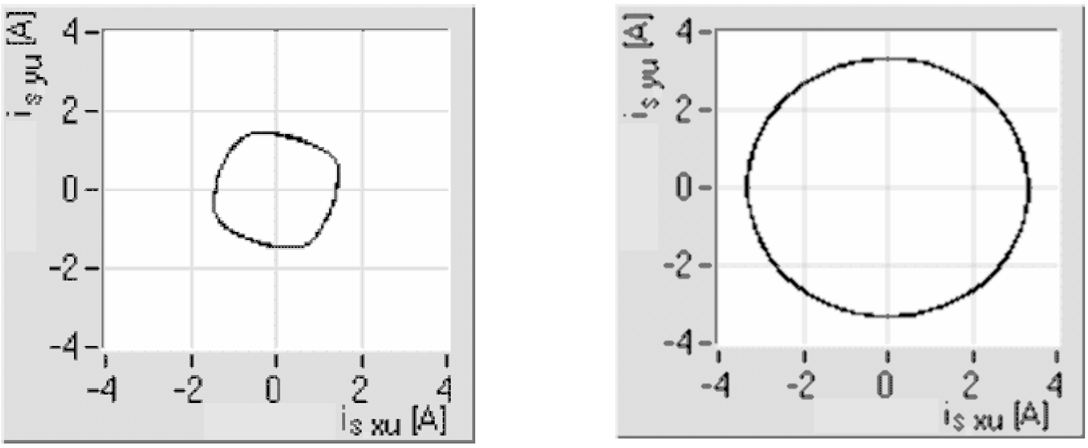

a) reference b) with unbalance acting

Fig 3.12: coil current orbit is_yu vs. is_xu

At a rotor speed of 876 rpm (ω = 92 s^{-1}) a force of 694 N caused by eccentricities of the rotor is acting in the reference state. With the simulated unbalance a disturbance force F_u is added:

$$F_u = m \cdot e \cdot \omega^2 = 846 \ N . \tag{3.23}$$

with:
mass of the unbalance m = 10 kg
eccentricity e = 0,01 m
angular frequency ω = 92 s^{-1}

The rms value of the shaft displacement increases from 9,5 µm to 21,5 µm, the rms value of the coil current increases from 1,01 A to 2,33 A. The acting rotating force calculated with equation 3.3 increases to 1683 N and consists of the unbalance force F_u and an additional force caused by the increased orbit of the shaft displacement (143 N).

The unbalance is localizable by using the ratios of the disturbance forces in the different level radial bearings and the phase angles of the unbalance force vector.

Influence of the electric drive (motor)

Fig. 3.13 and Fig 3.15 show the influence of the electric drive (motor) on the orbits of the shaft displacement. The additional rotating force of the motor increases the orbit. The rotating speed is detectable as a characteristic frequency in the amplitude spectrum (Fig 3.14 and 3.16).

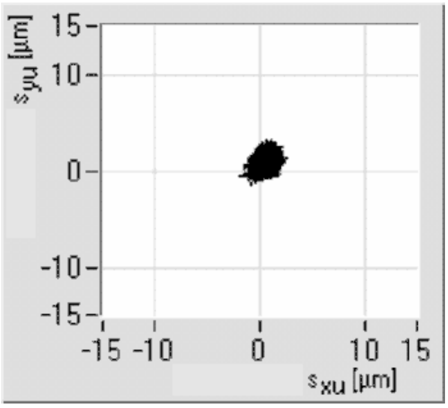

Fig. 3.13:
Shaft displacement orbit s_{yu} vs. s_{xu} at 780 rpm, motor off

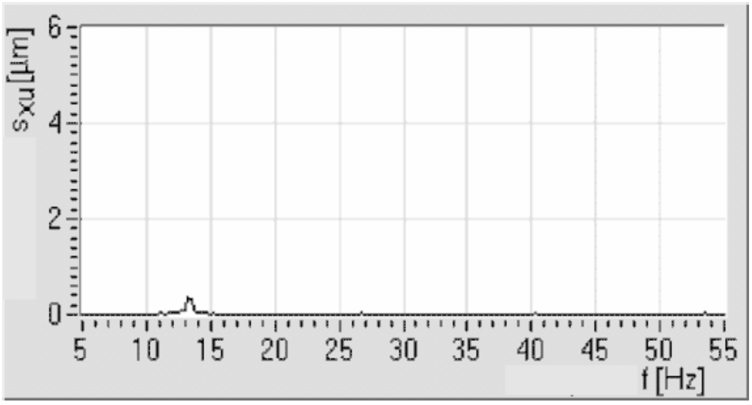

Fig. 3.14:
Amplitude spectrum of the shaft displacement s_{xu} at 780 rpm, motor off

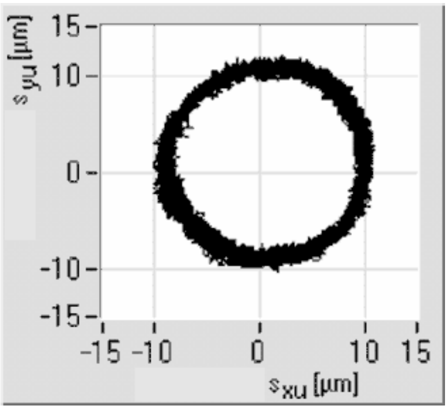

Fig 3.15:
Shaft displacement orbit s_{yu} vs. s_{xu} at 780 rpm, motor on

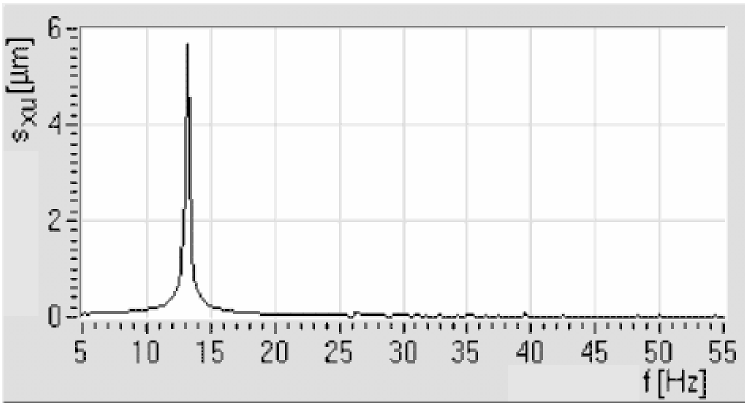

Fig. 3.16:
Amplitude spectrum of the shaft displacement s_{xu} at 780 rpm, motor on

Rotating of the rotor shaft in the catcher bearings

If the AMB is switched off and the rotor shaft rotates in the catcher bearing it is possible to detect faults und wear of the catcher bearing. Fig. 3.17 and 3.18 depict the shaft displacement orbits and the amplitude spectrum of the shaft displacement for this case. Out of the deformation of the orbits and the characteristic frequencies information on the catcher bearing condition can be made.

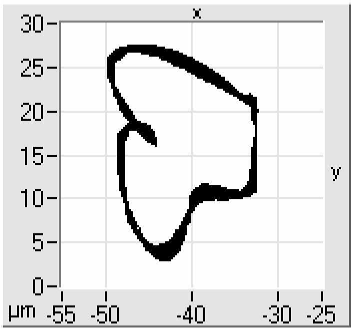

Fig. 3.17:
Shaft displacement orbit s_{yu} vs. s_{xu} at 780 rpm, AMB and motor off

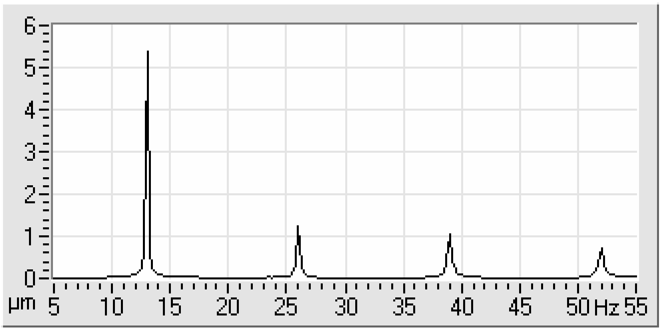

Fig. 3.18:
Amplitude spectrum of the shaft displacement s_{xu} at 780 rpm, AMB and motor off

Algorithms for diagnosis on conventional roller bearings which will be tested at further experiments with the FLP 500 are described in [5].

Significant frequencies of conventional roller bearings are:

- the bearing cage rotation frequency whose magnitude increases with cage faults

$$f_C = \frac{1}{2} f_n \cdot (1 - \frac{DW}{DT} \cdot \cos\alpha) \tag{3.24}$$

- the roll over frequency of the outer bearing ring whose magnitude increases with defects of the outer bearing ring

$$f_O = \frac{1}{2} f_n \cdot z \cdot (1 - \frac{DW}{DT} \cdot \cos\alpha) \tag{3.25}$$

- roll over frequency of the inner bearing ring whose magnitude increases with defects of the inner bearing ring

$$f_I = \frac{1}{2} f_n \cdot z \cdot (1 + \frac{DW}{DT} \cdot \cos\alpha) \tag{3.26}$$

- rolling elements rotation frequency whose magnitude increases with defects of the rolling elements

$$f_R = \frac{1}{2} f_n \cdot \frac{DW}{DT} \cdot (1 - \frac{DW}{DT} (\cos\alpha)^2) \tag{3.27}$$

with:

z	number of rolling elements
DW	diameter of the bearing
DT	rotating circle diameter
f_n	relative rotation between inner and outer ring
α	bearing specific constant

3.4 Monitoring

The extracted magnitudes of the features are monitored on exceeding of limits and trends. The exceeding of a limit determines the occurrence of a fault and results in an alarm. The limit value checking gives a fast way to detect critical changes of the machine condition.

Table 3.1 shows the used features for the limit value checking and the causes for the exceeding.

Signal	feature	fault
shaft displacement	maximum/ minimum	exceeding of the measurement range by defect of the sensor or cable circuit breaks
shaft displacement	maximum gradient	exceeding of gradients, overloading of the controller
magnitude of the shaft displacement signal vector	maximum	danger of damage by rotor-stator contact
coil current	maximum 1	Short circuit, overload of the power amplifier
coil current	minimum 1	circuit break, defect of the power amplifier
coil current	maximum 2	coil currents near the possible maximum current, nonlinear behaviour
coil current	minimum 2	coil current to low, nonlinear behaviour

Table 3.1: Overview of the used features for the limit value monitoring

The main feature is the peak value of the shaft displacement. Limit value checking of the coil currents displays the occurrence of short circuits, thermal overloads and broken wires. The plausibility of the signals was checked with fixed minimum and maximum values and signal gradients. Slowly increasing faults were recognizable by calculation of the trends of the features with methods of linear regression analysis.

3.5 Fault diagnosis

3.5.1 Selection of the diagnosis method

The results of simulation and experiments deliver the knowledge database for the diagnosis. Annex 2 shows characteristic magnitudes of features at the occurrence of selected faults in the AMB control loop that are generated from the knowledge database. The allocation of these feature magnitudes to the according faults is a problem of classification.

For the classification different methods can be used, e.g. statistical methods, neuronal networks or knowledge-based methods.

In the case of AMB diagnosis a knowledge-based concept utilizing rule-based fuzzy logic has been selected. Fuzzy logic [6] supports the possibility to consider uncertainties resulting from the modelling, the process and the data acquisition. The acquired information in the knowledge database can be easily transformed into fuzzy rules.

3.5.2 Creation of fault diagnosis models using fuzzy logic

The first step in the application of fuzzy logic is the fuzzification of the input information (feature magnitudes). The features were defined as linguistic input variables with membership functions (fuzzy sets). For every fuzzy set a membership value is calculated according to the present feature magnitudes. This value serves as symptom for the diagnosis.

The classification of the faults was carried out with production rules in the form of

IF symptom s_1 AND symptom s_2 ... AND symptom s_n THAN fault class f_m.

The symptoms represent the premises of the rule, the fault classes represent the according conclusion. The fuzzy inferenz process calculates with these rules the degree of fulfilment μ of the fault classes.

After processing each rule a degree of fulfilment is calculated for each fault class. The fault classes are sorted by their degree of fulfilment and the class with the highest degree is displayed as the result of the diagnosis. For this diagnosis result the knowledge-base delivers information such as cause of fault, recommended measures and the method of calculation for size and location of the fault.

3.5.3 Definition of the fuzzy sets and fuzzy operators

Because of the high number of input and output variables a concept minimizing the calculation effort has been developed. The fuzzification for each selected feature is done using the overlapping fuzzy sets *S* (small), *N* (normal) and *B* (big). Figure 3.19 shows the definition of the sets on the example of the linguistic variable $\tilde{s}$ (rms value of the shaft displacement).

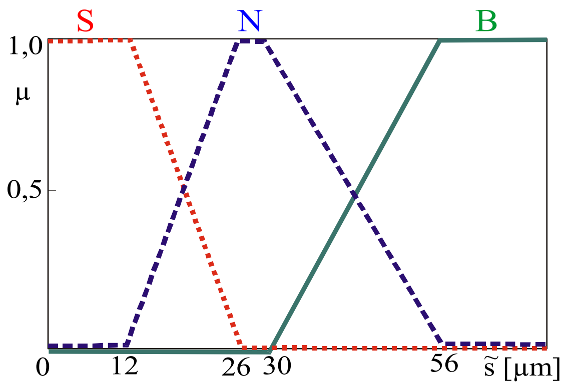

Fig. 3.19:
Fuzzy sets of the linguistic variable $\tilde{s}$

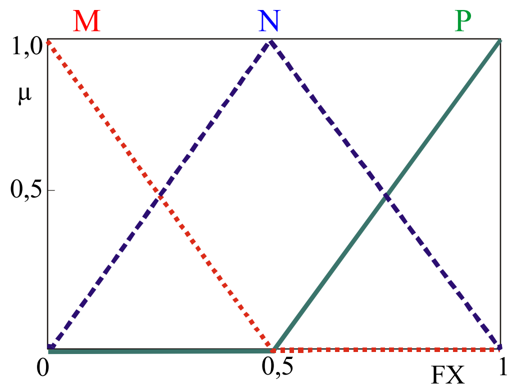

Fig. 3.20:
Fuzzy sets of the fault classes FX

In order to minimize the time of calculation the faults *FX*+ and *FX*- according to Annex 2 were combined into a fault *FX* with the fuzzy sets *M* (minus), *N* (normal) and *P* (plus) as shown in Fig. 3.20. The calculated membership values were used as the degrees of fulfilment μ of the fault classes. Therefore no defuzzification was necessary.

Operator for the fuzzy AND is the algebraic product, for the fuzzy OR the algebraic sum und for the accumulation of the individual conclusions the maximum operator.

3.5.4 Creating of the fuzzy rule bases

The creating of the fuzzy rule bases is shown exemplarily for the diagnosis "increased offset bias current, actuator" (*FA*2+) and "decreased offset bias current, actuator" (*FA*2-) which are combined to the fault *FA*2. The basic rule using the features $\bar{u}$ and Io is

$$\text{IF} \quad \bar{u} \quad \text{AND} \quad Io \quad \text{THEN} \quad FA2.$$

Table 3.2 contains the rule matrix.

Table 3.2: Rule matrix for fault *FA*2

FA2		$\bar{u}$		
		S	**N**	**B**
Io	**S**	**N**	**M**	**N**
	N	**N**	**N**	**N**
	B	**N**	**P**	**N**

Variation of the feature magnitudes resulted in the characteristic fields shown in Fig. 3.21 and 3.22 for the diagnosis statements "*FA*2 = *M*" and "*FA*2 = *P*" calculated with the relevant individual rules

$$\text{IF} \quad \bar{u} = N \quad \text{AND} \quad Io = S \quad \text{THEN} \quad FA2 := M$$

and

$$\text{IF} \quad \bar{u} = N \quad \text{AND} \quad Io = B \quad \text{THEN} \quad FA2 := P.$$

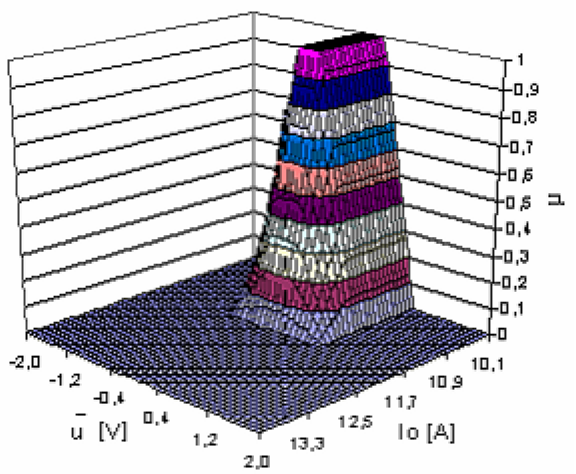

Fig. 3.21: Characteristic field of the diagnosis statement *FA*2 = *M*

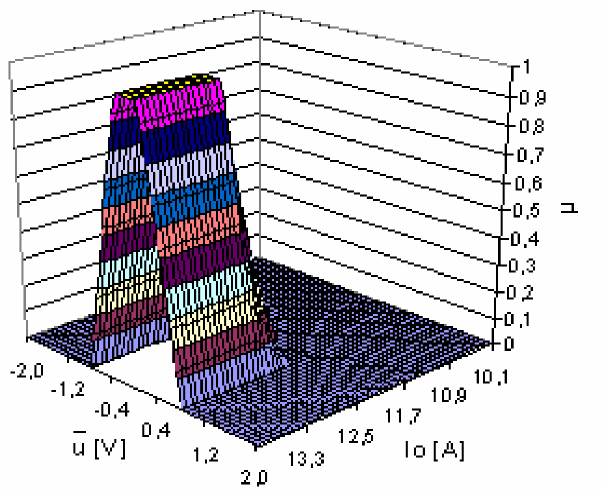

Fig. 3.22: Characteristic field of the diagnosis statement *FA*2 = *P*

The result of the calculation of the diagnosis statement "*FA*2 = *N*" with the rule base from Table 3.2 is shown in Fig. 3.23. If the calculation of *N* uses a large number of rules the calculation time can be minimized and the shape of the characteristic field can be optimized by calculating the degree of fulfilment of the set *N* from the degrees of the sets *M* and *P* with equation 3.28

$$\mu(FX=N) := MIN\,((1 - \mu(FX=M)),\ (1 - \mu(FX=P))) \tag{3.28}$$

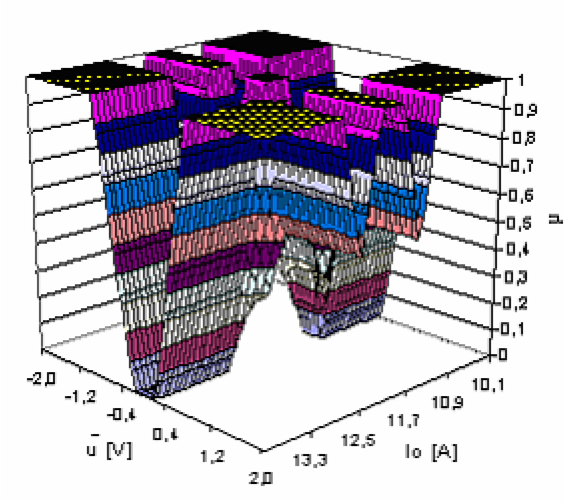

Fig. 3.23:
Characteristic field of the diagnosis statement *FA*2 = *N,* calculated with the rule base in Table 3.2

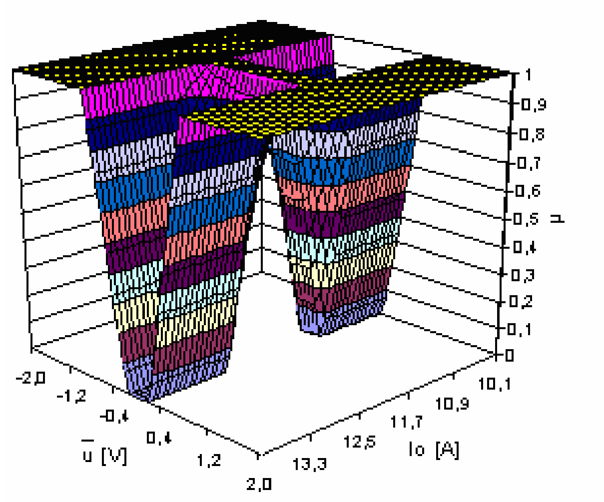

Fig. 3.24:
Characteristic field of the diagnosis statement *FA*2 = *N,* reduced calculation with equation 3.28

The characteristic field of this reduced calculation for "*FA*2 = *N*" is shown in Fig. 3.24. It shows not the deformations like Fig. 3.23, so the calculation with equation 3.28 is the better and faster way.

The fuzzy sets and rules were defined for all selected faults according to Annex 2.

To minimize the calculation time only the relevant features and rules for each fault class were processed. The following rule sets were created:

RULE SET FC1

IF	*R* = *S*	THEN	*FC1* := *P*
IF	*R* = *N*	THEN	*FC1* := *N*
IF	*R* = *B*	THEN	*FC1* := *M*

RULE SET FC2

IF	$\bar{s}$ = *S*	THEN	*FC2* := *P*
IF	$\bar{s}$ = *N*	THEN	*FC2* := *N*
IF	$\bar{s}$ = *B*	THEN	*FC3* := *M*

RULE SET FA1

IF	$\bar{u}$ = *S*	AND	$\bar{i}_s$ = *N*	AND	*Io* = *N*	AND	$\bar{f}$ = *N*	AND	*V* = *N*	THEN *FA1* := *P*
IF	$\bar{u}$ = *N*									THEN *FA1* := *N*
IF	$\bar{u}$ = *B*	AND	$\bar{i}_s$ = *N*	AND	*Io* = *N*	AND	$\bar{f}$ = *N*	AND	*V* = *N*	THEN *FA1* := *M*

RULE SET FA2

IF $\bar{u}$ = *N* AND *Io* = B AND *V = N* THEN *FA2 := P*
IF *Io = N* THEN *FA2 := N*
IF $\bar{u}$ = *N* AND *Io = S* AND *V = N* THEN *FA2 := M*

RULE SET FA3

IF $\bar{u}$ = *S* AND *Io = B* AND *V = N* THEN *FA3 := P*
IF $\bar{u}$ = *N* AND *Io = N* THEN *FA3 := N*
IF $\bar{u}$ = *B* AND *Io = S* AND *V = N* THEN *FA3 := M*

RULE SET FA4

IF $\bar{u}$ = *B* AND *Io = B* AND *V = N* THEN *FA4 := P*
IF $\bar{u}$ = *N* AND *Io = N* THEN *FA4 := N*
IF $\bar{u}$ = *S* AND *Io = S* AND *V = N* THEN *FA4 := M*

RULE SET FA6

IF *Io = N* AND *A = S* THEN *FA6 := P*
IF *A = N* THEN *FA6 := N*
IF *Io = N* AND *A = B* THEN *FA6 := M*

The following rule sets use the fuzzy sets of the variables $\tilde{F}$ and $\bar{F}$ of the other axis which are labeled $\widetilde{Foa}$ and $\overline{Foa}$.

RULE SET FA5

IF $\tilde{s}$ = *N* AND $\bar{F}$ = *S* AND $\bar{i}_s$ = *S* AND $\overline{Foa}$ = *N* THEN *FA5 := P*
IF $\bar{i}_s$ = *N* AND $\bar{F}$ = *N* AND $\overline{Foa}$ = *N* THEN *FA5 := N*
IF $\tilde{s}$ = *N* AND $\bar{F}$ = *B* AND $\bar{i}_s$ = *B* THEN *FA5 := M*

RULE SET FS1

IF $\bar{F}$ = *B* AND $\overline{Foa}$ = *N* THEN *FS1 := P*
IF $\bar{F}$ = *N* THEN *FS1 := N*
IF $\bar{F}$ = *S* AND $\overline{Foa}$ = *N* THEN *FS1 := M*

RULE SET FS2

IF *W = N* AND $\bar{i}_s$ = *N* AND $\tilde{F}$ = *S* AND $\widetilde{Foa}$ = *N* THEN *FS2 := P*
IF $\tilde{F}$ = *N* THEN *FS2 := N*
IF *W = N* AND $\bar{u}$ = *N* AND $\tilde{F}$ = *B* AND $\widetilde{Foa}$ = *N* THEN *FS2 := M*

3.5.5 Diagnosis results

Using the defined rules and sets from chapter 3.5.3 and 3.5.4 the degrees of fulfilment have been examined by simulation of the faults of one AMB control loop.

The simulation was done with an angular frequency ω of 92 s^{-1}, according to a rotor speed of about 1000 rpm. The features were calculated over a full spin of the rotor, that resulted to a simulation cycle time of 0,1 s. The fault was activated at t = 0,5 s, the first reaction can be seen at t = 0,6 s.

Fig. 3.24 to 3.27 show the degrees of fulfilment µ for the diagnose "*FA1 = P*" (increased offset, actuating signal). With an offset of 0,06 A the fault class has a degree of 0,1 which rises to 0,8 by an offset of 0,12 A. The maximum degree of 1,0 is reached with an offset of 0,15 A. Fig. 3.27 shows results with an oversized offset fault of 5 A. The fault class "*FA1 = P*" is correct displayed and there are no other faults displayed after the system has stabilized at t = 1,4 s, even with this extreme error. Right after the activating of the fault there are some different faults displayed for a short time. The controller needs some time to stabilize the system.

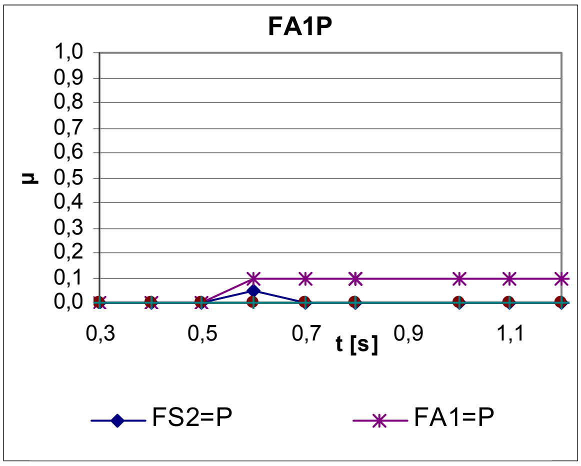

Fig. 3.24: Fault *FA1+*, offset actuating signal = +0,06 A

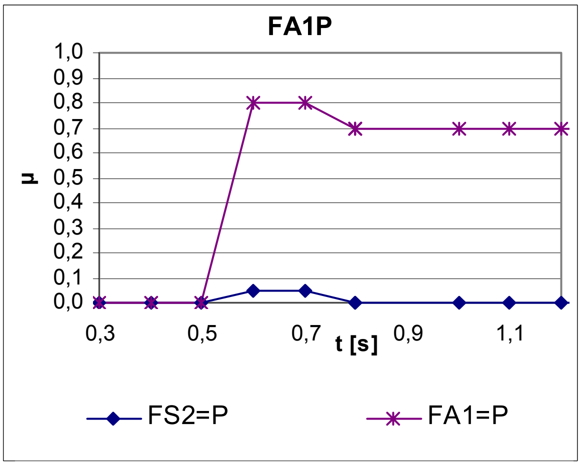

Fig. 3.25: Fault *FA1+*, offset actuating signal = +0,06 A

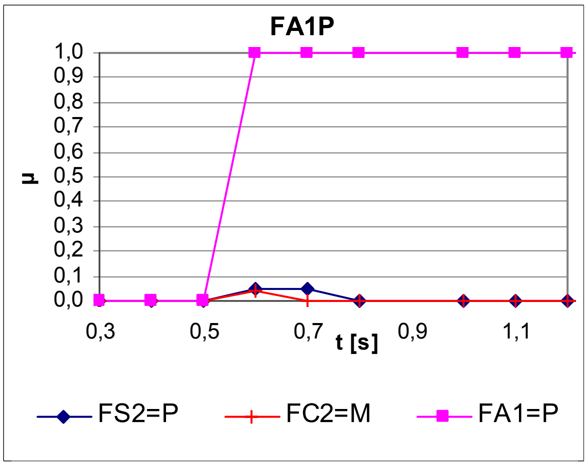

Fig. 3.26: Fault *FA1+*, offset actuating signal = +0,15 A

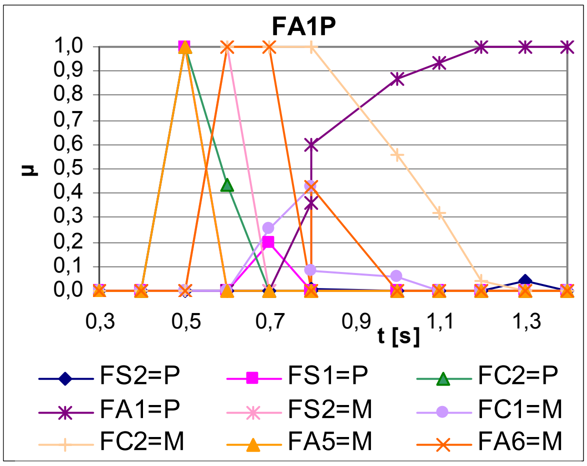

Fig. 3.27: Fault *FA1+*, offset actuating signal = +5,0 A

The Fig. 3.28 to 3.34 show the diagnosis results for the other faults according to Annex 2. Results are shown for fulfilment degrees over 0,5. In all cases the simulated faults were clearly distinguishable from other faults, therefore the simulated faults are correctly identified.

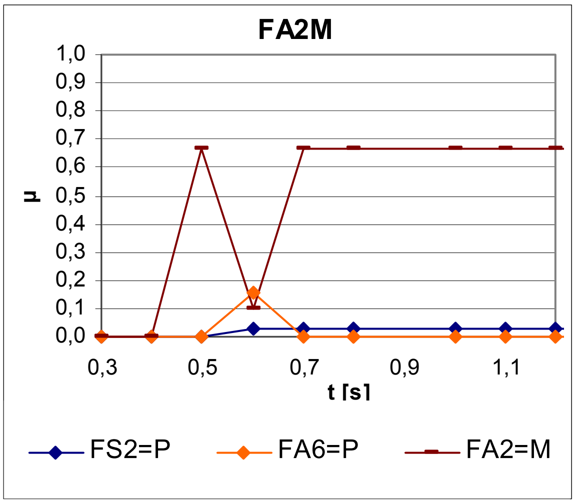

Fig. 3.28: Fault *FA2*-, offset bias current = - 0,6 A

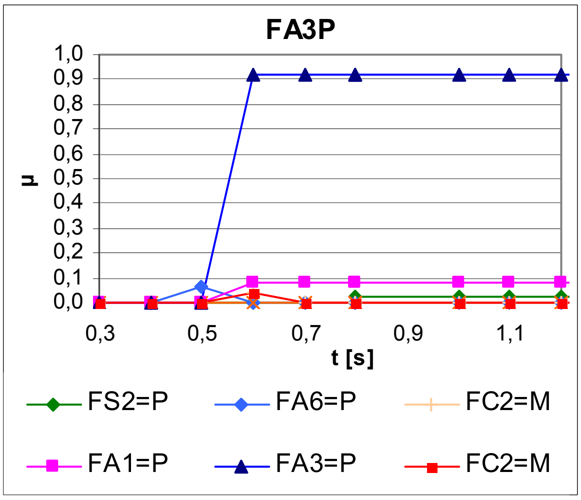

Fig. 3.9: Fault *FA3*+, offset current positive coil = + 1,5 A

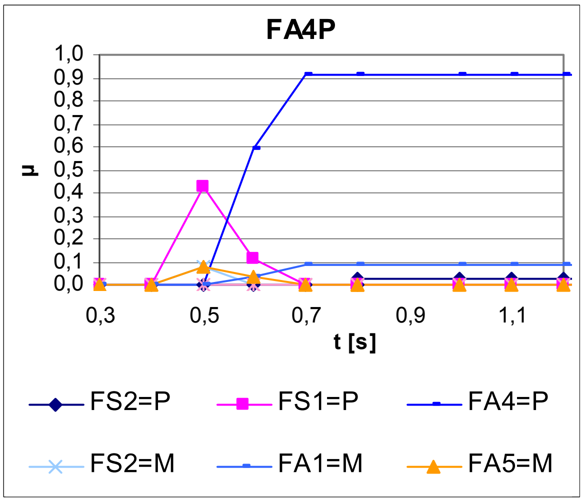

Fig. 3.30: Fault *FA4*+, offset current negative coil = + 1,5 A

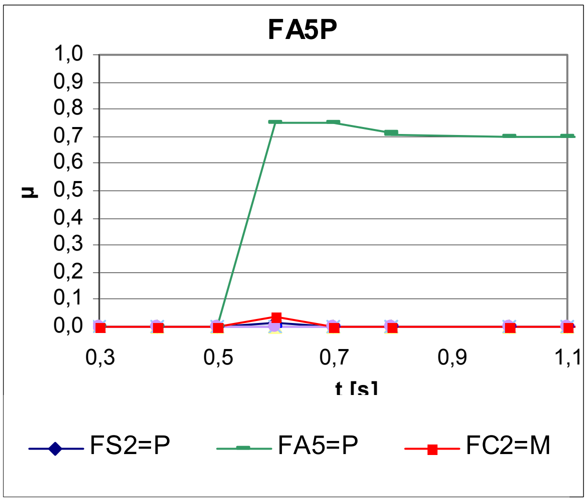

Fig. 3.31: Fault *FA5*+, positive force offset = + 400 N

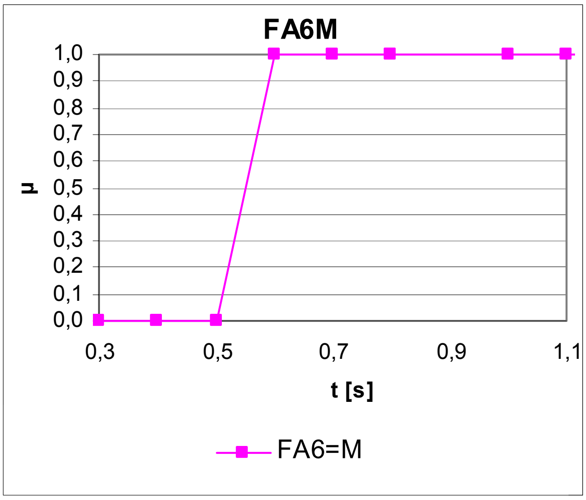

Fig. 3.32: Fault *FA6-*, decreased actuator gain = - 20 %

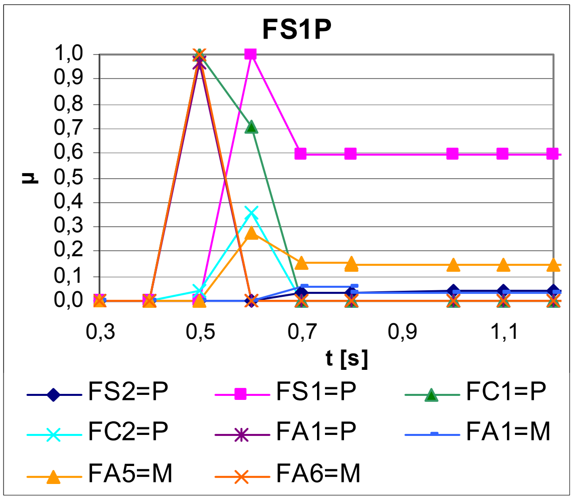

Fig. 3.33: Fault *FS1+*, increased sensor offset = 30 µm

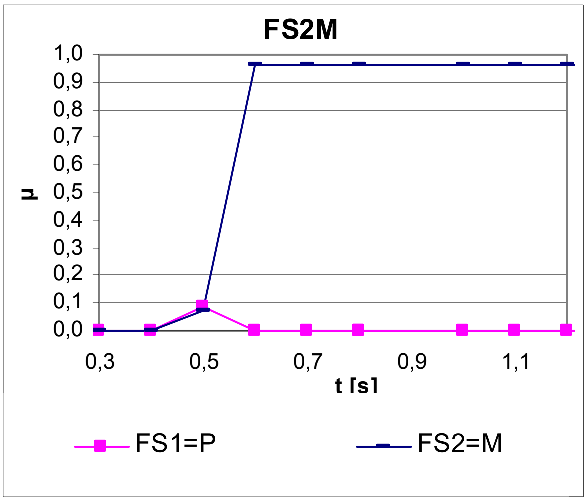

Fig. 3.34: Fault *FS2-*, decreased sensor gain = - 50 %

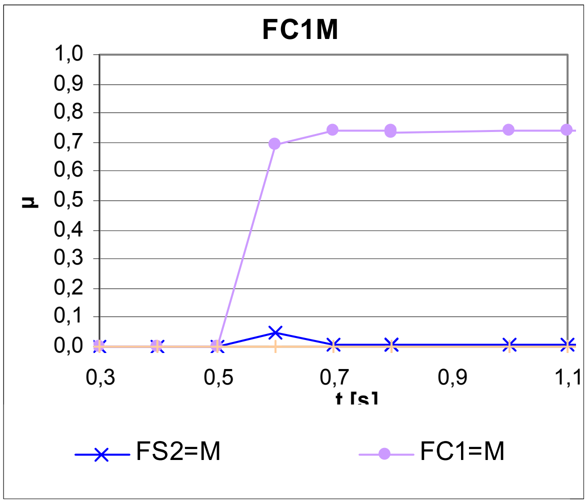

Fig. 3.35: Fault *FC1-*, decreased controller gain = - 40 %

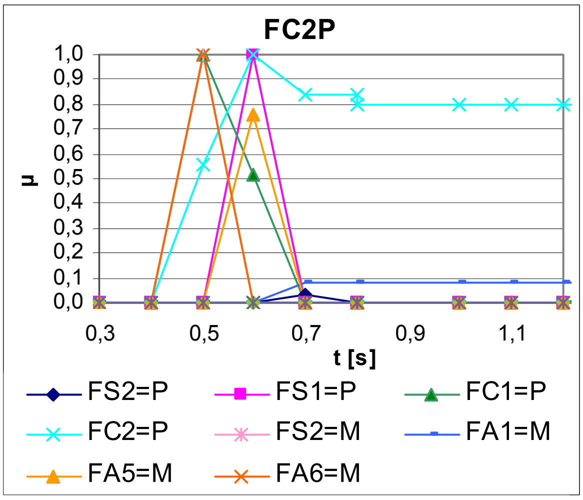

Fig. 3.36: Fault *FC2+*, increased controller set point = + 25 µm

3.5.6 Cascading of fuzzy logic modules

Diagnosing the whole system results in a complex set of rule bases. A hierarchical structure [7] in the shape of fault trees was designed and auxiliary linguistic variables were introduced to increase the transparency. These auxiliary variables represent the result of sub-rules, they can be used by each individual rule set. In such a way the calculation time was decreased.

In this hierarchical structure fuzzy logic modules (FLM) were cascaded. The FLM realize the inference processing of the individual rule sets. The inputs of the FLM are linguistic input variables which are fuzzified by the FLM or the results of sub-rules.

This is shown in the diagnosis example "radial force" at the FLP 500. Figure 3.37 shows the cascading of the fuzzy logic modules FLM 1 – 3 for the diagnosis of radial forces.

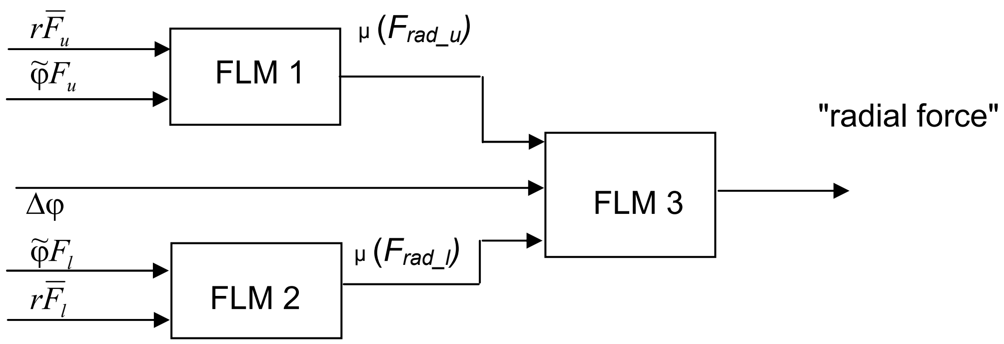

Fig. 3.37: Cascaded fuzzy logic modules (FLM) for the diagnosis "radial force"

The inputs for FLM 1 and FLM 2 are the mean values $r\overline{F}$ of the force vector magnitudes of the upper and lower radial magnetic bearing and the rms values $\tilde{\varphi}F$ of the force vector angles. FLM 1 and FLM 2 calculate the auxiliary variables F_{rad_u} and F_{rad_l} with the individual rules

IF	$\tilde{\varphi}F_u = S$	AND	$r\overline{F}_u = B$	THAN	$F_{rad\_u} := B$
IF	$\tilde{\varphi}F_o = S$	AND	$r\overline{F}_l = B$	THAN	$F_{rad\_l} := B$

F_{rad_u} and F_{rad_l} are used by FLM 3 together with the phase difference $\Delta\varphi$ between the force vectors from the upper and lower bearing. The fuzzy sets of $\Delta\varphi$ are defined as shown in Fig. 3.38.

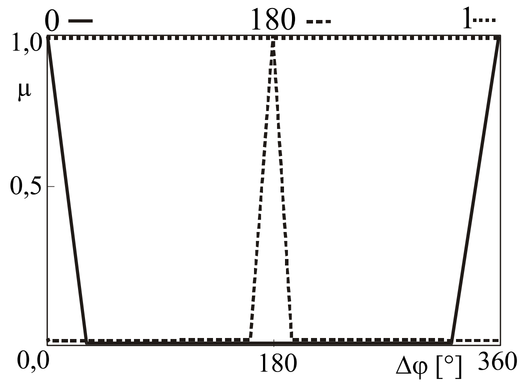

Fig 3.38:
Fuzzy sets of the linguistic variable Δφ

FLM 3 calculates the diagnosis "radial force" using the basic rule

IF F_{rad_u} AND F_{rad_l} AND Δφ THAN *radial force*

and the rule base shownin Table 3.3.

				Δφ		
				0	**180**	**1**
F_{rad_u}	**S**	F_{rad_o}	**S**	**N**	**N**	**N**
	S		**B**	**N**	**N**	**Frub**
	B		**S**	**N**	**N**	**Frlb**
	B		**B**	**Frbb**	**Frob**	**N**

Table 3.3: Rule base of FLM 3

The output of FLM 3 is the diagnosis "radial force" with the fulfilment degrees of the sets of the fault classes:

- *Frub*: radial force in the upper bearing level
- *Frlb*: radial force in the lower bearing level
- *Frbb*: radial force between the upper and lower bearing level
- *Frob*: radial force below the lower or over the upper bearing level

Figure 3.39a shows diagnosis results with simulated radial forces. The force acted below the lower bearing starting from t = 1.5 s. The degree of fulfilment of the corresponding fault class *Frob* fired correctly with the value of 0.98, the other degrees remained below 0.1.

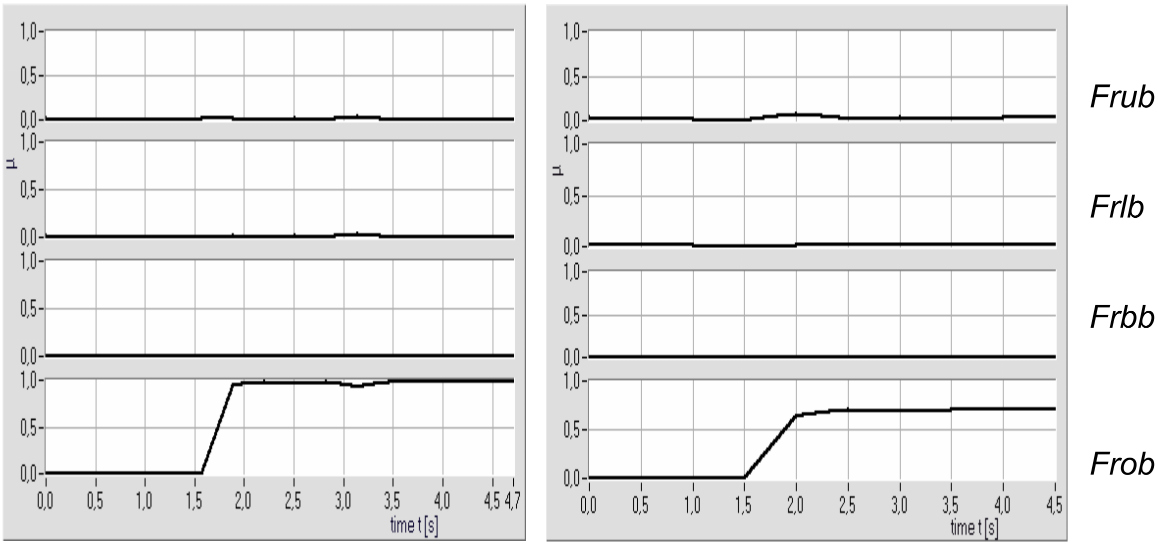

a) Simulation with *MLDyn* b) Experiment on the FLP 500

Fig. 3.39: Degrees of fulfilment of the fault classes with the occurrence of the fault "radial force below the lower magnetic bearing"

Results of analogous experiments on the test facility FLP 500 are shown in Fig. 3.39b. The fault was also correctly identified with a degree of fulfilment of 0.7.

3.6 Diagnosis system *MLDia*

For the technical realisation of the diagnosis concept the diagnosis system *MLDia* has been developed. It works with the software LabVIEW [8]. This software supports the data acquisition with a variety of hardware components and comprises a lot of signal analysis function. LabVIEW is used in a Windows-Version, but supports also Macintosh, Sun-workstations, HP-UX and Linux.

MLDia is modular based. The present implementation comprises the modules:

- data acquisition,
- signal based feature extraction,
- parameter estimation,
- shaft displacement monitoring,
- controller output monitoring,
- coil current monitoring,
- bearing force calculation and monitoring,
- trend recording and display,
- limit value checking and adaptation,
- diagnosis.

The module **data acquisition** records a maximum of 16 channels with a sampling rate of 100 kHz which is enough for the diagnosis tasks. Higher sample rates and more channels are available if different acquisition hardware is used. The data acquisition records the signals shaft displacement, controller output and coil currents of 4 radial and 1 axial AMB controller loops. Additional the rotating speed is measured. In the **signal based feature extraction** the features according to chapter 3.2 are calculated, stored and available for the monitoring and diagnosis. The module **parameter estimation** calculates the controller parameters of each axis. The **monitoring** modules display the main features vs. time and the orbits of the radial signals. Fig. 3.40 shows a screen shot of the shaft displacement display. Limit checking barriers can be displayed in the according orbits.

Trends and gradients of selected signals and features are calculated, recorded and displayed with the module **trend recording and display**. The generating of long term trends is realised with the calculation of the mean values over a variable time. This mean values are also used for the adaptation of limit values.

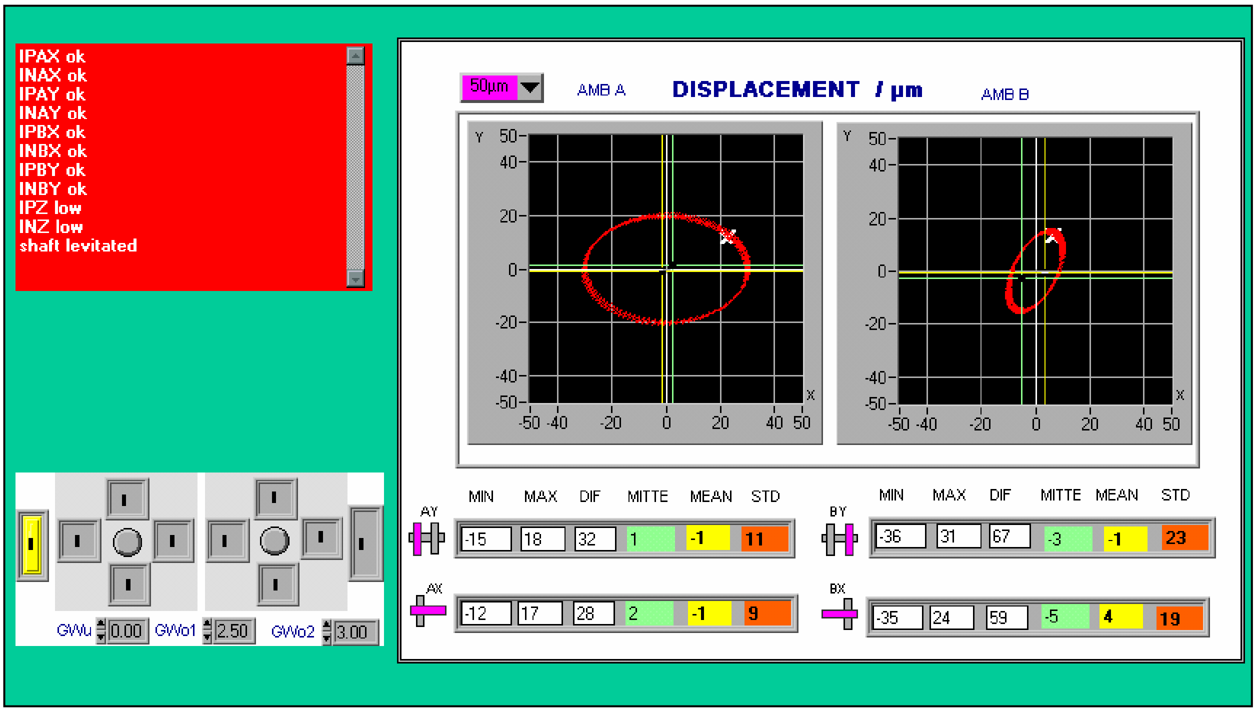

Fig 3.40: Shaft displacement monitoring in *MLDia*

The **limit value checking** is carried out for the mean values, rms values and the minimum and maximum values of the shaft displacement and coil current signals. It is possible to adapt the limit values automatically if the machine condition is altered. That is useful for the unattended long time monitoring of experimental AMB systems. The exceeding of limits can start a recording of the signals and features and it can trigger alarms.

The module **diagnosis** uses the fuzzy based models created in chapter 3.5. The processing of the algorithms is carried out in sub modules. The fuzzy sets are adaptable to different machine conditions. After the fuzzification the rules are processed hierarchically. At first the fulfilment values for the faults in every axis are calculated, from these values the diagnosis results of the different levels. In a third step it is possible to use additional feature sets for the increasing or decreasing of the fulfilment degrees.

At the end all diagnosis results are displayed in the order of their fulfilment degrees in a textbox.

3.7 Conclusion

In this document the concept of diagnosis for AMB using system inherent signals was presented. Results of simulations and experiments were implemented in a knowledge-base for the monitoring and diagnosis. Knowledge-based models for the diagnosis using fuzzy logic have been successfully tested and verified. The defined fuzzy sets, operators and the selected rules realise a correct identification of occurring faults with a minimized effort of calculation. Using the concept of cascaded fuzzy logic modules the transparency of the whole systems was preserved even with a large number of features and rules.

The experiments have been carried out at the test rack FLP 500. The diagnosis concept is adaptable to different AMB configurations.

References

[1] Isermann, R.: Überwachung und Fehlerdiagnose. VDI Verlag, 1994
[2] Isermann, R.: Identifikation dynamischer Systeme, Springer Verlag, 1992
[3] Büttner, W.: Digitale Regelungssysteme, Vieweg Verlag, 1991
[4] Document N°: HTR-E-03/01-D-3-3-1
[5] Sturm, A.: Wälzlagerdiagnose an Maschinen und Anlagen, Verlag TÜV-Rheinland, 1986
[6] Zadeh, L.A.: Fuzzy Algorithms, Information and Control 12, 1968
[7] Hampel, R., Chaker, N.: Cascading of Multidimensional Fuzzy Controllers. Proceedings 5th Zittau Fuzzy-Colloquium, 1997
[8] http://www.ni.com/labview

Annex 1 – Results of controller test

1. Speed levels and unbalances

PID controller

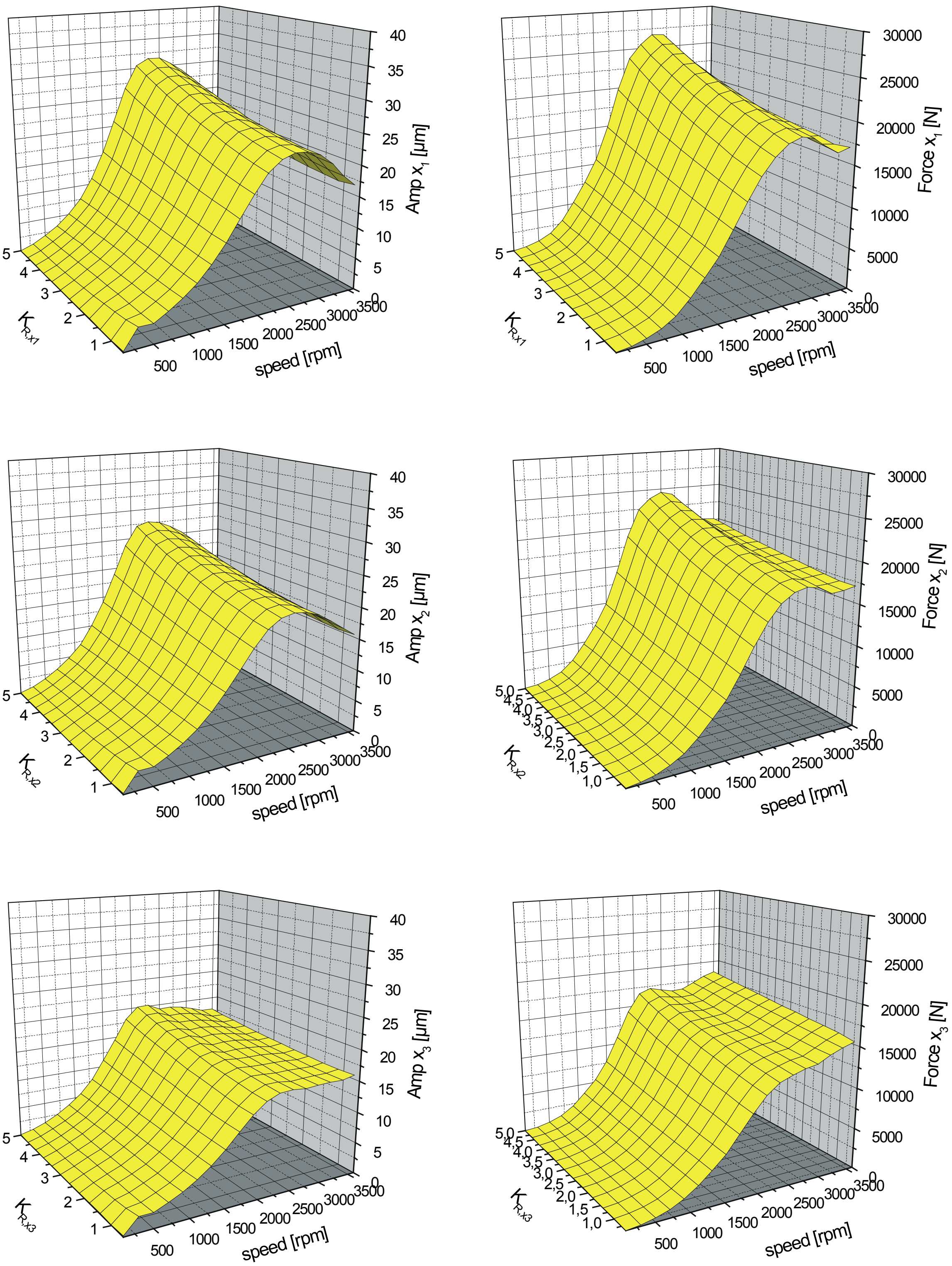

Amplitude of rotor position and bearing force vs. speed and controller gain for radial AMB 1...3

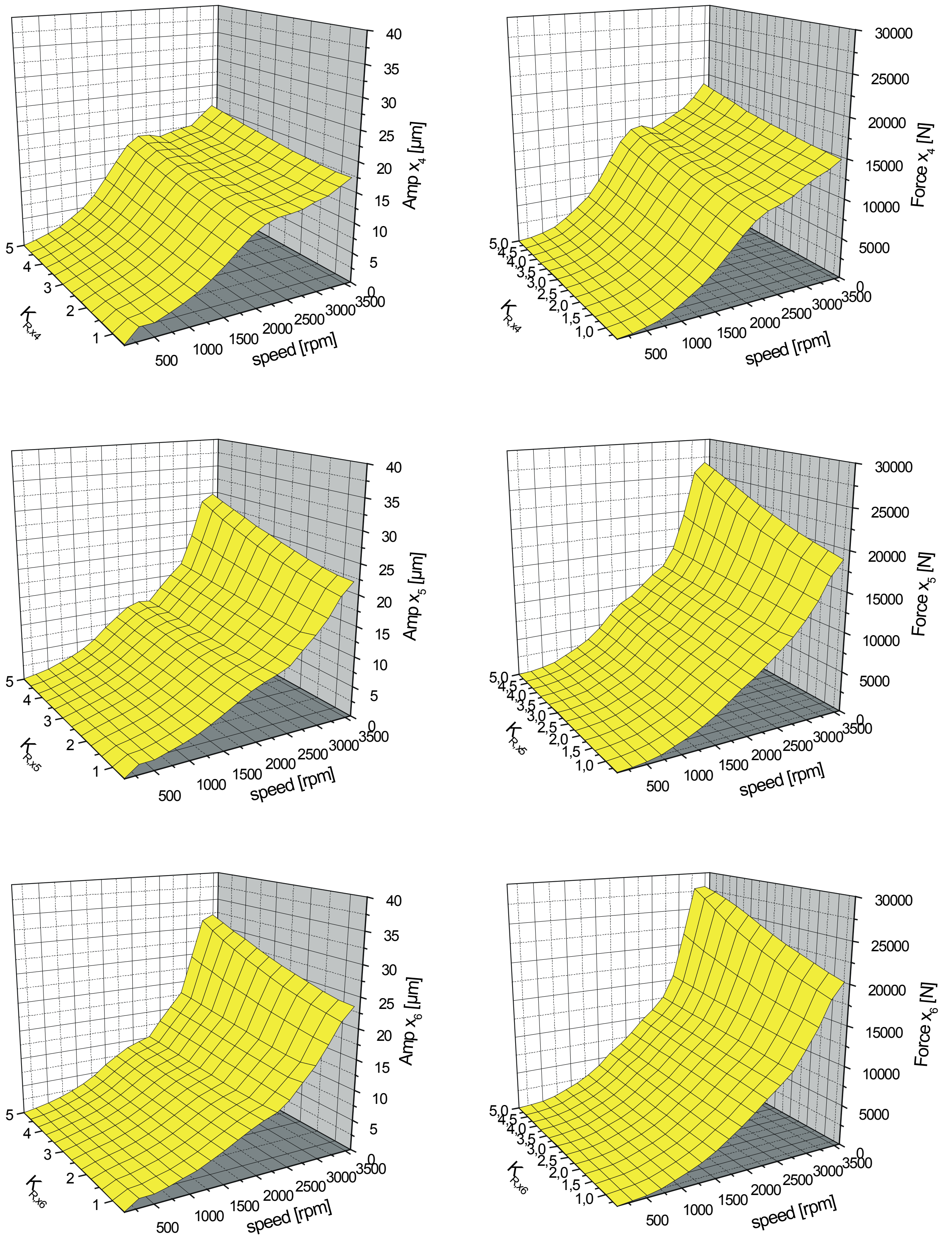

Amplitude of rotor position and bearing force vs. speed and controller gain for radial AMB 4...6

Fuzzy controller

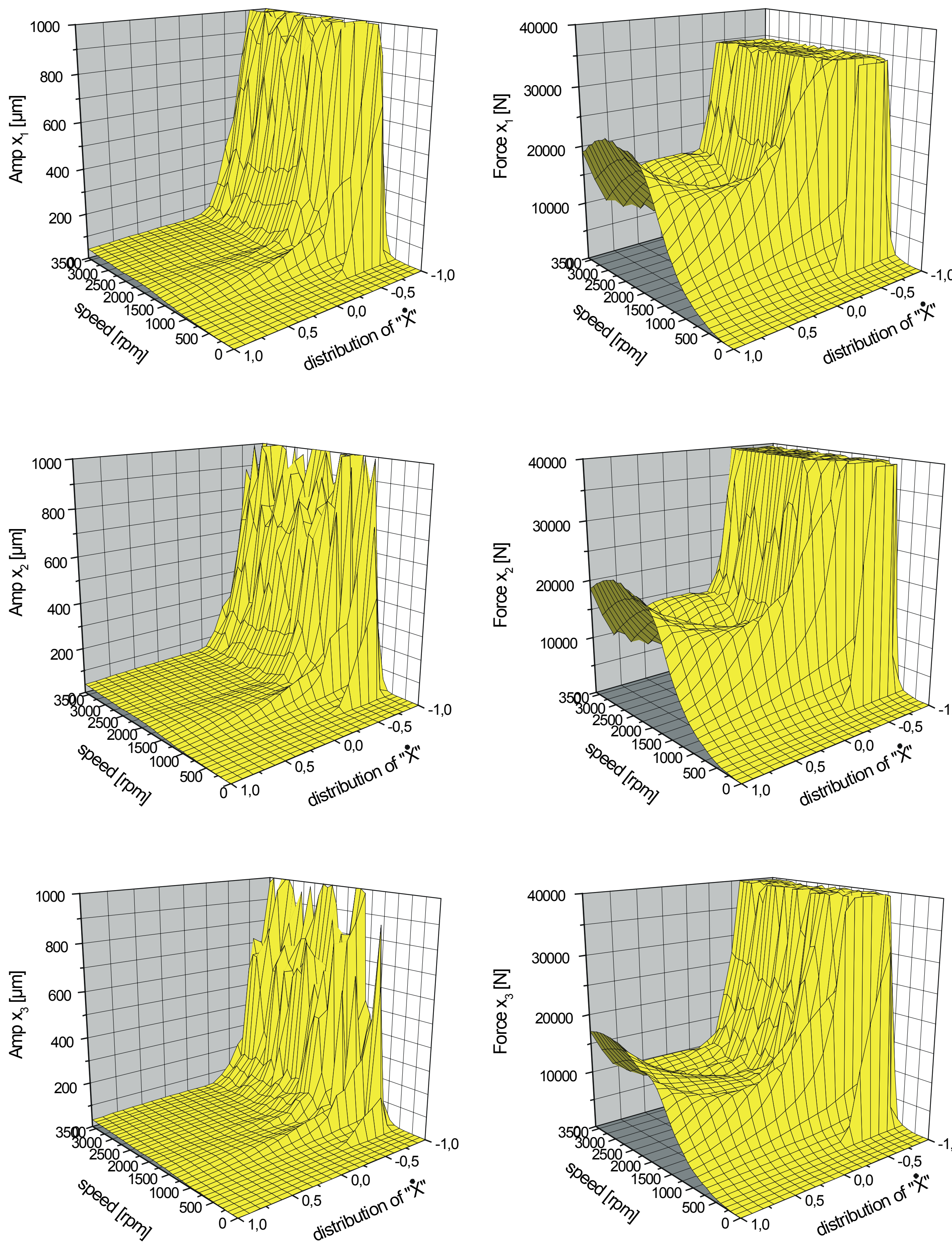

Amplitude of rotor position and bearing force vs. speed and normalized distribution of set „ $\dot{X}$ “ for radial AMB 1...3

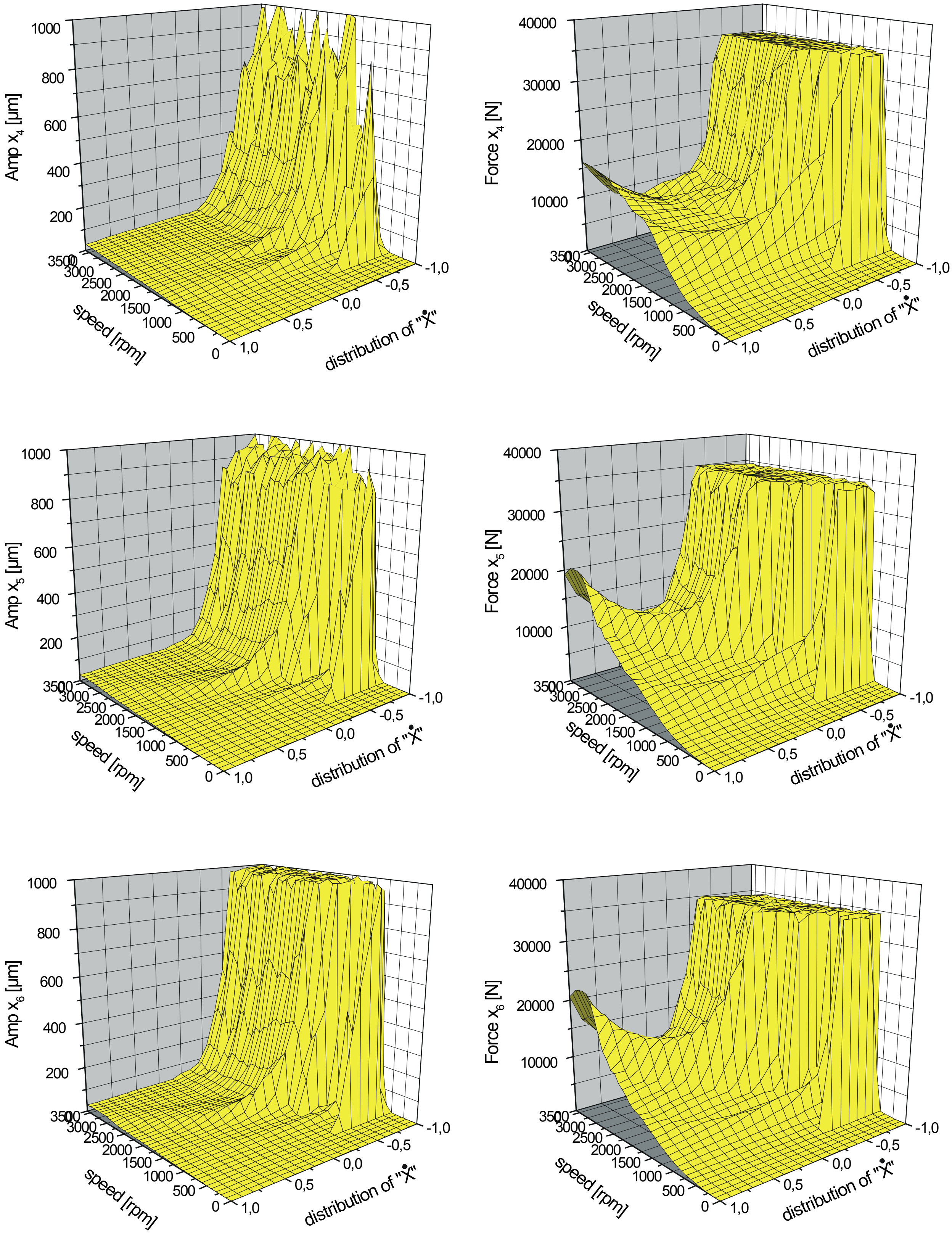

Amplitude of rotor position and bearing force vs. speed and normalized distribution of set „ $\dot{X}$ “ for radial AMB 4...6

Fuzzy gain adaptation

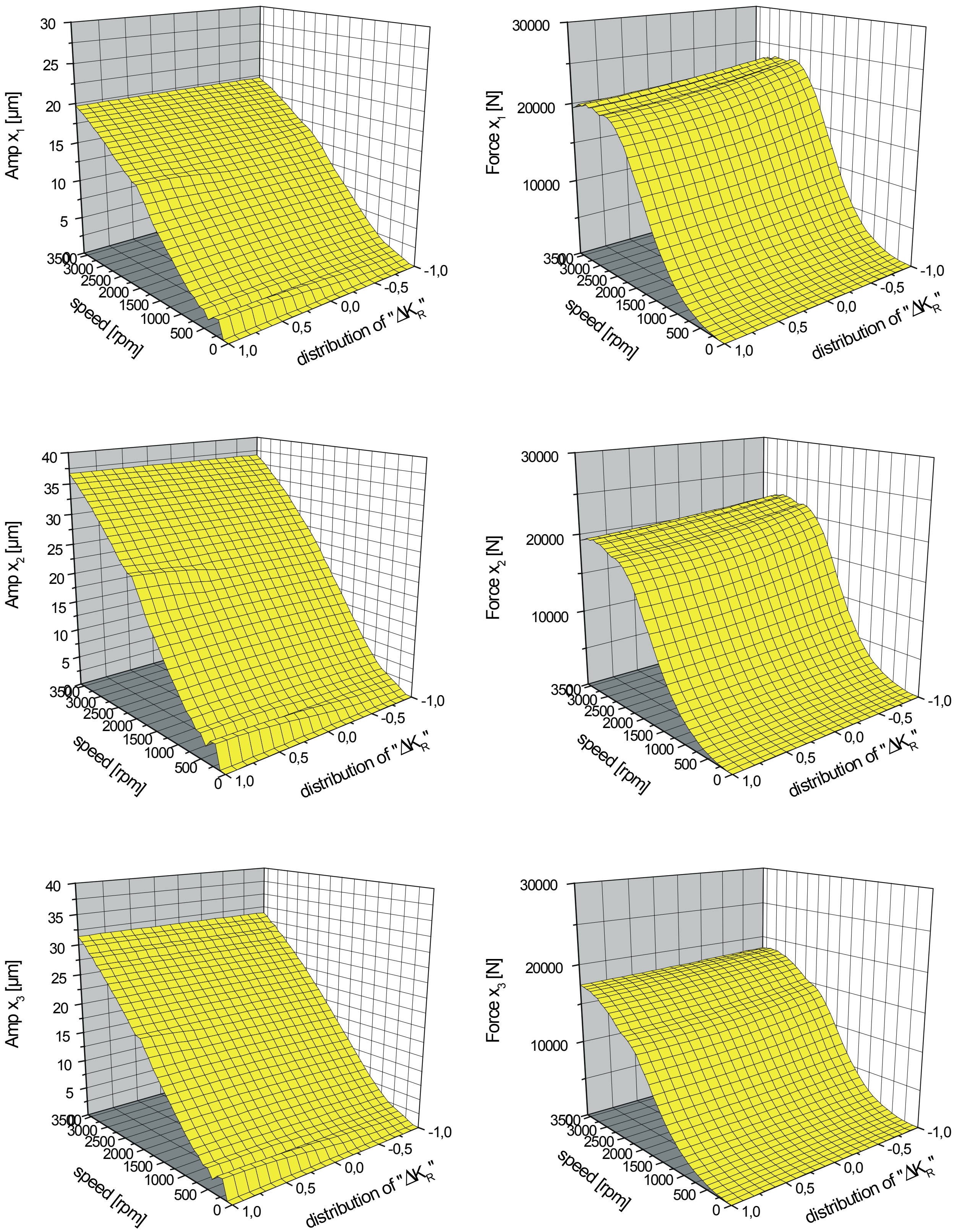

Amplitude of rotor position and bearing force vs. speed and normalized distribution of set „ΔK_R“ for radial AMB 1...3

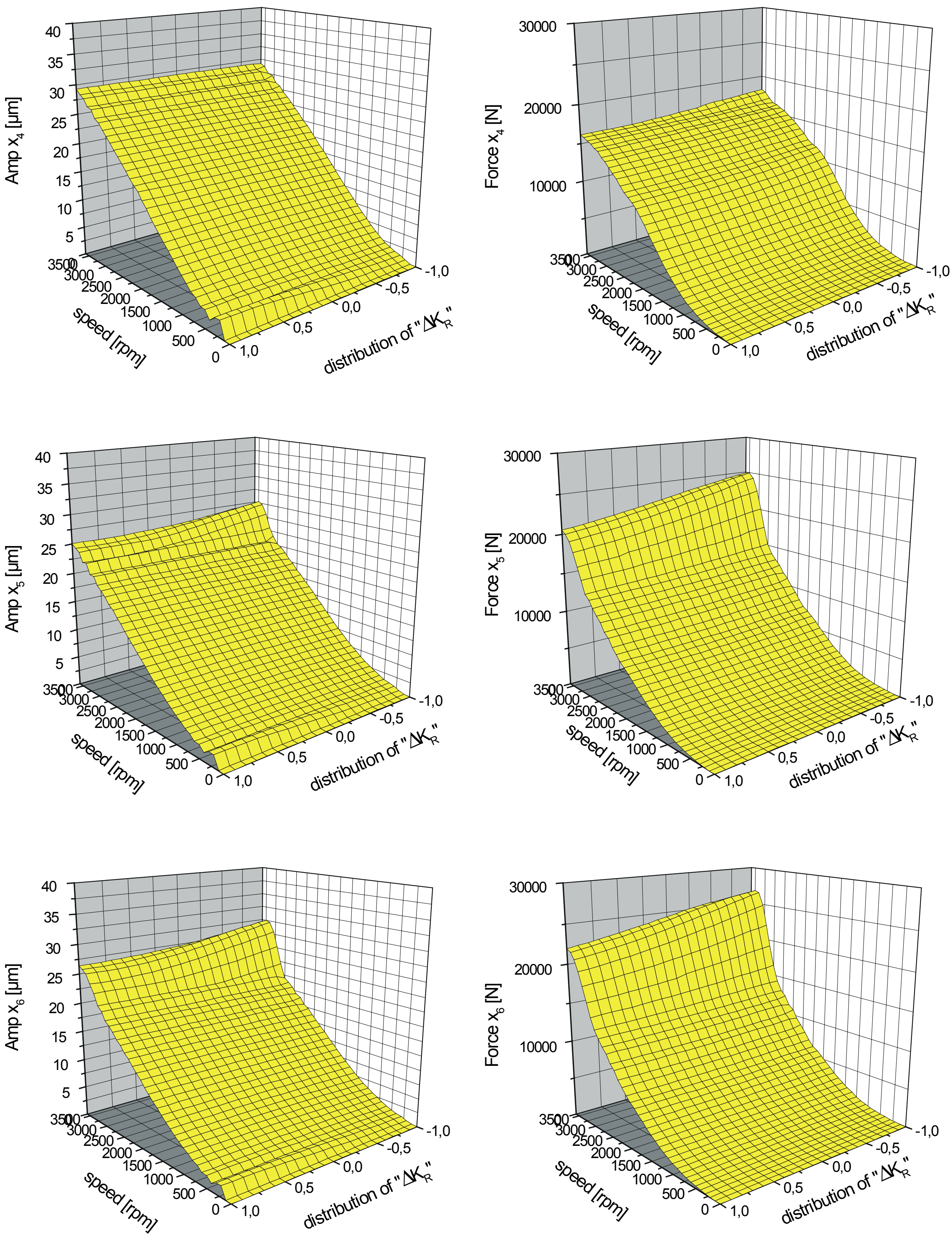

Amplitude of rotor position and bearing force vs. speed and normalized distribution of set „ΔK_R“ for radial AMB 4...6

2. Static Loads at radial AMB‘s

PID controller

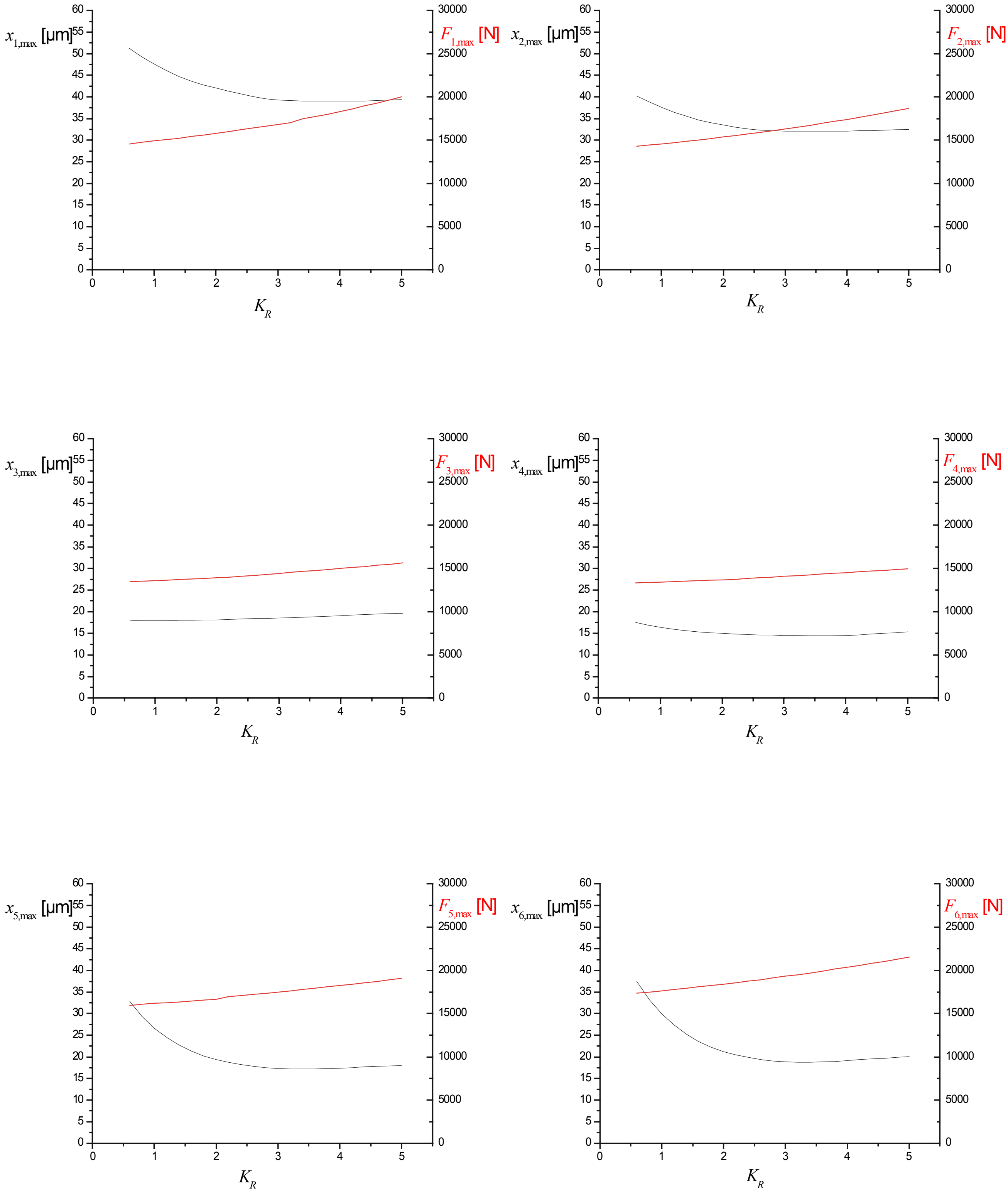

Amplitude of rotor position and bearing force vs. controller gain for radial AMB 1...6

Fuzzy controller

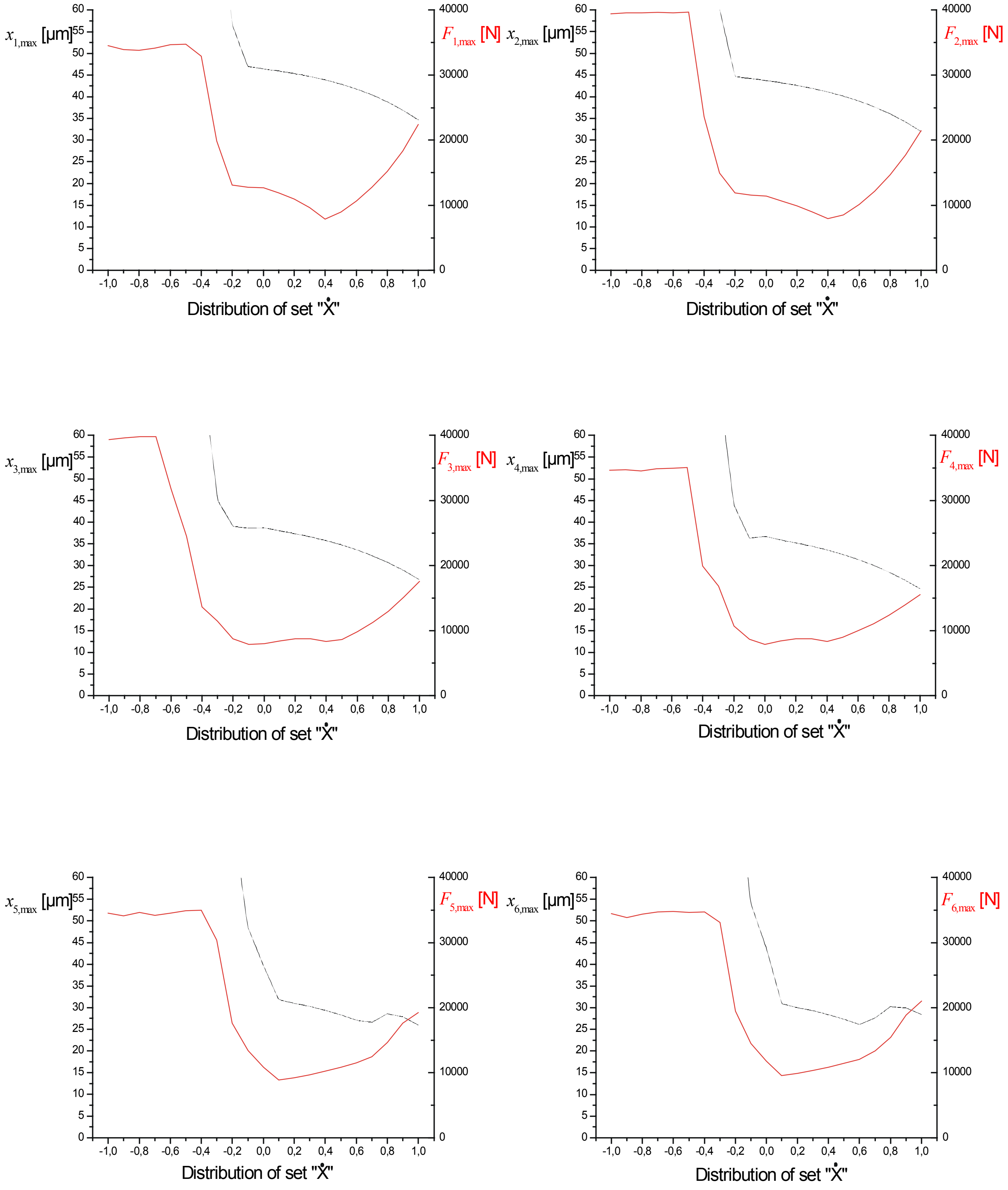

Amplitude of rotor position and bearing force vs. normalized distribution of set „ $\dot{X}$ “ for radial AMB 1...6

Fuzzy gain adaptation

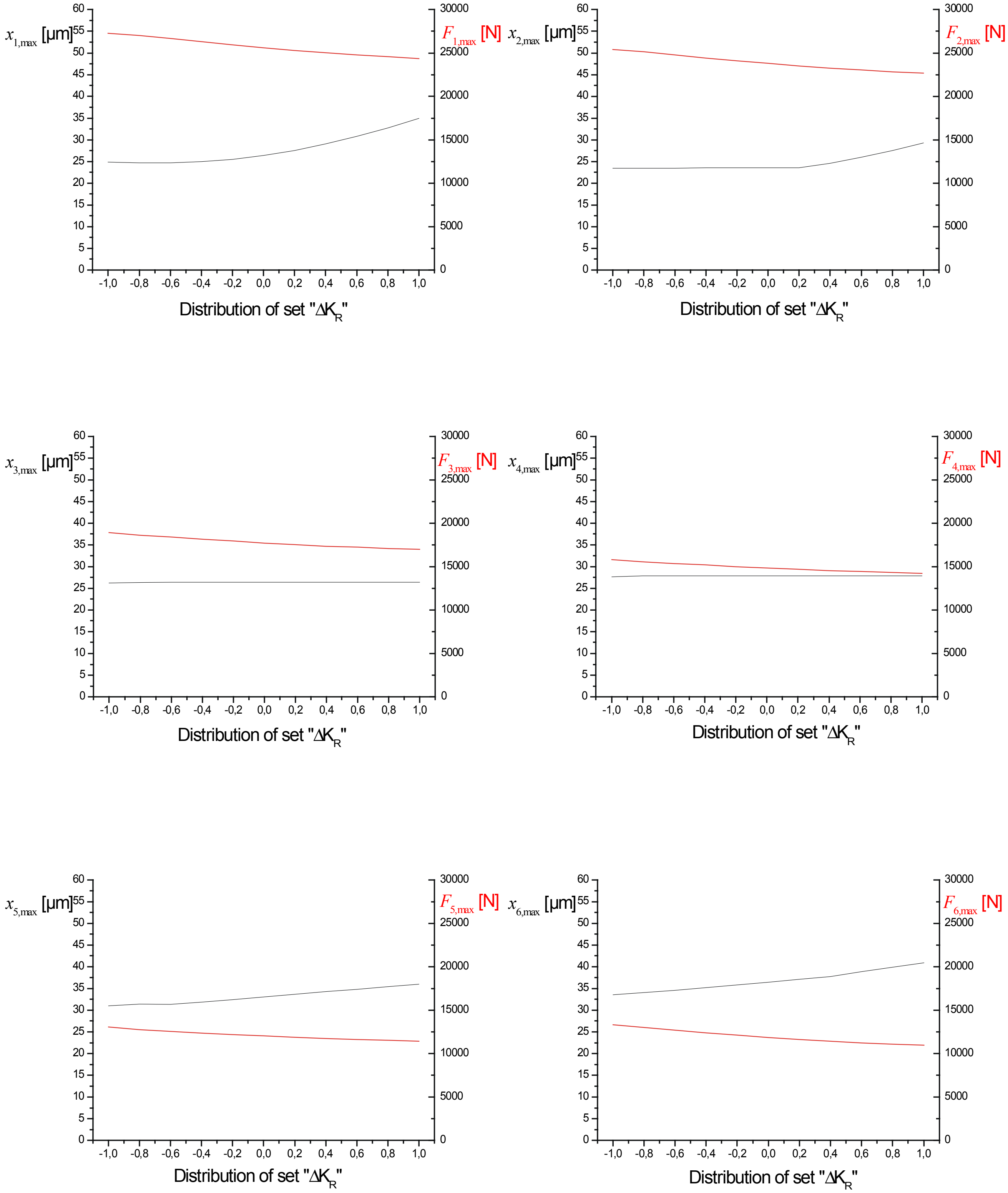

Amplitude of rotor position and bearing force vs. normalized distribution of set „ΔK_R“ for radial AMB 1...6

3. Dynamic loads at radial AMB's

PID controller

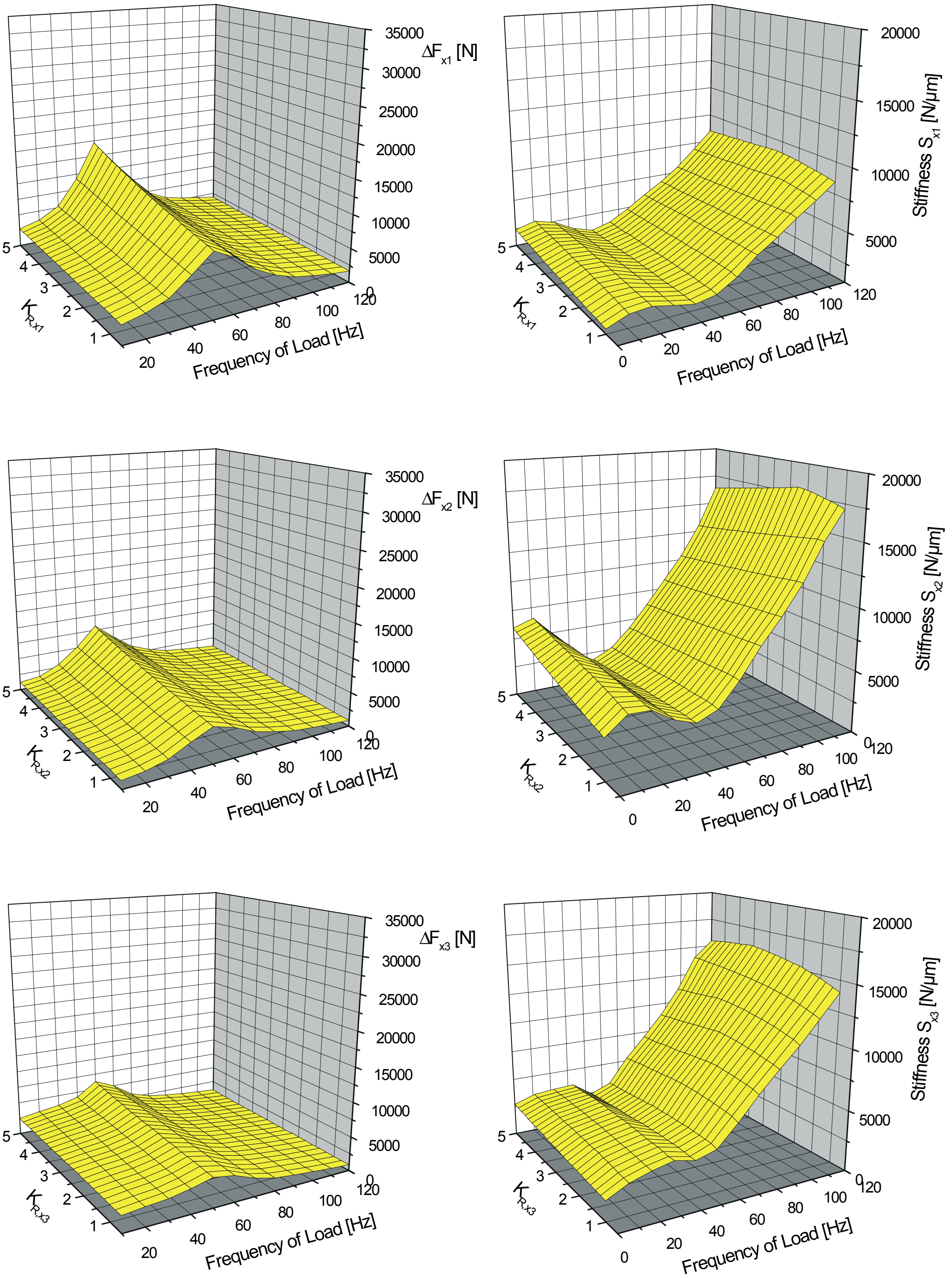

Bearing force and dynamic stiffness vs. freqency of load and controller gain for radial AMB 1...3

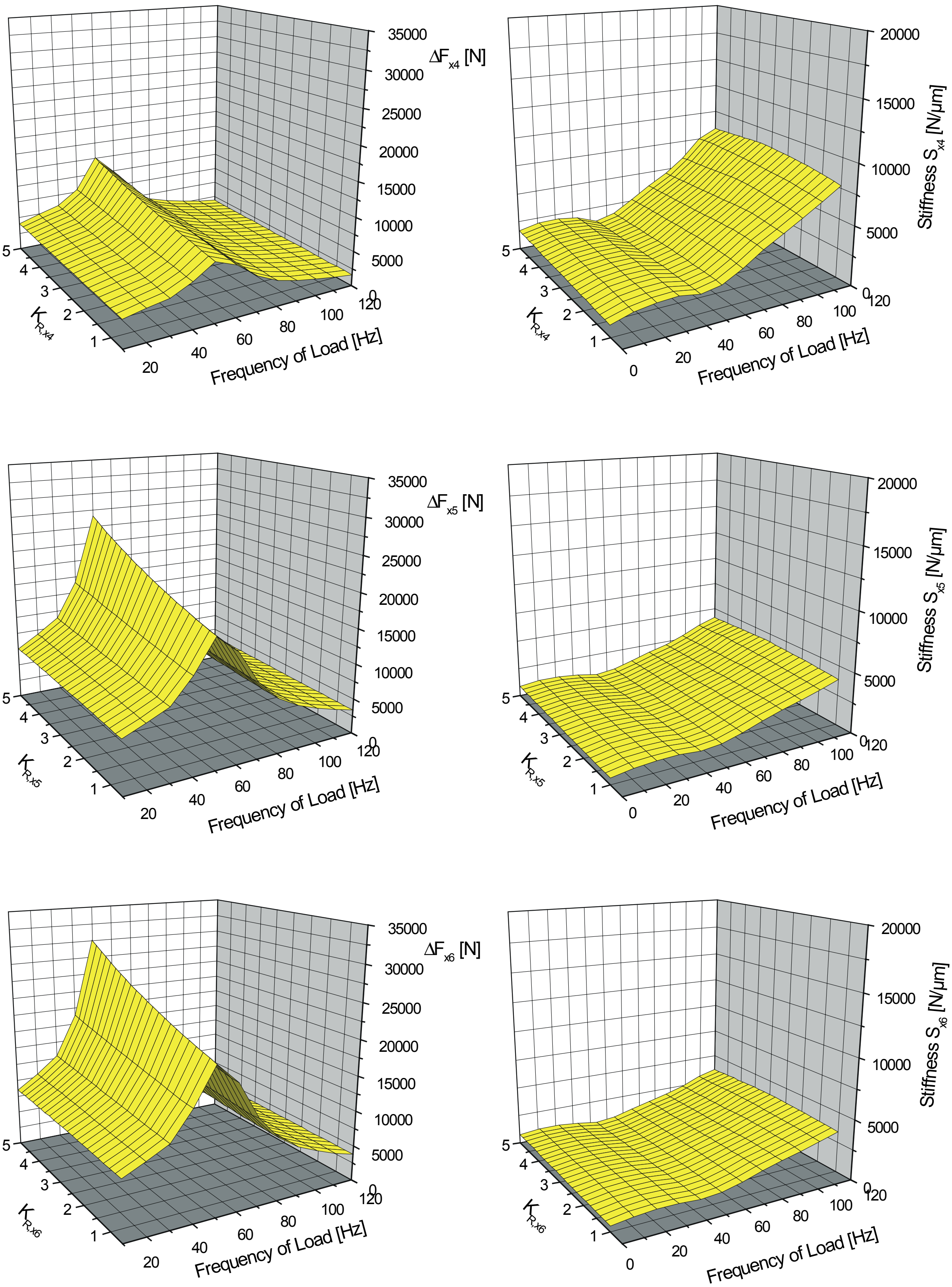

Bearing force and dynamic stiffness vs. freqency of load and controller gain for radial AMB 4...6

Fuzzy controller

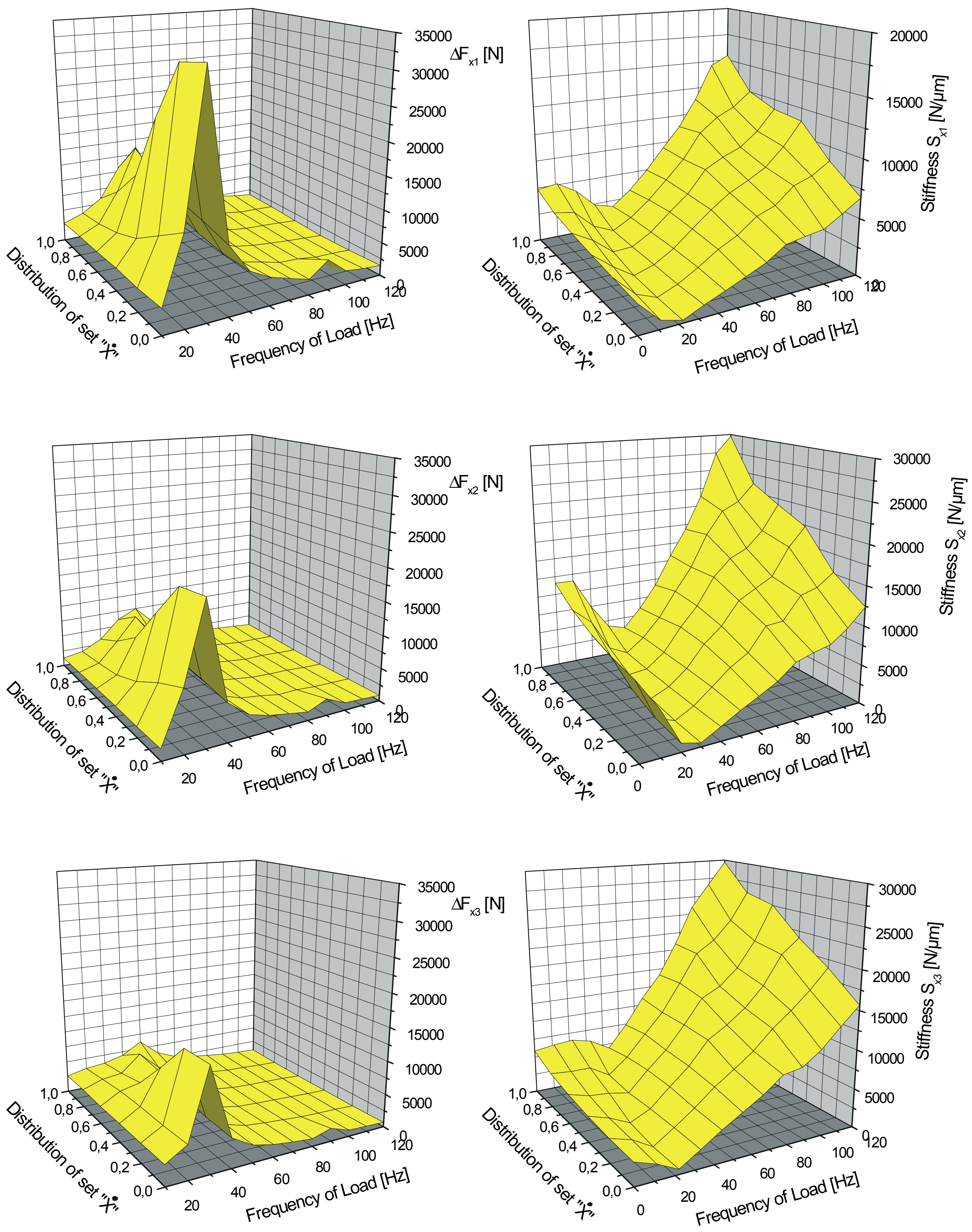

Bearing force and dynamic stiffness vs. freqency of load and normalized distribution of set „ $\dot{X}$ “ for radial AMB 1...3

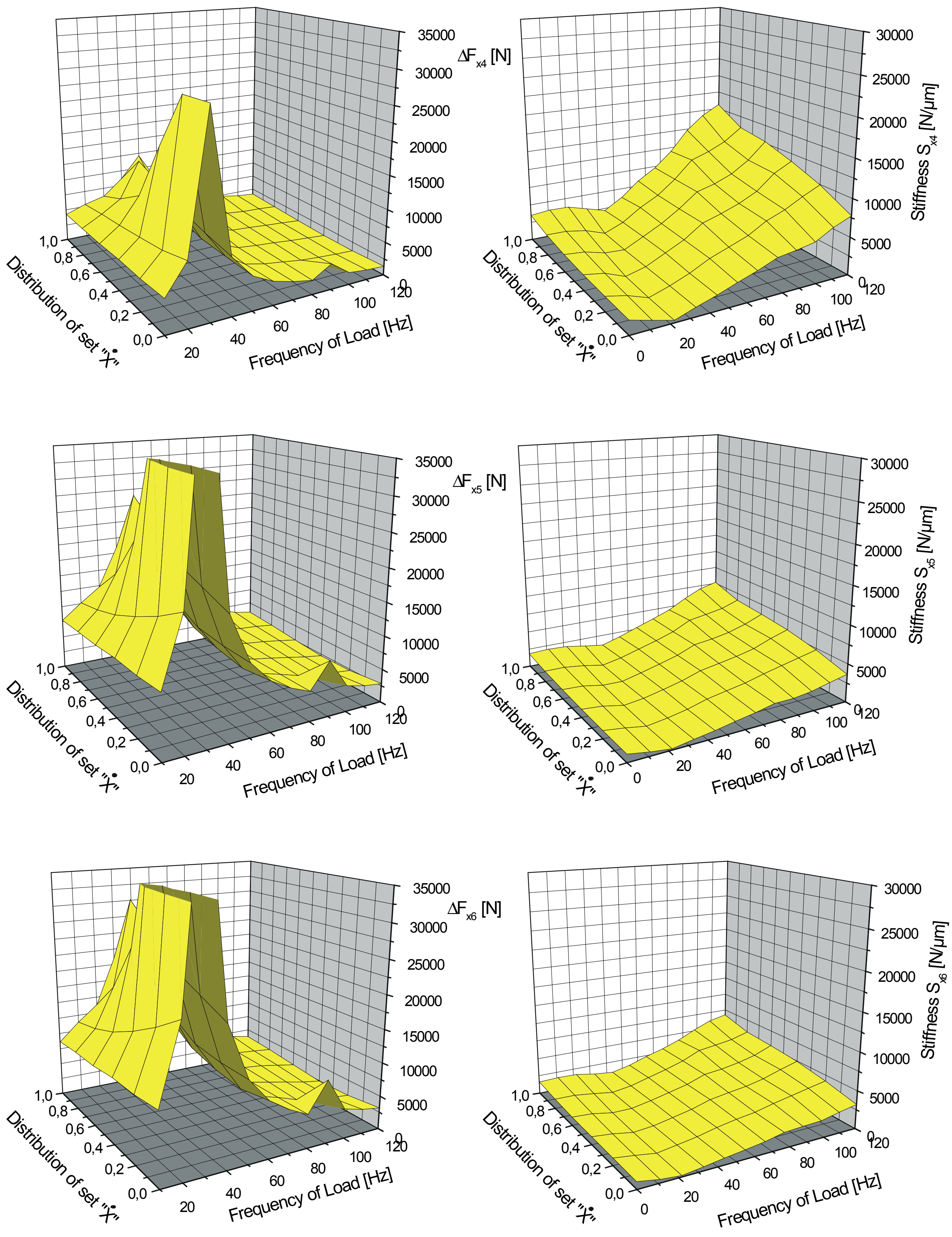

Bearing force and dynamic stiffness vs. freqency of load and normalized distribution of set „ $\dot{X}$ “ for radial AMB 4...6

Fuzzy gain adaptation

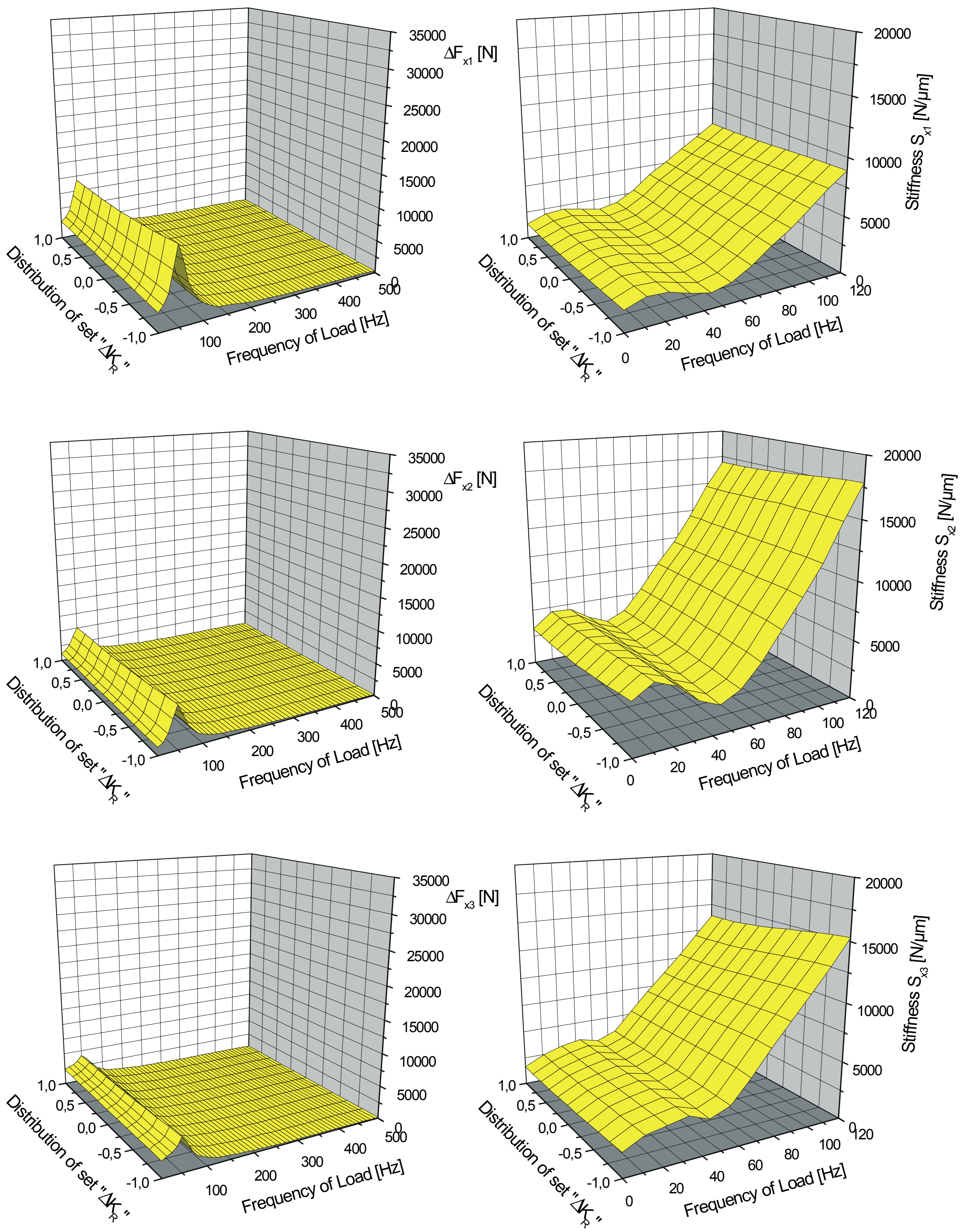

Bearing force and dynamic stiffness vs. freqency of load and normalized distribution of set „ΔK_R“ for radial AMB 1...3

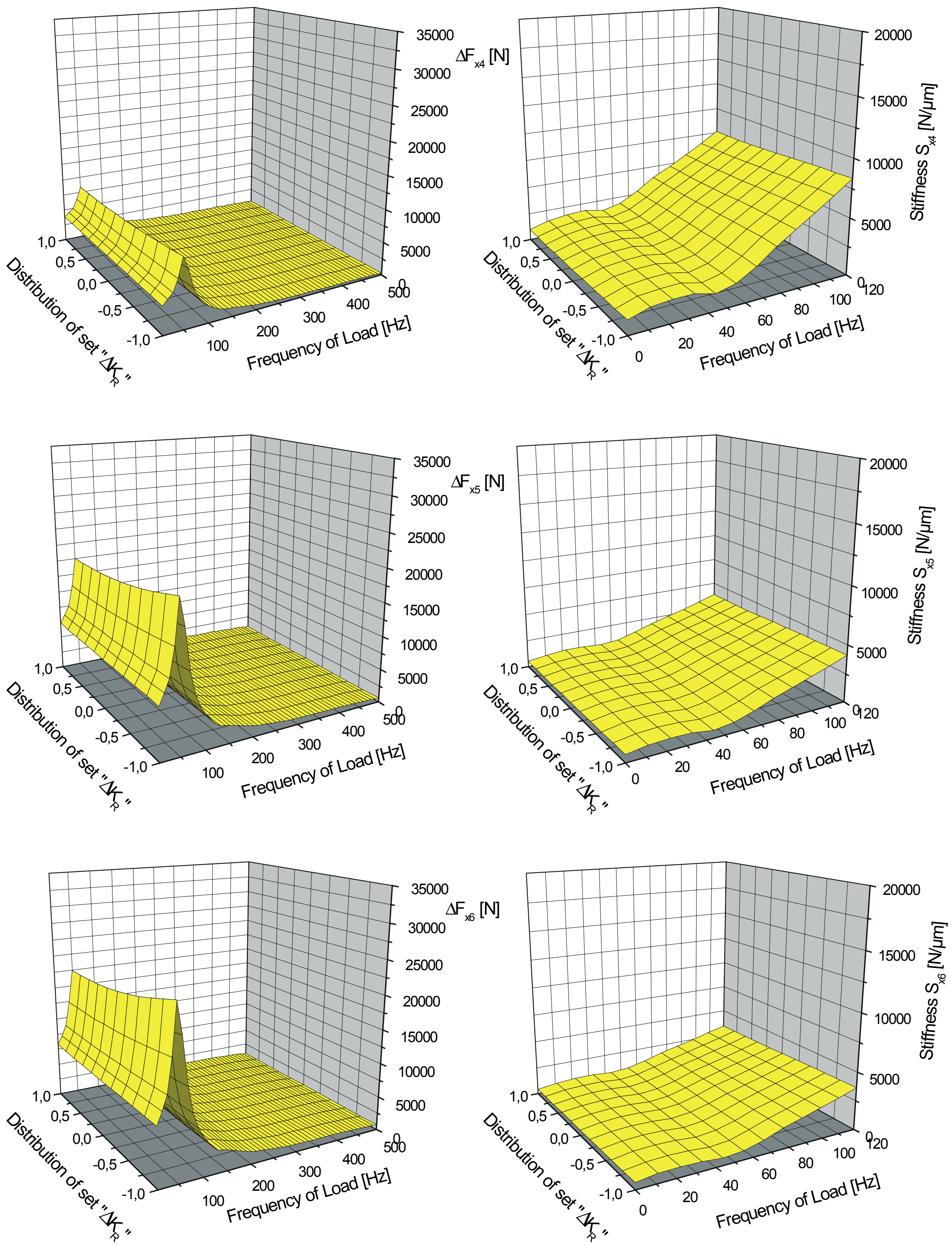

Bearing force and dynamic stiffness vs. freqency of load and normalized distribution of set „ΔK_R“ for radial AMB 4...6

Annex 2 – Feature magnitudes of the axis at selected faults (scaled into a range of -5 to +5)

fault	Explanation	feature											
		$\tilde{s}$	$\bar{s}$	$\tilde{u}$	$\bar{u}$	Io	i_s	W	R	A	V	$\tilde{F}$	$\bar{F}$
FS1+	increased offset, sensor	-1	0	-1	4	0	5	0	0	0	0	0	5
FS1-	decreased offset, sensor	-1	0	-1	-4	0	-5	0	0	0	0	0	-5
FS2+	increased gain, sensor	-5	0	-5	0	0	0	0	0	0	0	-5	0
FS2-	decreased gain, sensor	5	0	5	0	0	0	0	0	0	0	5	0
FC1+	increased gain, controller	-5	0	-5	0	0	0	5	-5	0	0	-5	0
FC1-	decreased gain, controller	5	0	5	0	0	0	-2	5	0	0	5	0
FC2+	increased setpoint, controller	-1	-5	-1	3	0	5	0	5	0	0	1	0
FC2-	decreased setpoint, controller	-1	5	-1	-3	0	-5	0	-5	0	0	1	0
FA1+	increased offset, actuating signal	0	0	0	-5	0	0	0	0	0	0	0	0
FA1-	decreased offset, actuating signal	0	0	0	5	0	0	0	0	0	0	0	0
FA2+	increased offset bias current, actuator	-4	0	-2	0	5	0	0	0	0	0	0	0
FA2-	decreased offset bias current, actuator	4	0	2	0	-5	0	0	0	0	0	0	0
FA3+	increased offset, positive coil, actuator	-1	0	-2	-5	5	0	0	0	0	0	0	0
FA3-	decreased offset, positive coil, actuator	1	0	2	5	-5	0	0	0	0	0	0	0
FA4+	increased offset, negative coil, actuator	-1	0	-2	5	5	0	0	0	0	0	0	0
FA4-	decreased offset, negative coil, actuator	1	0	2	-5	-5	0	0	0	0	0	0	0
FA5+	positive force offset, actuator	0	0	0	-5	0	-5	0	0	0	0	0	-5
FA5-	negative force offset, actuator	0	0	0	5	0	5	0	0	0	0	0	2
FA6+	increased gain, actuating signal	-5	0	-5	0	0	0	0	0	-4	0	-5	0
FA6-	decreased gain, actuating signal	5	0	5	0	0	0	0	0	4	0	5	0